CALIFORNIA INSTITUTE OF TECHNOLOGY

ELECTRON TUBE AND MICROWAVE LABORATORY



# SLOW WAVE PROPAGATION IN PLASMA WAVEGUIDES

by

A. W. Trivelpiece

TECHNICAL REPORT NO. 7

May 1958

A REPORT ON RESEARCH CONDUCTED UNDER

CONTRACT WITH THE OFFICE OF NAVAL RESEARCH

# SLOW WAVE PROPAGATION IN PLASMA WAVEGUIDES

by

A. W. Trivelpiece

CALIFORNIA INSTITUTE OF TECHNOLOGY

Pasadena, California

A Technical Report to the Office of Naval Research

Prepared for

Office of Naval Research Contract

Nonr 220(13)

May 1958

ACKNOWLEDGEMENT

I wish particularly to thank Professor Roy W. Gould and Professor Lester M. Field for their advice, interest, and encouragement throughout this investigation. Mr. Gary Boyd is thanked for his advice on construction of the experimental plasma tubes. Thanks is also extended to Professor Joel Franklin and Mr. Ken Hebert who prepared the computer programs; to Mr. Tom Hays, who assisted in the computations; to Mr. Pete Carpenter, Mr. Eric Gelin, and Mr. Bob Stratton, who constructed the experimental equipment; and to Mrs. Ruth Stratton, who prepared the manuscript.

ABSTRACT

It is shown that the space charge wave modes of propagation which are usually associated with the drifting motion of an electron beam can also propagate and carry energy in stationary electron beams or plasmas of finite transverse cross section. The properties of these modes of propagation have been studied by considering the plasma as a dielectric and solving the field equations. The effect of d.c. magnetic fields have been included, while ion motion and thermal velocities have been neglected. These modes have phase velocities which are generally much less than the velocity of light. Two distinct types of propagation are reported; the first involves charge density variation within the plasma (body wave) and the second involves a perturbation of the surface of the plasma (surface wave). Both of these types have modes which exist down to zero frequency as well as backward wave modes. The angular dependent modes can exhibit Faraday rotation.

One of the potentially useful features of these modes of propagation is that of plasma diagnostics. The effect of radial charge density variation within the plasma column has been investigated and methods for experimentally determining this variation, as well as the average charge density, are suggested. The effect of collisions on wave attenuation is examined approximately.

The interaction of a moving electron beam with these modes is considered, as well as the backward wave start oscillation conditions for backward wave interaction. A qualitative explanation of these modes is given in terms of an equivalent electrical circuit transmission line. Many of the features of these modes have been verified experimentally by measuring the phase velocity along a mercury arc discharge column in an axial magnetic field.

TABLE OF CONTENTS

# I INTRODUCTION

One of the fundamental limitations in the generation of higher microwave frequencies with conventional negative grid vacuum tubes comes from the fact that an electron may spend an appreciable fraction of a cycle in the cathode grid region. To overcome the deleterious effects (1) of such a condition, the Heil brothers (2) and the Varian brothers (3) proposed a device (Klystron) which utilizes a drifting electron beam to produce dense current bunches which are passed through a cavity resonator where the r.f. energy can be extracted. Webster (4) made the first satisfactory analysis of a klystron using a kinematic or bunching theory. He assumed a single velocity electron beam to be passed through a narrow-gap cavity resonator which perturbs the average velocity of the electrons in the beam, sinusoidally in time. The electrons which were decelerated by the cavity fields will be overtaken by electrons which were accelerated by the cavity fields, but which left the cavity at a slightly later time. This results in dense bunches of electrons at some distance down the beam centered about the electron which passed through the cavity when the cavity fields were changing from decelerating to accelerating. The operating characteristics of the klystron can then be determined by investigating the problem of passing these dense current bunches through a narrow gap cavity resonator similar to the one used to perturb the electron velocities. Although the kinematic theory satisfactorily accounts for klystron operation in most cases, it is by no means complete since the mutual repulsion (space charge) forces between electrons have been neglected.

A more general theory including space charge was worked out by Hahn (5) and Ramo (6). One of the problems they considered was that of a

drifting, ion-neutralized, cylindrical electron beam in an infinite axial magnetic field. They found in general that there are two space charge waves associated with the drifting motion of an electron beam; one of these space charge waves has a phase velocity slightly greater than the average velocity of the electron beam (fast space charge wave) and the other has a phase velocity which is, in the case of a one-dimensional electron beam, an equal amount less than the average electron beam velocity, (slow space charge wave). The propagation equation for these space charge waves in a one-dimensional electron beam is*

$$\omega_p^2 - (\omega - \beta u_{oz})^2 = 0 \qquad \text{(I.1)}$$

where $\omega_p^2 = -\frac{\rho_o e}{\epsilon_o m}$ is the electron plasma frequency, $u_{oz}$ is the average electron beam velocity, and all quantities are assumed to have $\exp\ [j(\omega t - \beta z)]$ dependence. The solutions of this equation are

$$\beta = \frac{\omega + \omega_p}{u_{oz}} \qquad \text{(I.2)}$$

$$\beta = \frac{\omega - \omega_p}{u_{oz}} \qquad \text{(I.3)}$$

These traveling wave solutions have different phase velocities ($v_{phase} = \omega/\beta$)

$$v_{ph} = \frac{\omega}{\omega - \omega_p} u_{oz} \qquad \text{(fast space charge wave)} \qquad \text{(I.4)}$$

$$v_{ph} = \frac{\omega}{\omega + \omega_p} u_{oz} \qquad \text{(slow space charge wave)} \qquad \text{(I.5)}$$

but have the same group velocity ($v_g = d\omega/d\beta$)

$$v_g = u_{oz} \quad . \qquad \text{(I.6)}$$

---

*A simple derivation is given in Appendix 1.

The group velocity represents the rate of energy transfer, and as can be seen from I.6, a stationary ($u_{oz} = 0$) one-dimensional electron beam does not propagate space charge disturbances. These space charge waves are just the natural plasma oscillations bodily transported at the average drift velocity of the plasma so that an observer moving with the drift velocity would see a plasma resonance which does not depend on the wavelength of the disturbance. As will be shown in this paper, however, an average velocity of the electron beam is not essential to the propagation of space charge disturbances when the electron beam has finite transverse geometry. The propagation equations derived by Hahn (5) and Ramo (6) predict this behavior; however, their interest was confined to the drifting electron beam solutions and the possibility of propagation along a stationary electron beam was not considered.

Rigrod and Lewis (7) considered the somewhat more difficult problem of an electron beam formed in a region of zero d.c. axial magnetic field injected into a region of non-zero axial magnetic field; the magnetic field being chosen to be of the proper value to produce an inward force on the electrons which just cancels the outward space charge force and the centrifugal force on the electrons. This type of focusing is known as Brillouin Flow (8). They found two types of space charge wave propagation. One of these types of propagation involves a perturbation in the average charge density, and the other type involves a rippling of the surface of the electron beam with no perturbation of the average charge density.

Brewer (9) and Labus (10) have recently treated the even more difficult problem of space charge wave propagation on an eletron beam in an axial d.c. magnetic field of arbitrary strength. Such an analysis

was appropriate since the magnetic fields available in the laboratory are less than the infinite value assumed by Hahn and Ramo, but greater than the value necessary to produce Brillouin Flow.

Although none of these later investigators considered the problem of space charge wave propagation in the absence of any drifting motion of the electron beam, the problem of electromagnetic wave propagation in waveguides filled with stationary ion-neutralized plasmas in arbitrary axial magnetic fields has received considerable attention. Suhl and Walker (11), Gamo (12), Van Trier (13) and others, have examined how the well-known electromagnetic modes of propagation in a waveguide are modified by the introduction of a plasma into the waveguide system. In particular they examined how the cutoff frequencies of the various modes of propagation which exist in the system are perturbed by the presence of the plasma and how the plane of polarization of the angular dependent modes is rotated (Faraday rotation) as a function of distance along the waveguide. They found in general that the mode cutoff frequencies are increased by the presence of the plasma and that the combined presence of plasma and axial magnetic field results in Faraday rotation. They did not find, however, that there exist slow wave space charge modes of propagation analogous to those on a drifting beam at frequencies which are usually well below the cutoff frequency for the empty waveguide system (actually below the plasma frequency for the plasma-filled waveguide when the d.c. magnetic field is infinite).

One of the useful applications of the space charge wave theory described earlier is that of calculating the amount of noise power contributed to the output of a klystron or traveling-wave tube (14) by the electron beam in order to determine what combination of parameters is

required to make this noise power a minimum (15), (16), (17), (18). At the cathode or potential minimum of an electron gun or diode producing an electron beam, there are two sources of noise (19) which serve as the boundary conditions for the two space charge waves. These noise disturbances propagate along the electron beam according to the space charge wave theory, ultimately appearing at the output of the amplifier, which utilizes the electron beam, with some finite value. The extent to which this noise power can be minimized determines the ultimate sensitivity or noise figure* of the amplifier. In most microwave devices using electron beams, the plasma frequency is the order of hundreds of megacycles and the operating frequency is the order of thousands of megacycles. This condition permits the effects of finite geometry on space charge wave propagation to be included as a slight modification to the one-dimensional space charge wave theory. The modification involves using a plasma frequency which is less than that appropriate to the average charge density. This reduced plasma frequency is, just as with the one-dimensional electron beam, the plasma oscillation as seen by an observer moving with the electron beam. The plasma oscillation frequency is reduced because some of the electric field now terminates on the charges induced in the conducting wall (assuming the electron beam is contained in a conducting cylinder), thereby reducing the longitudinal restoring force. The amount by which the plasma frequency is reduced depends on both the wavelength of the disturbance and the transverse geometry. For short wavelength disturbances, the fields do not extend very far outside the electron beam, and

*The sum of the amplified thermal noise associated with the input impedance and the noise power from the electron beam divided by the amplified thermal noise.

if the conducting wall is far removed, there is only a slight reduction in the plasma frequency. However, for long wavelength disturbances, the fields do extend from the plasma and the reduction in plasma frequency is quite significant; in fact, the plasma frequency is reduced to zero for disturbances of infinite wavelength. Thus the propagation constants for space charge waves in finite geometry can be expressed

$$\beta = \frac{\omega \pm R\,\omega_p}{u_{oz}} \tag{I.7}$$

where the reduction factor R is in this case a function of the geometry, beam velocity, and operating frequency. In the case of traveling wave amplifiers operating at low frequencies, however, it is possible to realize operating conditions where the plasma frequency near the potential minimum may exceed the operating frequency. In the course of investigating the consequences of this situation on the propagation of noise disturbances near the potential minimum (20), it became evident that the approximate method of including the effects of finite geometry just described, was unsatisfactory. In fact, it became evident that there were associated with very slowly moving and stationary electron beams, modes of propagation other than the slow and fast space charge waves (21). Presumably these additional modes of propagation are of significance in determining how noise disturbances propagate from the potential minimum and may have a marked influence on the minimum noise figure of a traveling-wave tube operating in this region. However, these additional modes of propagation were of sufficient interest to warrant investigation for their own sake; the noise figure investigation therefore terminated in favor of a study of their properties. Smullin and Chorney (22) have also recently reported the existence of these modes

of propagation.

It is the purpose of this paper to investigate the propagation of space charge wave disturbances in stationary ion-neutralized plasmas of finite geometry, to describe the experimental measurements made to verify their existence, and to demonstrate their relation to space charge waves on moving electron beams.

## II. PLASMAGUIDE MODES IN AN INFINITE AXIAL MAGNETIC FIELD

All of the "plasmaguide"* modes of propagation which will be treated in this paper are slow waves, i.e., the phase velocity of the waves is much less than the velocity of light. The properties of these slow wave modes can be adequately described by an approximate analysis which neglects the a.c. magnetic fields (quasi-static approximation); however, it is appropriate to examine at least one of these modes of propagation including the a.c. magnetic field. For small signals the case of the plasma-filled guide in an infinite axial d.c. magnetic field provides an example which can be treated by the complete Maxwell equations without becoming unduly complicated. This treatment can then be compared with the approximate analysis for the same solution.

Definition of Plasma. The term plasma will be used in this paper to denote a partially ionized gas which, in the absence of disturbances, is electrically neutral. Unless otherwise noted, it will be assumed for this plasma that: the ions are stationary, the electrons have no thermal or random velocities and suffer no collisions, and the neutral gas molecules play no role at all. Ionization and recombination will also be neglected. Such a plasma as described above might be termed an ideal electron plasma.

The Plasma-Filled Waveguide. Consider now a perfectly conducting cylindrical waveguide completely filled with an ideal electron plasma and let there be an infinite axial magnetic field, $B_o = \infty$.**

* The term "plasmaguide" will be used throughout this paper to denote any of the slow wave modes on a non-drifting, ion-neutralized, plasma column.

**Subscripts zero and one will be used to denote d.c. and a.c. quantities respectively.

To study the propagation of waves in this system, the Maxwell equations will be used,

$$\nabla \times \underline{E} = - \frac{\partial \underline{B}}{\partial t} \tag{II.1}$$

$$\nabla \times \underline{H} = \underline{J} + \frac{\partial \underline{D}}{\partial t} \tag{II.2}$$

$$\nabla \cdot \underline{D} = \rho \tag{II.3}$$

$$\nabla \cdot \underline{B} = 0 \tag{II.4}$$

$$\underline{B} = \mu \underline{H} \tag{II.5}$$

$$\underline{D} = \epsilon \underline{E} \tag{II.6}$$

along with the equation of motion,

$$\frac{\partial \underline{v}}{\partial t} + (\underline{v} \cdot \nabla) \underline{v} = - \frac{e}{m} \underline{E} - \frac{e}{m} \underline{v} \times \underline{B} , \tag{II.7}$$

and the equation of continuity,

$$\nabla \cdot J = - \frac{\partial \rho}{\partial t} , \tag{II.8}$$

where the convection current density $\underline{J} = \rho \underline{v}$ , is assumed to be due to the electrons only, and the symbol "e" is used to denote the magnitude of the electronic charge only.

Assuming that all quantities have an average value plus a small harmonic time dependent perturbation,

$$\underline{F}(r,t) = \underline{F}_o(r) + \underline{F}_1(r) \, e^{j\omega t} , \tag{II.9}$$

and are wave-like in nature,

$$\underline{F}_1(x,y,z) = \underline{F}_1(x,y) \, e^{-\Gamma z} , \tag{II.10}$$

where $\Gamma$ is the complex propagation constant,

$$\Gamma = \alpha + j\beta \,, \tag{II.11}$$

allows II.1 and II.2 to be written in component form for cylindrical coordinates in terms of the a.c. quantities as follows:

$$\frac{1}{r}\frac{\partial E_{1z}}{\partial \theta} + \Gamma E_{1\theta} = -j\,\omega\,\mu_o\,H_{1r} \tag{II.12}$$

$$-\Gamma E_{1r} - \frac{\partial E_{1z}}{\partial r} = -j\,\omega\,\mu_o\,H_{1\theta} \tag{II.13}$$

$$\frac{1}{r}\frac{\partial}{\partial r}(r\,E_{1\theta}) - \frac{1}{r}\frac{\partial E_{1r}}{\partial \theta} = -j\,\omega\,\mu_o\,H_{1z} \tag{II.14}$$

$$\frac{1}{r}\frac{\partial H_{1z}}{\partial \theta} + \Gamma H_{1\theta} = j\,\omega\,\epsilon_o\,E_{1r} \tag{II.15}$$

$$-\Gamma H_{1r} - \frac{\partial H_{1z}}{\partial r} = j\,\omega\,\epsilon_o\,E_{1\theta} \tag{II.16}$$

$$\frac{1}{r}\frac{\partial}{\partial r}(r\,H_{1\theta}) - \frac{1}{r}\frac{\partial H_{1r}}{\partial \theta} = j\,\omega\,\epsilon_o\,E_{1z} + J_{1z} \tag{II.17}$$

where $J_{1r}$ and $J_{1\theta}$ have been set equal to zero since the electrons cannot move in the r- or $\theta$-directions. The above equations, II.12 through II.17, can be combined to give the field components $E_{1r}$, $E_{1\theta}$, $H_{1r}$, $H_{1\theta}$, in terms of $E_{1z}$ and $H_{1z}$ only

$$E_{1r} = -\frac{1}{(\Gamma^2 + k^2)}\left[\Gamma\frac{\partial E_{1z}}{\partial r} + \frac{j\omega\mu_o}{r}\frac{\partial H_{1z}}{\partial \theta}\right] \tag{II.18}$$

$$E_{1\theta} = \frac{1}{(\Gamma^2 + k^2)}\left[-\frac{\Gamma}{r}\frac{\partial E_{1z}}{\partial \theta} + j\omega\mu_o\frac{\partial H_{1z}}{\partial r}\right] \tag{II.19}$$

$$H_{1r} = \frac{1}{(\Gamma^2 + k^2)}\left[\frac{j\omega\,\epsilon_o}{r}\frac{\partial E_{1z}}{\partial \theta} - \Gamma\frac{\partial H_{1z}}{\partial r}\right] \tag{II.20}$$

$$H_{1\theta} = \frac{-1}{(\Gamma^2 + k^2)} \left[ j\omega\epsilon_o \frac{\partial E_{1z}}{\partial r} + \frac{1}{r} \frac{\partial H_{1z}}{\partial \theta} \right] , \qquad \text{(II.21)}$$

where $k^2 = \omega^2 \mu_o \epsilon_o$ is the free-space wave number. This demonstrates that all field components can be derived from $E_{1z}$ and $H_{1z}$. The differential equations which $E_{1z}$ and $H_{1z}$ must satisfy are

$$\nabla_T^2 E_{1z} + \Gamma^2 E_{1z} + k^2 E_{1z} = j\omega\mu_o J_{1z} - \Gamma \frac{\rho_1}{\epsilon_o} \qquad \text{(II.22)}$$

$$\nabla_T^2 H_{1z} + (\Gamma^2 + k^2) H_{1z} = 0 \quad , \qquad \text{(II.23)}$$

where the symbol $\nabla_T^2$ denotes the transverse Laplacian which for cylindrical coordinates is

$$\nabla_T^2 = \frac{1}{r} \frac{\partial}{\partial r} \left( r \frac{\partial}{\partial r} \right) + \frac{1}{r^2} \frac{\partial^2}{\partial \theta^2} \quad . \qquad \text{(II.24)}$$

Since the differential equation for $H_{1z}$ does not depend on the presence of the electrons it can be concluded that the H-modes, i.e., those modes which can be derived from $H_{1z}$ only, are not affected by the electrons. This is argued physically by noting that the infinite axial magnetic field constrains the electrons to z-motion only and the H-modes have no electric field component along the z-coordinate to act on the electrons. The H-mode solutions are therefore not of interest in this analysis.

The E-modes, i.e., those modes which can be derived from $E_{1z}$ only, are influenced by the presence of the electrons. The solutions of the differential equation II.22 together with the appropriate boundary conditions leads to the propagation equation for the plasmaguide modes. This analysis is identical with the derivation for the ordinary Hahn-Ramo space charge waves (5),(6), which are associated with the drifting motion

of an electron beam; however, it will be shown that even in the absence of any drift motion of the plasma, propagation of an electromechanical nature can exist down at frequencies below the E-mode cutoff frequency and the plasma frequency.

Neglecting the forces on the electrons due to the a.c. magnetic fields and eliminating the a.c. convection current density and a.c. charge density from II.22 by means of the equations of motion II.7, and continuity II.8, leads to

$$\left\{ \nabla_T^2 + (\Gamma^2 + k^2) \left[ 1 - \frac{\omega_p^2}{\omega^2} \right] \right\} E_{1z} = 0 \qquad \text{(II.25)}$$

where $\omega_p^2 = - \frac{\rho_o e}{\epsilon_o m}$ is the electron plasma frequency. The differential equation in $E_{1z}$ is a linear approximation in that products and higher order combinations of the a.c. perturbation quantities have been neglected. Making the identification

$$T^2 = (\Gamma^2 + k^2) \left[ 1 - \frac{\omega_p^2}{\omega^2} \right] \quad , \qquad \text{(II.26)}$$

the solutions of II.25 are

$$E_{1z} = E_{1z}(0)\, J_n(Tr) \, , \qquad \text{(II.27)}$$

where $e^{jn\theta}$ angular dependence has been assumed and the second solution which is not finite at the origin has been omitted.

Since the plasma completely fills the conducting waveguide, application of the appropriate boundary condition that the tangential electric field must vanish on the waveguide surface, leads to

$$J_n(Ta) = 0 \quad , \qquad Ta = p_{n\nu} \quad , \tag{II.28}$$

where $a$ is the waveguide radius and $p_{n\nu}$ is the $\nu$th root of the nth order Bessel function of the first kind. Solving for the propagation constant in II.26 using II.28

$$\Gamma^2 = -\beta^2 = -k^2 + \frac{(p_{n\nu}/a)^2}{(1 - \frac{\omega_p^2}{\omega^2})} \quad . \tag{II.29}$$

For propagating waves, $\alpha = 0$ and $\Gamma^2 = -\beta^2$ where $\beta^2 > 0$ . Setting $\Gamma^2$ equal to zero and solving for the cutoff frequency leads to the familiar result that the E-mode cutoff frequency for a plasma-filled guide is just the cutoff frequency for the empty guide increased by the plasma frequency

$$\omega_{co}^2 = T^2 c^2 + \omega_p^2 \quad . \tag{II.30}$$

In addition to increasing the cutoff frequency, the presence of the plasma allows $\beta^2$ to take on positive real values for $\omega < \omega_p$ thus giving rise to a propagating wave. Figure 1 shows the phase velocity versus frequency characteristics* of this additional mode in relation to the perturbed electromagnetic waveguide mode. The lower branch represents the electromechanical or plasmaguide mode and has a high frequency cutoff at $\omega_p$ with no low frequency cutoff. Neglecting the free space wave number $k$ , the phase velocity of the plasmaguide wave at low frequencies is approximately

---

*These will be referred to as $\omega$-$\beta$ diagrams.

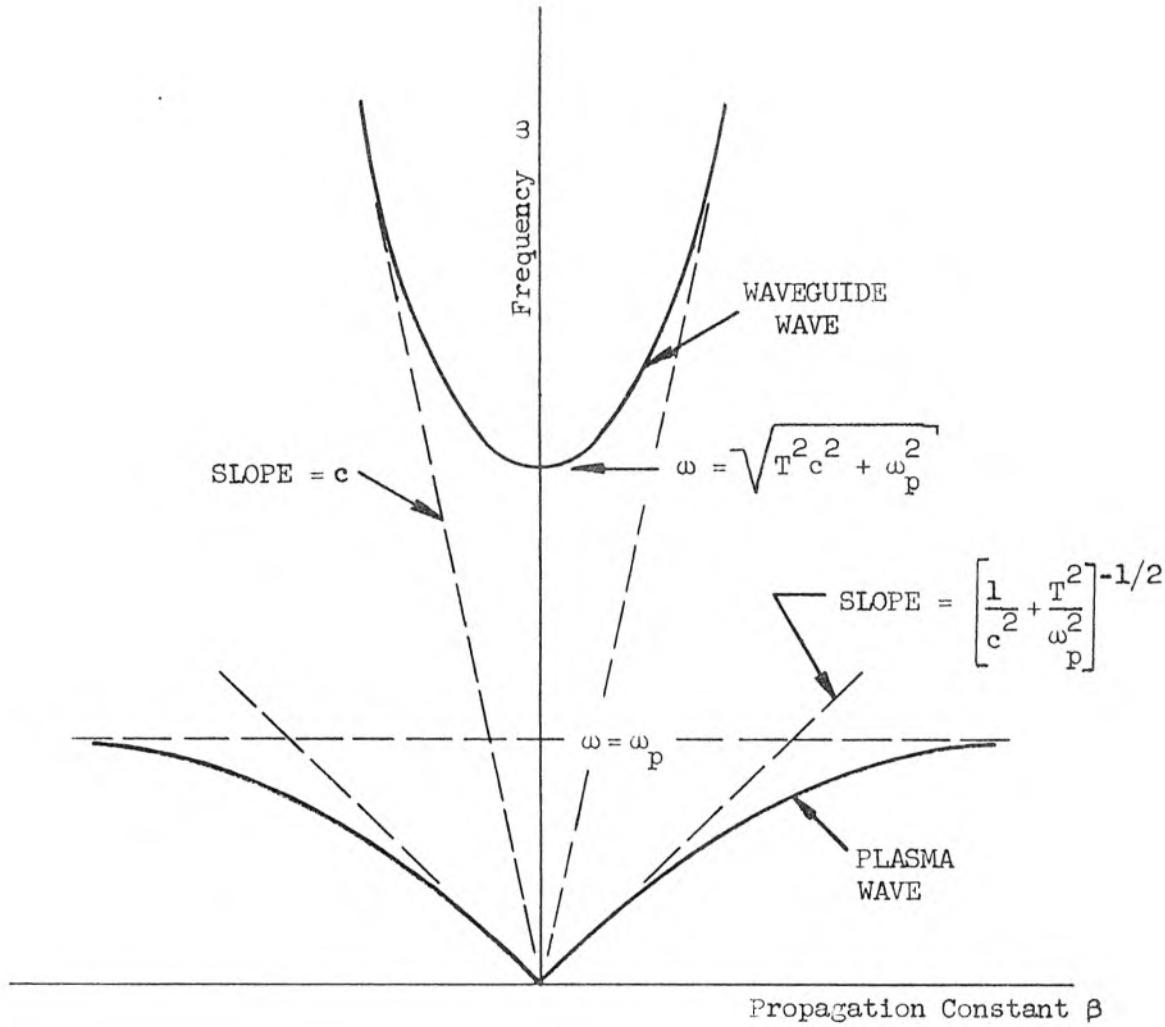


Figure 1. PHASE CHARACTERISTICS OF WAVES IN A PLASMA-FILLED WAVEGUIDE WITH AN INFINITE AXIAL MAGNETIC FIELD

$$v_{ph} = \frac{\omega_p a}{p_{n\nu}} \quad , \tag{II.31}$$

and can in principle always be made small compared with the velocity of light by choosing the guide radius sufficiently small $(\omega_p \ll \omega_{co})$, plasma frequency to be much less than the empty guide cutoff $(\omega_p \ll p_{n\nu} c/a)$. This would be a low phase velocity non-dispersive system at low frequencies. The phase velocity at higher frequencies is always less than the phase velocity at zero frequency, and is zero at $\omega = \omega_p$.

One of the interesting features of the plasmaguide modes is that the high frequency cutoff is independent of the geometry and depends only on the plasma frequency. This is in contrast with the electromagnetic waveguide modes where the cutoff frequency depends intimately on the geometry. Also in contrast with the electromagnetic waveguide modes where the number of modes which can propagate continues to increase as the frequency, is the fact that at any frequency within the passband $(0 < \omega < \omega_p)$, <u>all</u> the higher order $(n > 0,\ \nu > 1)$ modes will propagate simultaneously as well as the lowest order mode $(n = 0,\ \nu = 1)$, if they are excited.

<u>Power Flow</u>. The slope of the $\omega$-$\beta$ curve at any point indicates the group velocity or velocity at which energy is carried along in the system and for the plasmaguide mode the group velocity is non-zero implying that there is a real power flow associated with these modes.

The average power flow associated with these plasmaguide waves is given by

$$\bar{P}_z = \frac{1}{2} \mathrm{Re}\left\{ \int_{\sum} \underline{E}_1 \times \underline{H}_1 \, d\sigma \right\} \tag{II.32}$$

where $\sum$ is the guide area. For the lowest circularly symmetric mode II.32 becomes

$$\overline{P}_z = \frac{1}{2}\,\mathrm{Re}\left\{ 2\pi \int_0^a \frac{\omega\,\epsilon_o\,\beta\,E_{1z}^2(0)}{(k^2-\beta^2)^2}\; J_1^2(Tr)\;(Tr)\;d(Tr)\right\}$$

$$= \pi\,\frac{\omega\,\epsilon_o\,\beta}{(k^2-\beta^2)}\;E_{1z}^2(0)\;\frac{(Ta)^2}{2}\;J_1^2(Ta)$$

$$\pi\left(\frac{\omega}{\beta}\right)\left(\frac{1}{\beta^2}\right)\left(\frac{\epsilon_o}{2}\right)E_{1z}^2(0)\;(p_{01})^2\;J_1^2(p_{01})\quad , \tag{II.33}$$

where $k^2$ has been neglected as compared with $\beta^2$ in the last line. Notice that the total power flow will be the sum of the power flows over all of the modes which are excited. The phase velocity $\omega/\beta$ approaches a constant value at low frequencies and $\beta$ goes to zero as $\omega$. For constant power flow, therefore, the z-component of the electric field $E_{1z}$ becomes small at low frequencies and in the limit is zero.

Simple Physical Explanation for Plasmaguide Modes. A useful conceptual model in terms of electrical transmission lines can be given for the plasmaguide modes as follows. The total current density (convection plus displacement) which flows as a result of an applied field is, for the longitudinal and transverse coordinates,

$$J_{1zT} = j\omega\epsilon_o\left(1 - \frac{\omega_p^2}{\omega^2}\right)E_{1z} \tag{II.34}$$

$$J_{1rT} = j\omega\epsilon_o\,E_{1r}\quad . \tag{II.35}$$

Multiplying the current densities by an area to get the total current, and calculating the admittance gives

$$\left.\frac{I}{V}\right|_z = (\text{constant})\left(j\omega + \frac{\omega_p^2}{j\omega}\right) \tag{II.36}$$

$$\left.\frac{I}{V}\right|_r = (\text{constant})(j\omega)\quad . \tag{II.37}$$

The admittance of the plasma in the longitudinal direction is seen to be just that of a parallel L-C section and the admittance in the radial direction is just the susceptance of free space. Figure 2 shows a transmission line made of such elements and as can be seen, the passbands

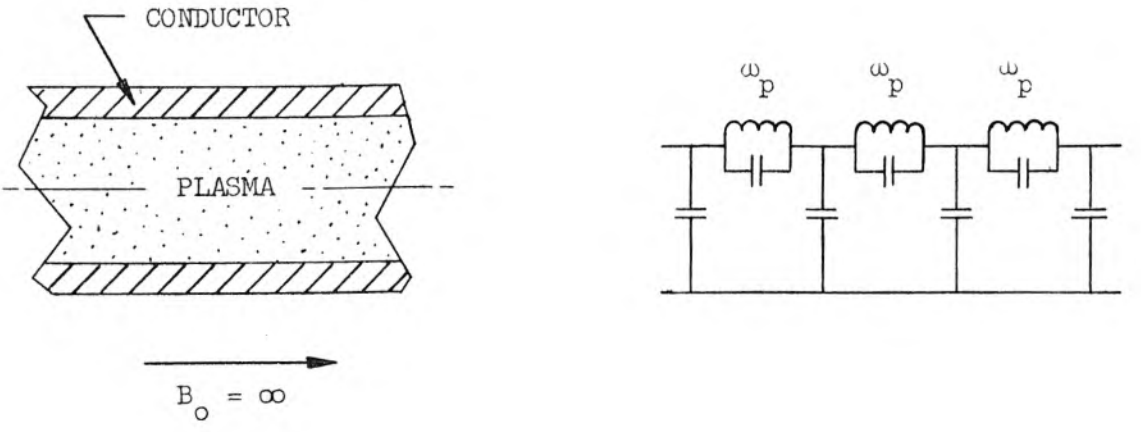


Figure 2. Equivalent Electrical Transmission Line for Plasmaguide Waves

of the iterative circuit are identical with that predicted by the field analysis, i.e., propagation is possible when the series branch is inductive $(0 < \omega < \omega_p)$ and is not possible when the series branch is capacitive $(\omega > \omega_p)$. Such a transmission line analog obviously does not predict the ordinary waveguide passbands.

Electromechanical Nature of the Plasmaguide Waves. As pointed out earlier these modes are electromechanical in nature, i.e., the wave propagation results from the interchange of the kinetic energy of the electrons, and stored energy in the electric field. To compare this with the electromagnetic modes of propagation where the wave propagation results from the interchange of the electric and magnetic stored energy, see Figure 3 which shows the electric and magnetic fields for the lowest E-mode in a cylindrical

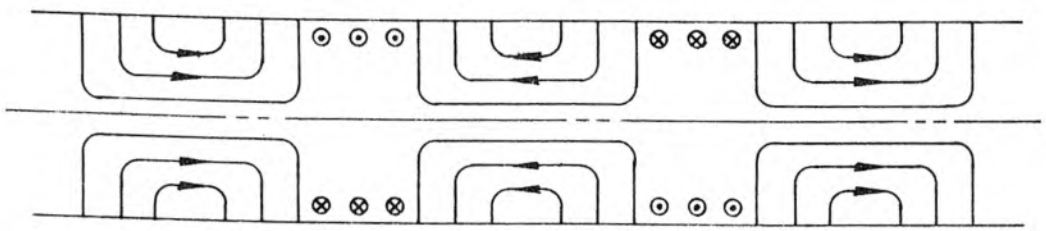

Figure 3a. Electric and Magnetic Field Configuration for the Lowest Circularly Symmetric Mode in a Cylindrical Waveguide.

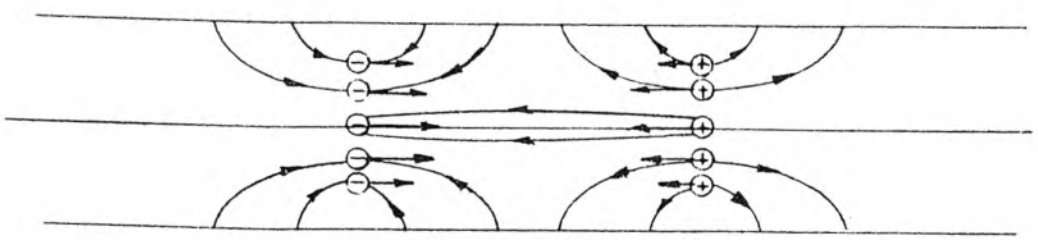

Figure 3b. Electric Field Configuration and Electron Velocities for Electromechanical Plasmaguide Modes.

waveguide and the electric field and electron velocity for the lowest plasmaguide mode in a cylindrical waveguide. Thus it is seen that the role of the magnetic field for the electromagnetic waveguide modes has been essentially taken over by the mass velocity of the electrons.

Review of the Features of Plasmaguide Propagation for an Infinite Axial Magnetic Field. The principal feature of plasmaguide propagation is that a plasma column can, in the absence of any drift motion, support a mode of wave propagation below the plasma frequency. The passband for this mode extends from zero frequency to the plasma frequency and does not depend on the geometry except to the extent that the cross section of the plasma column be finite. The phase velocity of the waves, however, depends both on the plasma frequency and the geometry, and very slow waves are possible for small waveguides. The presence of the metallic conductor around the plasma is not essential to the propagation of waves, i.e., a plasma column in free space would have the same qualitative but not quantitative propagation characteristics as the plasma-filled waveguide. All modes have the same passband and, if excited, will propagate simultaneously. At very low frequencies all of the modes are nondispersive if the guide-to-plasma radius ratio is finite. The phase velocities for typical plasmaguide waves range from a few tenths to a few hundredths the velocity of light. Plasmaguide modes are electromechanical in nature in that the role played by the magnetic field in electromagnetic propagation has been taken over by the mass velocity of the plasma electrons.

## III. PLASMAGUIDE MODES FOR FINITE D.C. MAGNETIC FIELDS

In the previous chapter, space charge wave propagation in a plasma-filled waveguide was examined for the case of an infinite axial magnetic field using the complete Maxwell equations. It is of interest to examine this problem for the case of finite magnetic fields and plasma columns only partially filling the waveguide system. The propagation equations which result from the use of the Maxwell equations are quite complicated (11), (12), (13), thus making a systematic study of the properties of the space charge wave solutions difficult. A result of the analysis given in the previous chapter was that the wave solutions had phase velocities much less than the velocity of light

$$v_{phase} = \frac{\omega}{\beta} \ll c \quad . \tag{III.1}$$

This means that a free-space wavelength is much longer than the wavelength of the disturbances in the waveguide system containing the plasma, and the instantaneous electric fields are to a good approximation given by a solution of Laplace's equation, or in the cases considered here, Poisson's equation, providing the solutions satisfy the same boundary conditions (23).

Dielectric Constant of a Plasma in a D.C. Magnetic Field. It is permissible to treat an ideal electron plasma as described in Chapter II as an equivalent charge-free region, frequency-dependent dielectric. The dielectric constant for the plasma in a uniform magnetic field is a tensor because the components of the electric field and the displacement are no longer related by a simple isotropic constant.

The components of this tensor are calculated by adding the convection current density* to the free-space displacement current density and

*This neglects the term $\rho_1 v_1$ which is assumed to be small, since it is the product of perturbation quantities.

equating the sum to the displacement current of the equivalent charge-free region. Thus

$$j\omega\epsilon_o \underline{E}_1 + \rho_o \underline{v}_1 = j\omega \underline{\underline{\epsilon}} \cdot \underline{E}_1 \quad , \tag{III.2}$$

where the $\underline{\underline{\epsilon}}$ is the tensor dielectric constant. Using the equation of motion II.7, the components of velocity are

$$j\omega v_{1r} = -\frac{e}{m} E_{1r} - \omega_c v_{1\theta} \tag{III.3}$$

$$j\omega v_{1\theta} = -\frac{e}{m} E_{1\theta} + \omega_c v_{1r} \tag{III.4}$$

$$j\omega v_{1z} = -\frac{e}{m} E_{1z} \quad , \tag{III.5}$$

where $\omega_c = \frac{eB_o}{m}$ is the cyclotron frequency. Solving for the components of velocity yields

$$v_{1r} = -\frac{e}{m}\left[\frac{-j\omega E_{1r} + \omega_c E_{1\theta}}{\omega - \omega_c^2}\right] \tag{III.6}$$

$$v_{1\theta} = -\frac{e}{m}\left[\frac{-j\omega E_{1\theta} - \omega_c E_{1r}}{\omega^2 - \omega_c^2}\right] \tag{III.7}$$

$$v_{1z} = -\frac{e}{m}\frac{E_{1z}}{j\omega} \quad . \tag{III.8}$$

Using these components of velocity in III.2 and solving for the tensor,

$$\underline{\underline{\epsilon}} = \epsilon_o \begin{Vmatrix} \epsilon_{rr} & j\epsilon_{r\theta} & 0 \\ -j\epsilon_{\theta r} & \epsilon_{\theta\theta} & 0 \\ 0 & 0 & \epsilon_{zz} \end{Vmatrix} \quad , \tag{III.9}$$

where

$$\epsilon_{rr} = \epsilon_{\theta\theta} = 1 + \frac{\omega_p^2}{\omega_c^2 - \omega^2} \tag{III.10}$$

$$\epsilon_{r\theta} = \epsilon_{\theta r} = \frac{\omega_c}{\omega} \frac{\omega_p^2}{\omega_c^2 - \omega^2} \qquad \text{(III.11)}$$

$$\epsilon_{zz} = 1 - \frac{\omega_p^2}{\omega^2} \quad , \qquad \text{(III.12)}$$

and $\omega_p^2 = -\frac{\rho_o e}{\epsilon_o m}$ is the electron plasma frequency.

Plasma Column in a Waveguide. Consider a perfectly conducting cylindrical waveguide of radius $b$ containing a plasma column of radius $a$ and let there be a finite axial magnetic field $B_o$. To study the propagation of waves in this system, the a.c. magnetic field will be set equal to zero

$$\nabla \times \underline{E}_1 = -j\omega \underline{B}_1 = 0 \quad , \qquad \text{(III.13)}$$

in accordance with III.1, permitting the a.c. electric field to be derived from a scalar potential

$$\underline{E}_1 = -\nabla \phi_1 \quad . \qquad \text{(III.14)}$$

Presumably the approximation is good for slow waves $(v_{phase}^2 \ll c^2)$; however, the solutions obtained should be examined to see if the magnetic fields are indeed negligible in determining the propagation characteristics. For the equivalent dielectric there is no free charge and

$$\nabla \cdot \underline{D}_1 = \nabla \cdot (\underline{\underline{\epsilon}} \cdot \underline{E}_1) = 0 \qquad \text{(III.15)}$$

which leads to the differential equation that the potential must satisfy

$$\nabla \cdot \underline{\underline{\epsilon}} \cdot \nabla \phi_1 = 0 \quad , \qquad \text{(III.16)}$$

i.e., Laplace's equation for an anisotropic medium. Written explicitly

in cylindrical coordinates III.16 becomes

$$\frac{1}{r}\frac{\partial}{\partial r}\left[ r\,\epsilon_{rr}\frac{\partial \phi_1}{\partial r} + j\,\epsilon_{r\theta}\frac{1}{r}\frac{\partial \phi_1}{\partial \theta}\right] + \frac{1}{r}\frac{\partial}{\partial \theta}\left[ -j\epsilon_{\theta r}\frac{\partial \phi_1}{\partial r} + \epsilon_{\theta\theta}\frac{1}{r}\frac{\partial \phi_1}{\partial \theta}\right] + \frac{\partial}{\partial z}\left[\epsilon_{zz}\frac{\partial \phi_1}{\partial z}\right] = 0 \quad , \tag{III.17}$$

where the fact that $\epsilon_{rz} = \epsilon_{zr} = \epsilon_{\theta z} = \epsilon_{z\theta} = 0$ has been used. Also using the fact that $\epsilon_{\theta\theta} = \epsilon_{rr}$ and $\epsilon_{\theta r} = \epsilon_{r\theta}$ leads to the following partial differential equation for the potential

$$\frac{1}{r}\frac{\partial}{\partial r}\left(r\frac{\partial \phi_1}{\partial r}\right) + \frac{1}{r^2}\frac{\partial^2 \phi_1}{\partial r^2} + \frac{\epsilon_{zz}}{\epsilon_{rr}}\frac{\partial^2 \phi_1}{\partial z^2} = 0 \quad . \tag{III.18}$$

To solve this partial differential equation, assume wave solutions of the form

$$\phi_1 = R(r)\, e^{-jn\theta}\, e^{-j\beta z} \tag{III.19}$$

and solve the resulting linear differential equation in the radial variable,

$$\frac{1}{r}\frac{d}{dr}\left(r\frac{dR}{dr}\right) - \frac{n^2}{r^2}R - \beta^2\frac{\epsilon_{zz}}{\epsilon_{rr}}R = 0 \quad . \tag{III.20}$$

Making the identification

$$T^2 = -\beta^2\frac{\epsilon_{zz}}{\epsilon_{rr}} = -\beta^2\,\frac{1 - (\omega_p^2/\omega^2)}{1 + [\omega_p^2/(\omega_c^2 - \omega^2)]} \quad , \tag{III.21}$$

permits the solutions of III.20 (the Bessel's equation) to be written

$$R(r) = A\,J_n(Tr) + B\,N_n(Tr) \quad , \tag{III.22}$$

where, in this case, $B = 0$, since the fields on the axis must be finite.

The complete time dependent potential and field components are:

$$\left.\begin{aligned} \phi_1(r,\theta,z,t) &= A\, J_n(Tr) && \text{(III.23)}\\ E_{1r}(r,\theta,z,t) &= -A\, T\, J_n'(Tr) && \text{(III.24)}\\ E_{1\theta}(r,\theta,z,t) &= A\, \frac{jn}{r}\, J_n(Tr) && \text{(III.25)}\\ E_{1z}(r,\theta,z,t) &= A\, j\beta\, J_n(Tr) && \text{(III.26)} \end{aligned}\right\} e^{j(\omega t - n\theta - \beta z)}, \quad r < a \ .$$

Outside the plasma $(a < r < b)$ the dielectric constant is $\epsilon_o$ and the differential equation for the potential is given by III.20 where $\epsilon_{zz} = \epsilon_{rr} = \epsilon_o$ . The solutions of this equation are the modified Bessel's functions of the first and second kind, and a suitable combination of these functions which satisfies the boundary condition at $r = b$ (i.e., the potential must vanish since $E_{1\theta}$ and $E_{1z}$ are proportional to $\phi_1$) is

$$R(r) = C\left[I_n(\beta r)\, K_n(\beta b) - I_n(\beta b)\, K_n(\beta r)\right] \quad , \quad a < r < b \ . \qquad \text{(III.27)}$$

Taking

$$A = \left[J_n(Ta)\right]^{-1} \qquad \text{(III.28)}$$

and

$$C = \left[I_n(\beta a)\, K_n(\beta b) - I_n(\beta b)\, K_n(\beta a)\right]^{-1} \qquad \text{(III.29)}$$

satisfies one boundary condition, i.e., the potential or tangential components of the electric fields must be continuous at $r = a$, the edge of the plasma. The remaining boundary condition at $r = a$ can be satisfied in either one of two ways which are equivalent. One of these methods is to calculate the charge perturbation at the surface of the plasma column due to the radial motion of the electrons and make the normal component

of the electric field discontinuous by the amount of the surface charge density associated with the perturbation. Since such a calculation determines the amount of radial polarization which is already accounted for in the tensor dielectric description of the plasma, it is equally correct to require that the normal component of the displacement be continuous; the dielectric constant in the plasma is that given by III.9. The latter of these two methods is easiest in application and will be used exclusively throughout the remainder of this paper. Requiring that the normal displacement be continuous leads to

$$\epsilon_{rr}(Ta)\,\frac{J_n'(Ta)}{J_n(Ta)} + n\,\epsilon_{r\theta} = K_e(\beta a)\left[\frac{I_n'(\beta a)\,K_n(\beta b) - I_n(\beta b)\,K_n'(\beta a)}{I_n(\beta a)\,K_n(\beta b) - I_n(\beta b)\,K_n(\beta a)}\right] \qquad \text{(III.30)}$$

where $K_e$ is the relative dielectric constant of the region outside the plasma. Prior to examining equation III.30 for the various solutions of interest, it will be useful to consider the solutions which result for the special case $b = a$, and see how the plasma-filled waveguide solutions treated in Chapter II are modified when the electrons are allowed transverse motion.

Properties of a Plasma-Filled Waveguide. When the plasma completely fills the conducting waveguide, the potential solution is

$$R = A\,J_n(Tr)\,, \qquad \text{(III.31)}$$

where $T$ is given by III.21. Requiring the potential to vanish at $r = a$ leads to

$$J_n(Ta) = 0\,, \qquad (Ta) = p_{n\nu}\,. \qquad \text{(III.32)}$$

Since $Ta$ is just a numerical constant depending on the particular mode of interest, the propagation constant can be expressed

$$\frac{\beta}{\Gamma} = \left[ \frac{(\omega_p^2/\omega^2) - 1}{1 + [\omega_p^2/(\omega_c^2 - \omega^2)]} \right]^{1/2} . \qquad \text{(III.33)}$$

This propagation equation is sketched in Figures 4a and 4b. Examination of these figures reveals that, in addition to modifying the infinite magnetic field plasmaguide waves, a non-infinite magnetic field introduces a backward wave, i.e., a wave whose phase and group velocities are oppositely directed. When the magnetic field is large $\omega_c > \omega_p$, the cutoff frequency of the forward wave remains at $\omega_p$; however, when the magnetic field is small $\omega_c < \omega_p$, the forward wave cutoff is now at the cyclotron frequency. The backward wave branches have the same high frequency cutoff at $\left[\omega_p^2 + \omega_c^2\right]^{1/2}$, but have different lower frequency limits, i.e., when $\omega_p < \omega_c$ the backward wave branch cuts in at $\omega_c$, and when $\omega_p > \omega_c$ it cuts in at $\omega_p$. The normalized phase characteristics for several values of $\omega_c/\omega_p$ are given in Figure 4c. It is of particular interest to note that this backward wave is "structureless" and is not a spatial harmonic of a periodic structure (24).

Perhaps the simplest physical explanation for the existence of a backward wave can be made with the aid of the equivalent electrical transmission line analog described in Chapter II. The longitudinal and radial admittances within the plasma for the finite magnetic field case are obtained from the tensor dielectric constant III.9

$$\left.\frac{I}{V}\right|_r = (\text{constant}) \left[ j\omega + \frac{\omega_p^2}{\frac{\omega_c^2}{j\omega} + j\omega} \right]$$

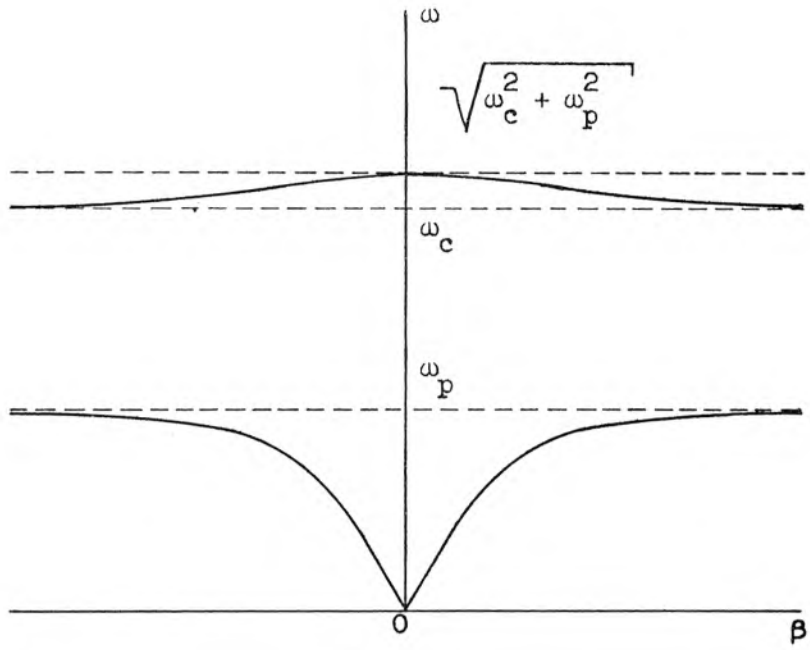


Figure 4a. $\omega_c > \omega_p$

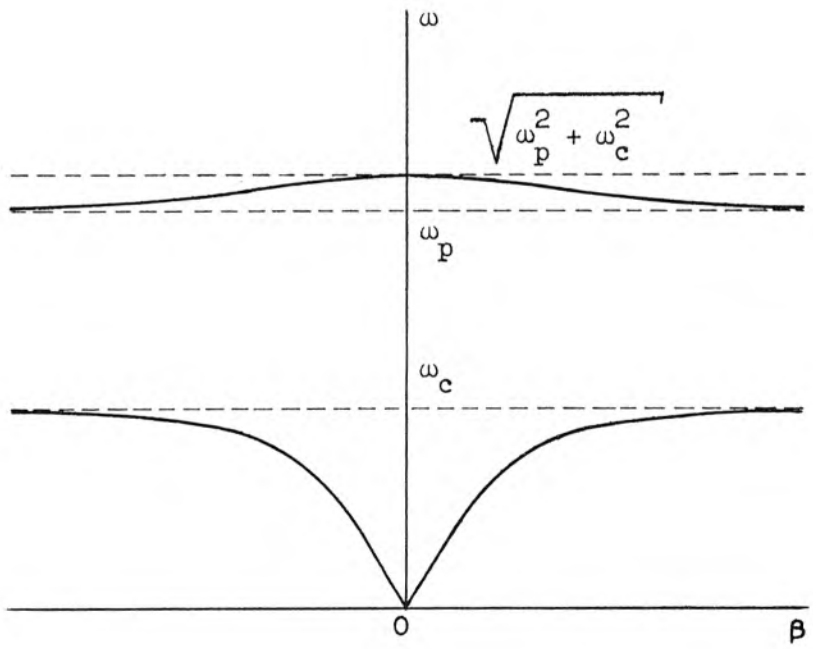


Figure 4b. $\omega_c < \omega_p$

PHASE CHARACTERISTICS OF WAVES IN A PLASMA-FILLED WAVEGUIDE

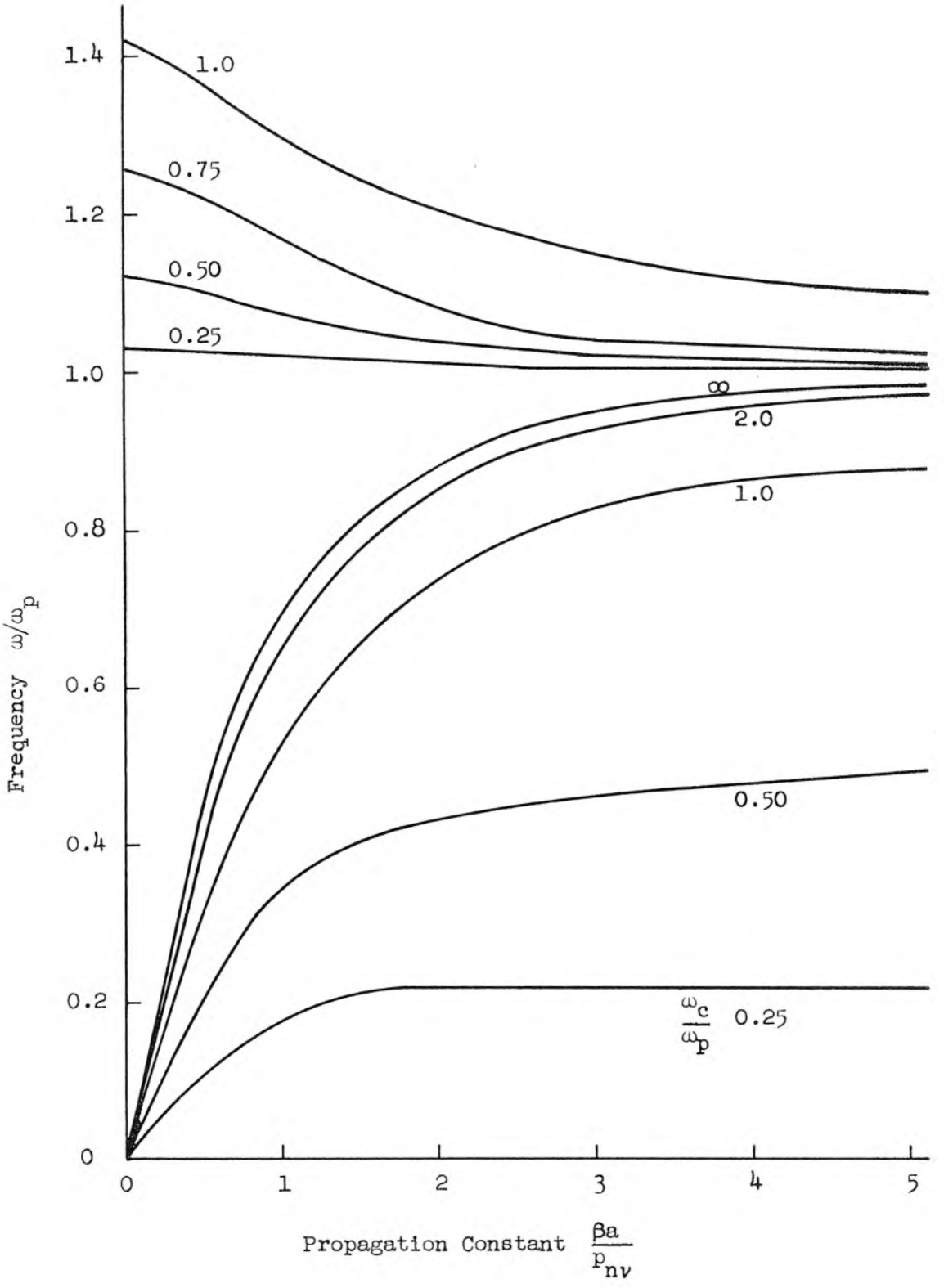


Figure 4c. Phase Characteristics of Plasma-Filled Waveguide. $p_{n\nu}$ is the $\nu$th zero of the nth Order Bessel Function of the First Kind.

$$\left.\frac{I}{V}\right|_z = (\text{constant}) \left(j\omega + \frac{\omega_p^2}{j\omega}\right) .$$

The transmission line analog including the capacity from the edge of the plasma column to the conducting waveguide is shown in Figure 5. The passbands, not including the effect of the dielectric surrounding the plasma, are in exact agreement with the field analysis. Although the shape of the phase characteristics obtained from this transmission line analog are in qualitative agreement with the field analysis, they are not quantitatively correct and will not be included.

The backward wave region, which is seen to be always above the plasma frequency, exists for two separate situations; $\omega_p > \omega_c$ and $\omega_p < \omega_c$. For the $\omega_p > \omega_c$ case the existence of a backward wave is justified by noting that above $\omega_p$ the plasma is capacitive in its longitudinal characteristics and inductive in its transverse characteristics. A lumped filter circuit having such a property is known to be of a backward wave nature (14), i.e., shifting the phase of a generator driving such a circuit causes some plane of known phase to be shifted oppositely to that of a forward wave. The same argument applies when $\omega_p < \omega_c$.

The value of the equivalent transmission line for plasma of finite geometry should not be underestimated. It provides a convenient conceptual tool toward understanding the propagation of waves in plasmas as well as predicting other modes of propagation. One mode of propagation which was predicted from transmission-line considerations is the backward wave which results when the d.c. magnetic field is made perpendicular to the guide axis. This mode will be treated in detail in a later section of this chapter; however, to illustrate the usefulness of

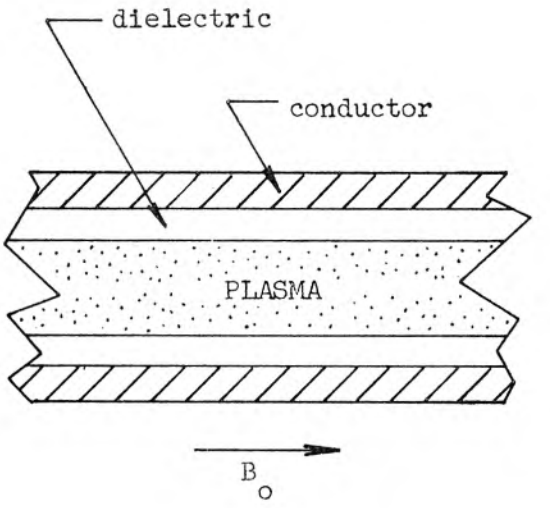


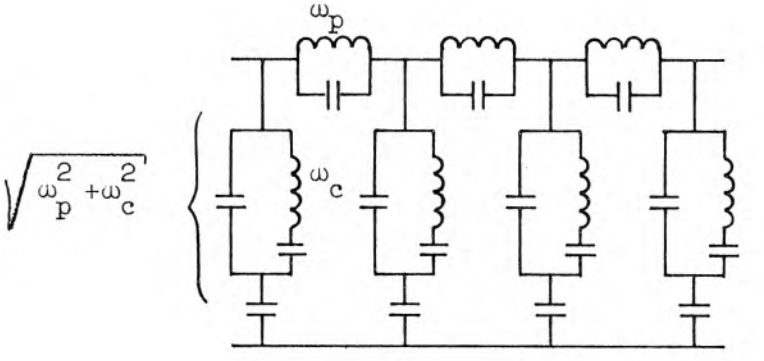


Figure 5. Waveguide Containing a Plasma Column and Equivalent Electrical Circuit Representation.

the transmission-line concept, the arguments for its existence will be given now.

For the case of infinite axial magnetic field plasma-filled waveguide, the transmission line reduces to series inductors and shunt capacitors below the plasma frequency. Imagine now that the waveguide is of rectangular cross-section and that the magnetic field is perpendicular to the guide axis. Since direction of the magnetic field defines the orientation of the inductive element, it can be easily seen that the rotation of the magnetic field has resulted in the interchanging of the elements of the transmission line of the axial magnetic field case. The circuit is now one of longitudinal capacitors and transverse inductors and is a backward-wave type.

Returning to the finite magnetic field plasma-filled guide, it should be pointed out that the properties of the lower branch are essentially the same as for the infinite magnetic field case with the notable exceptions of the cutoff frequency which is at $\omega_c$ when $\omega_c$ is less than $\omega_p$ and the low frequency phase velocity, which now depends on the magnetic field,

$$v_{ph} = \frac{\omega}{\beta} = \frac{a}{p_{n\nu}} \frac{\omega_p \omega_c}{(\omega_p^2 + \omega_c^2)^{1/2}}$$

$\omega^2 \ll \omega_p^2$ and $\omega_c^2$ .

It is now of interest to compare the magnitude of the field quantities as obtained by the rigorous treatment of Chapter I and the approximate method of this chapter. This comparison is made below:

Maxwell's Equation

$$E_{1r} = E_{1z}(0) \frac{-j\beta}{k^2 - \beta^2} T J_n'(Tr) \qquad \text{(III.34)}$$

$$E_{1\theta} = E_{1z}(0) \frac{-\beta}{k^2 - \beta^2} \frac{n}{r} J_n(Tr) \qquad \text{(III.35)}$$

$$E_{1z} = E_{1z}(0) J_n(Tr) \qquad \text{(III.36)}$$

Quasi-Static Approximation

$$E_{1r} = E_{1z}(0) \frac{j}{\beta} T J_n'(Tr) \qquad \text{(III.37)}$$

$$E_{1\theta} = E_{1z}(0) \frac{n}{\beta r} J_n(Tr) \qquad \text{(III.38)}$$

$$E_{1z} = E_{1z}(0) J_n(Tr) \quad . \qquad \text{(III.39)}$$

Note that neglecting $k^2$ as compared with $\beta^2$ in the Maxwell equation solution gives the same electric field components as the quasi-static approximation. Neglecting $k^2$ is consistent with the meaning of the quasi-static approximation which assumes the velocity of light to be infinite.

A. C. Magnetic Fields from Quasi-Static Approximation. The power flow calculation made in Chapter II involved the a.c. magnetic field which was shown early in this chapter to be sufficiently small to be neglected in determining the propagation characteristics of the plasmaguide waves. To obtain an estimate of the power flow for the case at hand, it will be necessary to calculate the a.c. magnetic field components approximately. A first order estimate of these field components is obtained using one of the Maxwell equations

$$\nabla \times \underline{H}_1 = j\omega \, \underline{\underline{\epsilon}} \cdot \underline{E}_1 \, , \qquad \text{(III.40)}$$

which in component form is

$$\frac{1}{r} \frac{\partial H_{1z}}{\partial \theta} - \frac{\partial H_{1\theta}}{\partial z} = j\omega \epsilon_o (\epsilon_{rr} E_{1r} + j \epsilon_{r\theta} E_{1\theta}) \qquad \text{(III.41)}$$

$$\frac{\partial H_{1r}}{\partial z} - \frac{\partial H_{1z}}{\partial r} = j\omega\epsilon_o \left(-j\,\epsilon_{\theta r}\, E_{1r} + \epsilon_{\theta\theta}\, E_{1\theta}\right) \qquad \text{(III.42)}$$

$$\frac{1}{r}\frac{\partial}{\partial r}\left(r\, H_{1\theta}\right) - \frac{1}{r}\frac{\partial H_{1r}}{\partial \theta} = j\omega\epsilon_o\, \epsilon_{zz}\, E_{1z} \qquad \text{(III.43)}$$

where $H_{1z}$ will be set to zero since it is the solution of a second independent differential equation. In a rigorous treatment the $H_{1z}$ would be required to match the boundary condition; however, for the quasi-static approximation the tangential electric field at the boundary which is derived from $H_{1z}$ is negligible. The comparison for the a.c. magnetic field components is given below for the plasma-filled waveguide.

From Maxwell's equation

$$B_{1\theta} = -j\,\frac{\omega}{(k^2 - \beta^2)}\,\frac{1}{c^2}\, E_{1z}(0)\, T\, J_n'(Tr) \qquad \text{(III.44)}$$

$$B_{1r} = \frac{\omega}{(k^2 - \beta^2)}\,\frac{1}{c^2}\,\frac{n}{r}\, E_{1z}(0)\, J_n(Tr) \quad . \qquad \text{(III.45)}$$

From Quasi-Static Approximation

$$B_{1\theta} = -j\,\frac{\omega}{\beta^2}\,\frac{1}{c^2}\, E_{1z}(0)\left[-\epsilon_{rr}\, T\, J_n'(Tr) - \epsilon_{r\theta}\,\frac{n}{r}\, J_n(Tr)\right] \qquad \text{(III.46)}$$

$$B_{1r} = -\frac{\omega}{\beta^2}\,\frac{1}{c^2}\, E_{1z}(0)\left[\epsilon_{\theta r}\, T\, J_n'(Tr) + \epsilon_{\theta\theta}\,\frac{n}{r}\, J_n(Tr)\right] \quad . \qquad \text{(III.47)}$$

Again in the limit of large magnetic field and neglecting $k^2$ as compared with $\beta^2$, the rigorous treatment using the Maxwell equations in Chapter II agrees with the results using the quasi-static approximation because $\epsilon_{rr} = \epsilon_o$ and $\epsilon_{r\theta} = 0$ .

Power Flow for Plasma-Filled Waveguide. To investigate the interaction of moving electron beams with the plasmaguide modes (see Chapter V) it will be necessary to evaluate the average power flow associated with

this mode. The power flow will be calculated here in association with the case discussed rather than in Chapter V where the results will be used.

The power flow for the plasma-filled guide in a finite magnetic field can be calculated using the appropriate field components from III.37 through III.39 and III.46 and III.47 in II.33 . For the axially symmetric modes

$$\bar{P}_z = \frac{1}{2} R_e \left[ 2\pi \int_0^a E_{1z}^2(0) \frac{\omega}{\beta^3} \epsilon_o \epsilon_{rr} J_1^2(Tr)\, d(Tr) \right]$$

$$= E_{1z}^2(0)\, \pi \frac{\omega}{\beta} \frac{1}{\beta^2} \frac{\epsilon_o}{2} \epsilon_{rr} (Ta)^2 J_1^2(Ta) \quad . \qquad \text{(III.48)}$$

Since $\epsilon_{rr}$ goes to unity at infinite magnetic field, the power flow given above agrees with the power flow calculated in Chapter II when $k^2 \ll \beta^2$ (see Equation II.34). Simplifying the above expression by using III.21 leads to,

$$\frac{2\bar{P}_z}{\pi a^2 \epsilon_o J_1^2(P_o) E_{1z}^2(0)} = \left(\frac{\omega_p^2}{\omega^2} - 1\right) \frac{\omega}{\beta} \qquad \text{(III.49)}$$

which is a sort of normalized power flow. This expression illustrates the fact that the backward wave passband will always be above the plasma frequency since the power flow and phase velocities can have opposite sign only if the exciting frequency is above the plasma frequency. The power flow calculated above using the approximate a.c. magnetic field is in agreement with a calculation of power flow made by multiplying the time average stored energy per unit length by the group velocity of the waves.*

Properties of a Plasma Column in a Waveguide. When the plasma does

---

* See Chapter V, Power Conservation for Plasmaguide Waves.

not completely fill the conducting waveguide, the properties of propagation are obtained by simultaneously solving III.21 and III.30. Contrary to the case of the plasma-filled guide, where one normalized $\omega$-$\beta$ diagram describes the properties of all the modes of higher order radial and angular variation, the partially filled guide exhibits quite diverse properties for the different modes. A limited study of these modes has been made with the aid of a digital computer. The results of the study will be presented for the circularly symmetric mode and the mode of one angular variation only.

For the lowest circularly symmetric mode, the forward wave phase characteristics are as shown in Figure 6. The limits of the passbands are obtained by large and small $\beta a$ approximations in III.30. For the geometry of Figure 6 the maximum frequency of transmission of the forward wave passband for $\omega_c < \omega_p$ occurs when

$$\omega = \frac{\omega_p}{\sqrt{2(K_e^2 - 1)}} \left\{ \left[ \left[ 2 - \frac{(K_e^2 - 1)\omega_c^2}{\omega_p^2} \right]^2 - 4 \frac{\omega_p^2 + \omega_c^2}{\omega_p^2} (K_e^2 - 1) \right]^{\frac{1}{2}} - \left[ 2 - \frac{(K_e^2 - 1)\omega_c^2}{\omega_p^2} \right] \right\}^{\frac{1}{2}} .$$

The cases $\omega_c = 0$ or $K_e = 1$ are particularly simple, $\omega_{max} = \left[ (\omega_p^2 + \omega_c^2)/2 \right]^{\frac{1}{2}}$; $K_e = 1$, $\omega_c \neq 0$, and $\omega_{max} = \omega_p (1 + K_e)^{-1/2}$; $K_e \neq 1$, $\omega_c = 0$ . This result was obtained by observing that the maximum frequency of transmission occurs when $\beta a = \infty$, and by using the fact that $\epsilon_{rr}$ and $\epsilon_{zz}$ are both negative when $\omega_c < \omega < \omega_p$, providing $\omega_c < \omega_p$. This means that $T^2 < 0$ and approaches infinity as $\beta^2$ so that III.30 becomes $\epsilon_{rr}\, \epsilon_{zz} = K_e^2$ . Substituting the explicit expressions for $\epsilon_{rr}$ and $\epsilon_{zz}$ and solving for $\omega$ yields the above result. When $\omega_c > \omega_p$ the passband extends to $\omega_p$ . This result is obtained by noting that $\epsilon_{rr} > 0$ while $\epsilon_{zz} < 0$ so that $T^2 > 0$ and that the right side of III.30 becomes proportional to $\beta a$ at large $\beta a$ so that $J_o(Ta)$ must approach zero if the equation is to be

satisfied. This means that $Ta$ must approach a constant, the value for a root of $J_o(Ta)$. In order that III.21 also be satisfied as $\beta a$ approaches infinity, $\epsilon_{zz}$ must approach zero. In the limit of large $\beta a$, $\omega = \omega_p$, thus defining the edge of the passband. The backward wave passbands are not influenced by the geometry for the situation considered here. The zero $\beta a$ limit is obtained by observing that the right side of III.30 is constant for $\beta a = 0$ so that the left side must also be constant. From III.21 $Ta = 0$ and the equation cannot be satisfied unless $\epsilon_{rr} = 0$. If $\epsilon_{rr} = 0$, $Ta \neq 0$ and III.30 can be satisfied providing $Ta$ is a root of $J_o$. Thus $\epsilon_{rr} = 0$ defines the zero $\beta a$ passband limit, $\omega = (\omega_p^2 + \omega_c^2)^{1/2}$ for $\omega_c > \omega_p$ and for $\omega_c < \omega_p$. The other limit of the backward wave passband occurs when $\beta a = \infty$. For this case, $J_o(Ta) = 0$ and $Ta$ is constant. To satisfy III.21, $\epsilon_{zz} = 0$ for $\omega_p > \omega_c$ and $\epsilon_{rr} = 0$ for $\omega_p < \omega_c$. The two limits are $\omega = \omega_p$ and $\omega = \omega_c$ respectively.

The principal difference in the phase characteristics for this case as compared with the completely filled guide is that the magnetic field is not essential to the propagation, and that when the cyclotron frequency is less than the plasma frequency, the lower branch of the phase characteristics is not cut off at the cyclotron frequency, i.e., the phase characteristics pass smoothly through the cyclotron frequency for this lowest circularly symmetric mode only. Below the cyclotron frequency the potential variation across the guide goes as $J_o(Tr)$ $(0 < Ta < p_{01})$. At the cyclotron frequency, $Ta = 0$ and the potential within the plasma is uniform. Above the cyclotron frequency (but within the passband) the potential variation goes as $J_o(jTr) = I_o(Tr)$ $(0 < jTa < \infty)$. These 3 cases are illustrated in Figure 7. As the frequency passes through the cyclotron frequency $(\omega_c < \omega_p)$ the mechanism of propagation passes smoothly from one which involves mostly charge accumulation within the plasma to one which

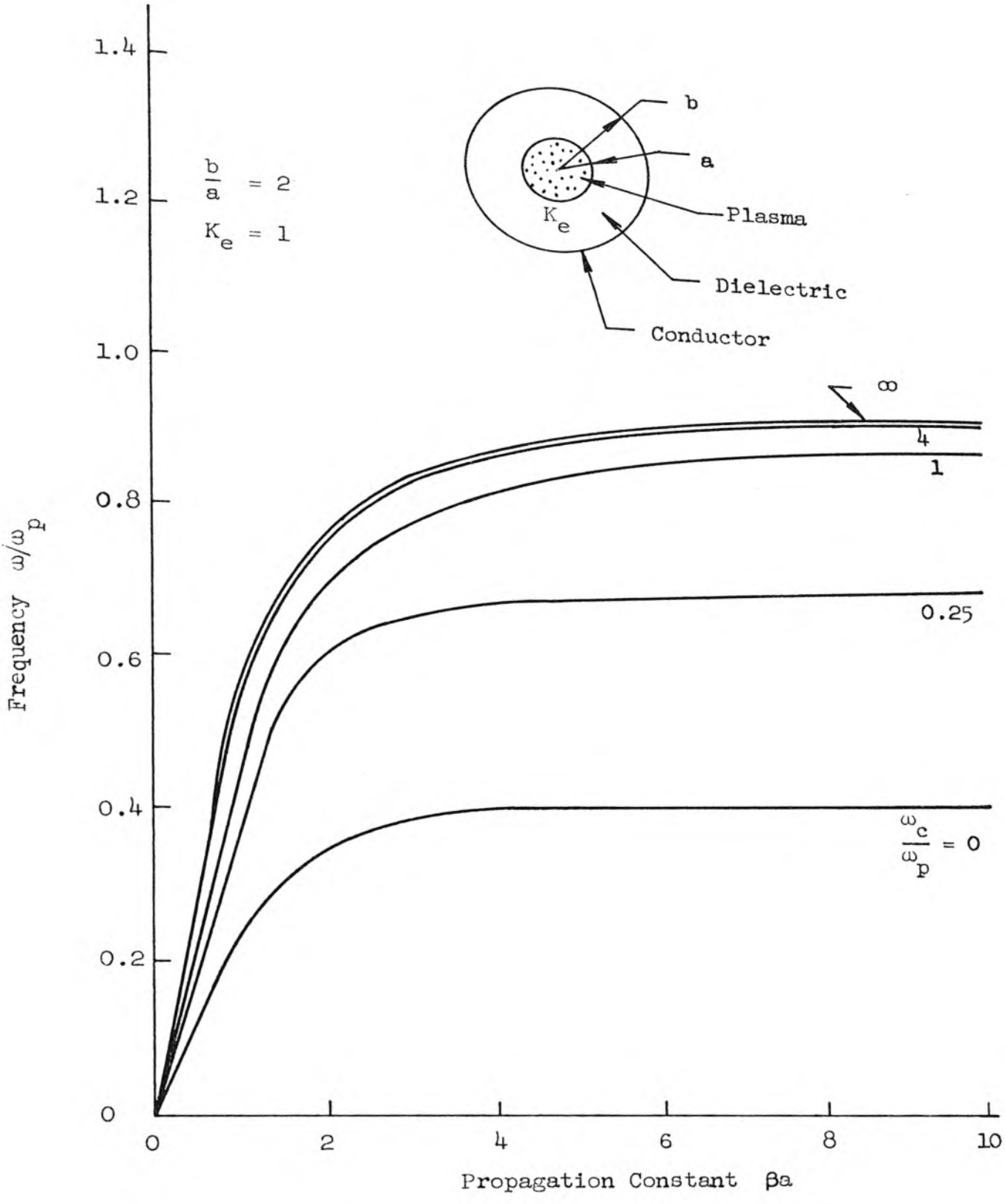


Figure 6. Phase Characteristics of Forward Wave Passband for Lowest Order Axially Symmetric Mode.

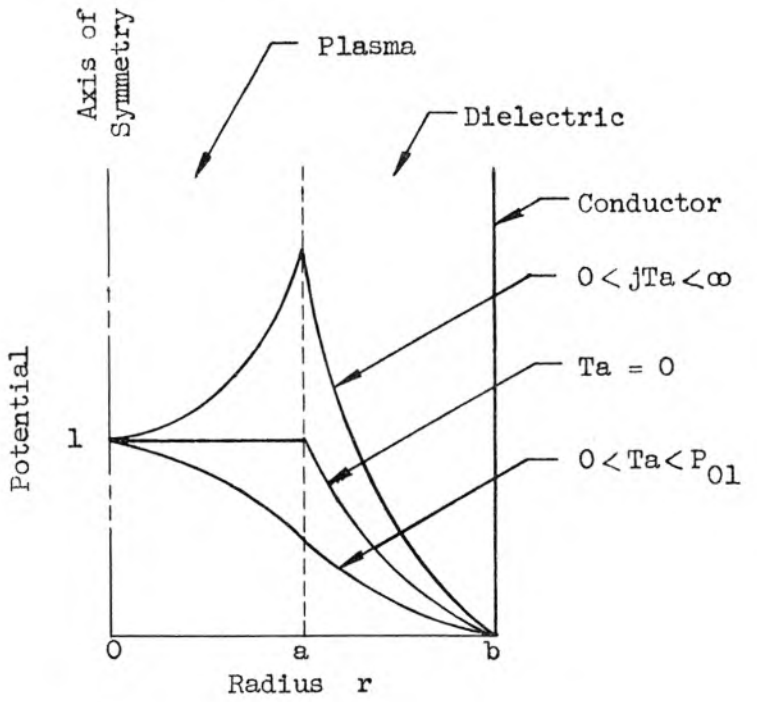


Figure 7. Potential Variation with Radius for Lowest Circularly Symmetric Mode.

involves mostly a perturbation or "rippling" of the surface of the plasma column. In the limit of no magnetic field ($\omega_c = 0$), there is no charge accumulation at all within the plasma. The properties of these "surface waves" are examined in detail in the next chapter.

The phase characteristics of the first few higher order circularly symmetric modes are shown in Figure 8. Notice that only the lowest mode has the behavior just described, i.e., the phase characteristics pass smoothly through the cyclotron frequency ($\omega_c < \omega_p$) for the lowest mode only. All the higher order radial modes with axial symmetry are cut off

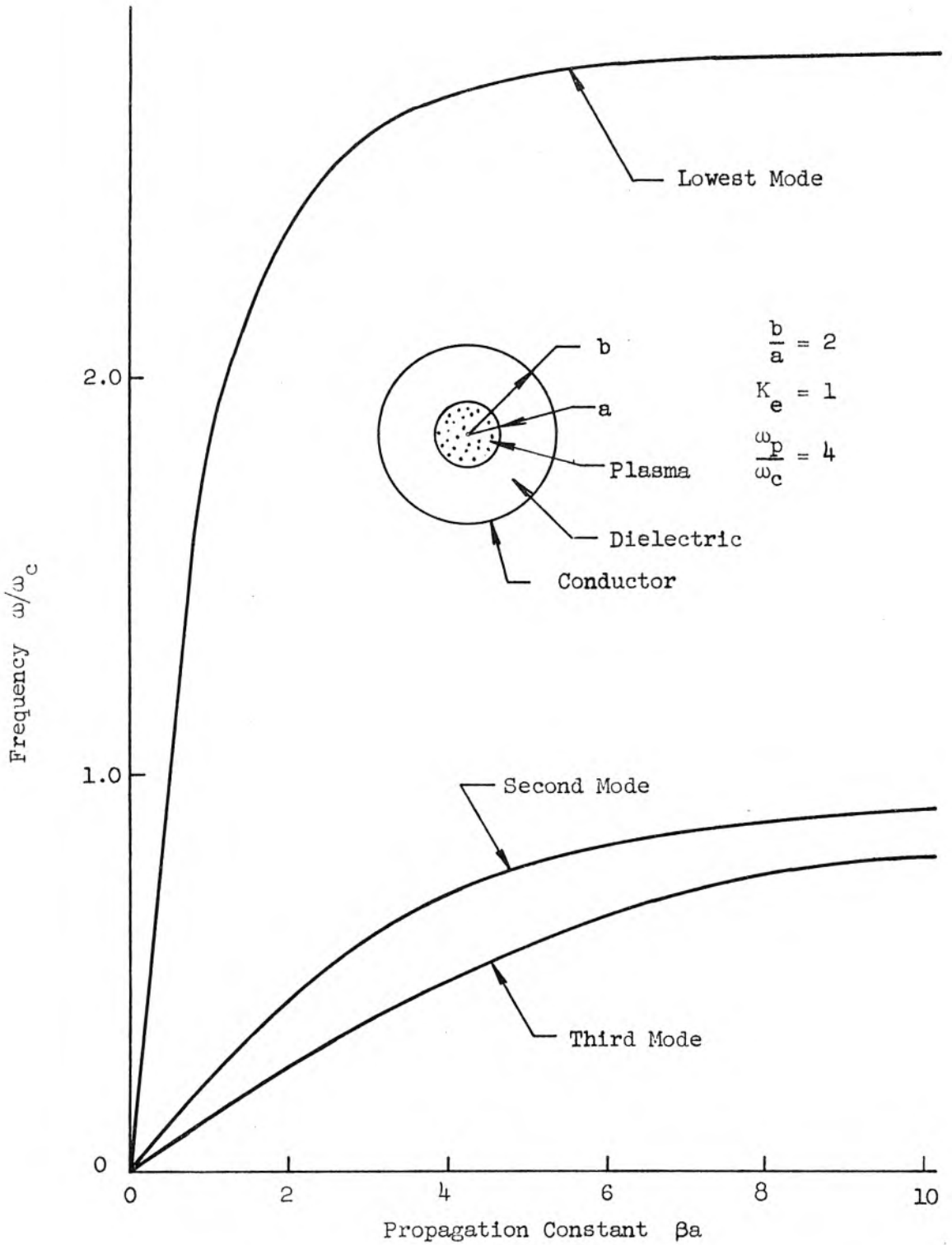


Figure 8. Phase Characteristics of Plasmaguide Waves Showing Higher Order Radial Modes in Relation to the Lowest Order Mode.

at the cyclotron frequency. This behavior is explained by considering the potential variation (see Figure 9) within the plasma column. The potential for the mode having one zero within the plasma goes as $J_o(Tr)$ $(p_{01} < Ta < p_{02})$ . As the cyclotron frequency is approached, Ta approaches $p_{01}$ and the potential outside the plasma approaches zero, which is to say that $\beta a$ is quite large. At the cyclotron frequency $\beta a$ is infinite, denoting the edge of the passband. Just above $\omega_c$ the propagation equation has no solution for $Ta > 0$ and a stop band exists.

Faraday Rotation. The principal reason for considering the mode of one angular variation was to investigate the possibility of Faraday rotation of the plane of polarization. Such considerations were of importance in the analysis of the perturbation of waveguide modes by the plasma (11) and seemed appropriate to investigate in this analysis. A superposition of the $n = +1$ and $n = -1$ modes of equal amplitudes yields a composite wave in which the transverse field is polarized in a certain direction. If the $n = +1$ and $n = -1$ modes have different phase velocities, the direction of polarization of the composite wave will be rotated as a function of distance along the guide. For the $n = +1$ and $n = -1$ modes to have different phase velocities, it is necessary for the propagation equation III.30 to be an odd function of $n$ . The propagation equation will be an odd function of $n$ as long as the plasma does not fill the waveguide. When the plasma fills the guide, all higher order modes of any angular or radial order have equal phase velocities for $n$ equal to plus and minus the same integer and there will be no Faraday rotation. Figure 10 shows the phase characteristics for the mode of one angular variation for the case of plasma frequency

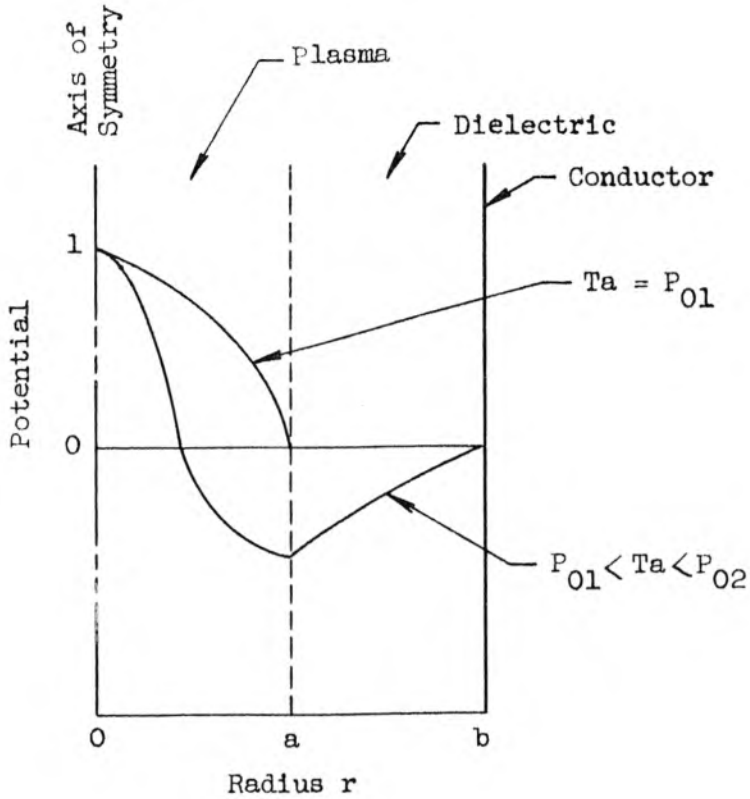


Figure 9. Potential Variation with radius for Circularly Symmetric Mode Having One Zero within the Plasma

twice the cyclotron frequency. The lower branches in Figure 10 do display different phase velocities for $n = \pm 1$ . The distance along the guide, measured in guide wavelengths, for one complete rotation of the plane of polarization is plotted in Figure 11.

In addition to the lower branches which were expected, there are other passbands. These other passbands are the surface waves which will be examined in the next chapter. These surface waves are degenerate in angular index in the absence of an axial magnetic field. The addition

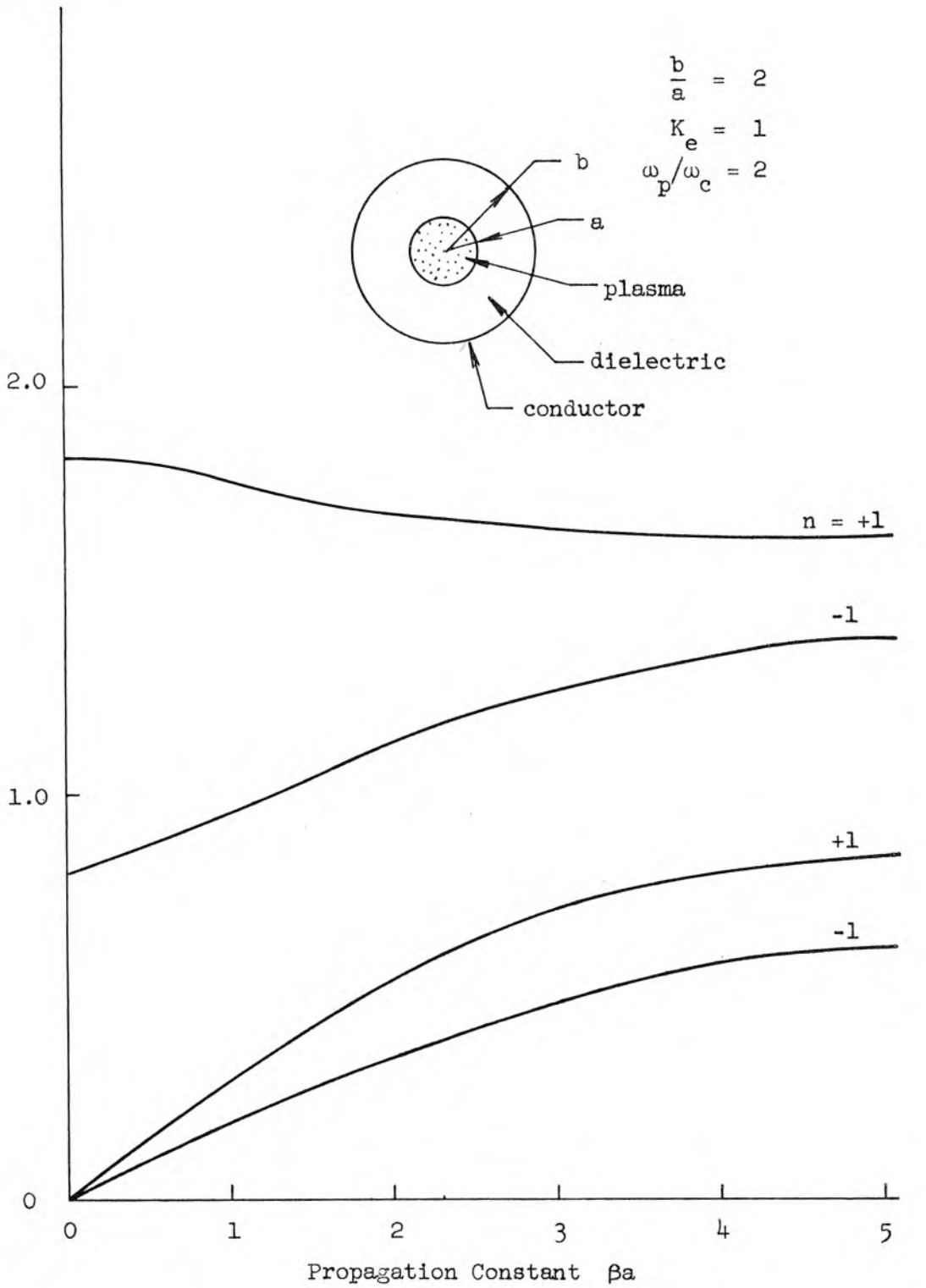


Figure 10. Phase characteristics for modes of one angular variation in a waveguide containing a plasma column.

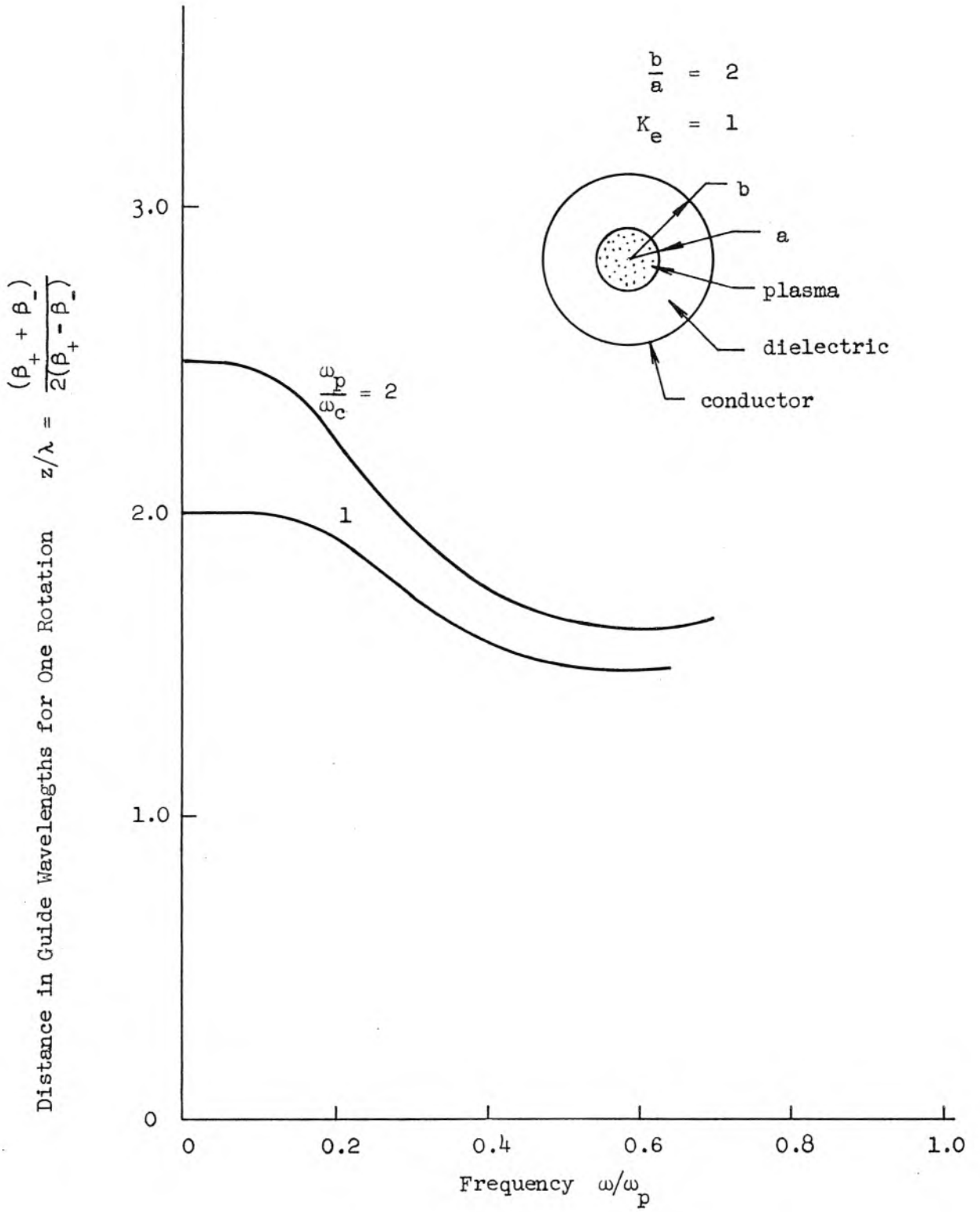


Figure 11. Faraday rotation of the plane of polarization for plasmaguide mode of one angular variation.

of the axial magnetic field removes this degeneracy and the modes are split as shown in Figure 10. For very small magnetic fields these surface waves can also exhibit Faraday rotation, however, no calculation of rotation is given for these upper modes.

Plasmaguide Mode for Magnetic Field Transverse to Direction of Propagation. As a final topic for plasmaguides in finite magnetic fields, consider a rectangular cross section waveguide completely filled with an ideal plasma as shown in Figure 12. The dielectric tensor is

$$\underline{\underline{\epsilon}} = \epsilon_o \begin{Vmatrix} \epsilon_{xx} & & \\ & \epsilon_{yy} & \pm j\epsilon_{yz} \\ & -j\epsilon_{zy} & \epsilon_{zz} \end{Vmatrix} \tag{III.50}$$

where

$$\epsilon_{xx} = 1 - (\omega_p^2/\omega^2) \tag{III.51}$$

$$\epsilon_{yy} = \epsilon_{zz} = 1 + \frac{\omega_p^2}{\omega_c^2 - \omega^2} \tag{III.52}$$

$$\epsilon_{yz} = \epsilon_{zy} = \frac{\omega_c}{\omega} \frac{\omega_p^2}{\omega_c^2 - \omega^2} \quad . \tag{III.53}$$

Paralleling the analysis for a plasma column in a waveguide (III.13 to III.18), the differential equation which must be satisfied by the small signal phasor potential is

$$\frac{\epsilon_{xx}}{\epsilon_{yy}} \frac{\partial^2}{\partial x^2} \phi_1 + \frac{\partial^2}{\partial y^2} \phi_1 + \frac{\partial^2}{\partial z} \phi_1 = 0 \quad . \tag{III.54}$$

Assuming wave solutions,

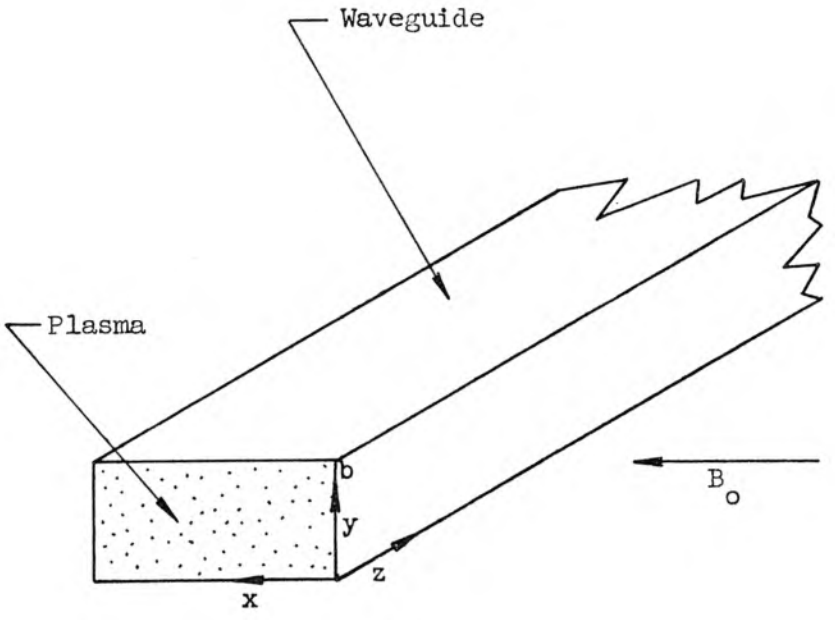


Figure 12. Coordinate System used in Transverse Magnetic Field Analysis.

$$\phi_1 = X(x)\, Y(y)\, e^{-j\beta z} \quad , \tag{III.55}$$

leads to

$$\frac{\epsilon_{xx}}{\epsilon_{yy}} \frac{1}{X} \frac{d^2X}{x^2} + \frac{1}{Y} \frac{d^2Y}{dy^2} - \beta^2 = 0 \, . \tag{III.56}$$

Setting

$$\frac{1}{X} \frac{d^2X}{dx^2} = -T^2 \tag{III.57}$$

gives solutions

$$X(x) = C_1 \sin (Tx) + C_2 \cos (Tx) \quad . \tag{III.58}$$

The equation in $Y$ is now given by

$$\frac{1}{Y}\frac{d^2Y}{dy^2} = \frac{\epsilon_{xx}}{\epsilon_{yy}}T^2 + \beta^2 = -S^2 \quad , \tag{III.59}$$

and the solutions are

$$Y(y) = C_3 \sin(Sy) + C_4 \cos(Sy) \quad . \tag{III.60}$$

The boundary condition at the waveguide surface ($E_{tangential} = 0$) is satisfied by taking $C_2 = C_4 = 0$, $T = m\pi/a$ and $S = n\pi/b$. The potential and field components are

$$\phi(x,y,z,t) = A \sin\left(\frac{m\pi x}{a}\right) \sin\left(\frac{n\pi y}{b}\right) \tag{III.61}$$

$$\left.\begin{aligned} E_{lx}(x,y,z,t) &= -A\left(\frac{m\pi}{a}\right) \cos\left(\frac{m\pi x}{a}\right) \sin\left(\frac{n\pi y}{b}\right) && \text{(III.62)} \\ E_{ly}(x,y,z,t) &= -A\left(\frac{n\pi}{b}\right) \sin\left(\frac{m\pi a}{a}\right) \cos\left(\frac{n\pi y}{b}\right) && \text{(III.63)} \\ E_{lz}(x,y,z,t) &= jA\beta \sin\left(\frac{m\pi x}{a}\right) \sin\left(\frac{n\pi y}{b}\right) && \text{(III.64)} \end{aligned}\right\} e^{j(\omega t - \beta z)} \quad .$$

The equation of propagation is obtained by substituting the values of $S$ and $T$, which satisfy the boundary condition, in the two terms on the right of equation III.59 and solving for the propagation constant $\beta$

$$\beta^2 = -\frac{\epsilon_{xx}}{\epsilon_{yy}}\left(\frac{m\pi}{a}\right)^2 - \left(\frac{n\pi}{b}\right)^2 \quad . \tag{III.65}$$

Substituting the explicit expressions for $\epsilon_{xx}$ and $\epsilon_{yy}$, III.65 may be written

$$\left(\frac{\beta b}{\pi}\right) = \left[\frac{(\omega_p^2 - \omega^2)(\omega_c^2 - \omega^2)}{\omega^2(\omega_p^2 + \omega_c^2 - \omega^2)}\left(\frac{m}{n}\frac{b}{a}\right)^2 - 1\right]^{1/2} \quad . \tag{III.66}$$

A typical $\omega$-$\beta$ diagram is shown in Figure 13. Examination of this figure reveals that, as predicted by the transmission line arguments given

$$\omega_1(-),\ \omega_2(+) = \frac{1}{\sqrt{2}} \left\{ (\omega_p^2 + \omega_c^2) \pm \left[ (\omega_p^2 + \omega_c^2)^2 - \frac{4}{1+\alpha}\, \omega_p^2\, \omega_c^2 \right]^{1/2} \right\}^{1/2}$$

$$\alpha = \left(\frac{nb}{ma}\right)^2$$

$m,n = 1,2,3, \cdots$

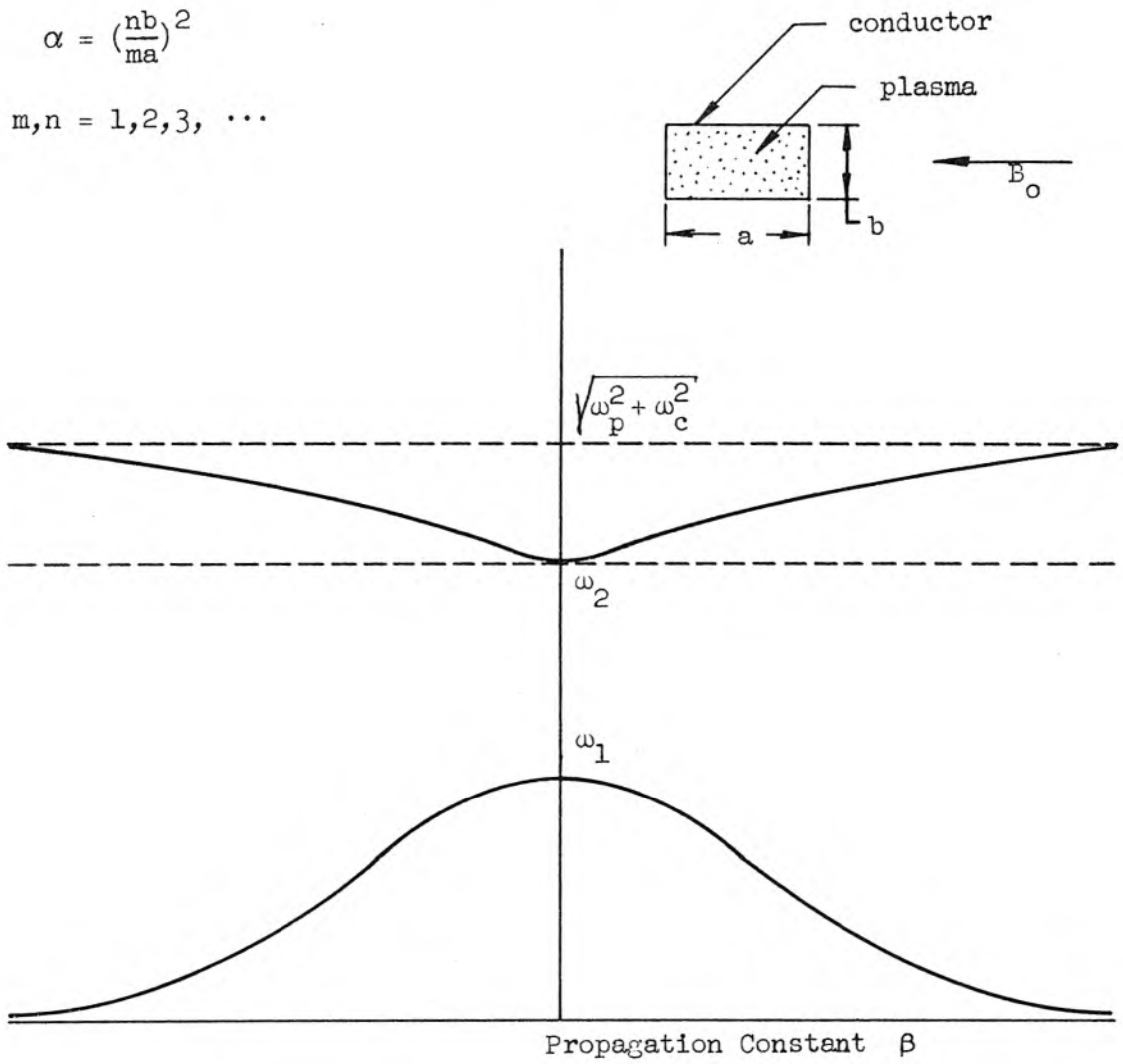


Figure 13. Phase characteristics for rectangular plasma-filled waveguide with a transverse d.c. magnetic field.

earlier in this chapter, there is a backward wave region from zero frequency up to some frequency which depends on the particular mode and the geometry. This upper frequency for the backward wave band is

$$\omega_1 = \frac{1}{2}\left[(\omega_p^2+\omega_c^2) - \left[(\omega_p^2+\omega_c^2)^2 - \frac{4}{1+\alpha}\omega_p^2\,\omega_c^2\right]^{1/2}\right]^{1/2}, \quad 0<\alpha<\infty \tag{III.67}$$

where $\alpha = (\frac{na}{mb})^2$. The fact that $\alpha$ must be finite means that a mode of propagation such as described here does not exist for two parallel planes with plasma between them for a d.c. magnetic field either parallel or perpendicular to the planes. Figure 13 also shows a forward wave region which has a passband from

$$\omega_2 = \frac{1}{2}\left[(\omega_p^2+\omega_c^2) + \left[(\omega_p^2+\omega_c^2)^2 - \frac{4}{1+\alpha}\omega_p^2\,\omega_c^2\right]^{1/2}\right]^{1/2}, \quad 0<\alpha<\infty \tag{III.68}$$

up to $\omega = \left[\omega_p^2 + \omega_c^2\right]^{1/2}$. This forward wave mode would have been predicted by the transmission line arguments if a finite magnetic field case had been considered; it is essentially the backward wave region of finite axial magnetic field plasma-filled waveguide where the transmission line elements have been rotated through $90^\circ$.

This analysis suggests the existence of still other interesting propagation phenomena at frequencies near or below the cyclotron or plasma frequency in other geometries. Although such are known to exist, the systematic investigation and presentation of the analyses would be lengthy and not germane to the purpose of this paper which is the presentation of the notion that electromechanical modes of a slow wave nature can propagate and carry energy below the plasma frequency in finite plasmas in the absence of any drifting motion to the plasma.

Review of the Properties of Plasmaguide Waves in Finite Magnetic Fields. In contrast to the infinite magnetic field case, the plasma-filled waveguide in a finite magnetic field has additional passbands above either the plasma frequency or the cyclotron frequency, whichever is largest. The phase characteristics of these passbands are backward wave. These backward waves are quite novel in that they are not spatial harmonics on a periodic structure. There is no Faraday rotation for the plasma-filled waveguide, and the passbands depend only on the cyclotron and plasma frequencies. The phase velocities of these waves are usually much less than the velocity of light and depend on the geometry as well as the cyclotron and plasma frequency. Propagation stops when the magnetic field is reduced to zero.

When the plasma does not completely fill the waveguide, propagation can exist at zero magnetic field as well as higher magnetic fields. For small magnetic fields the wave propagation involves both a perturbation of the average charge density and a rippling of the plasma surface. The phase velocities of the angular dependent modes are different for plus and minus the same angular index and Faraday rotation exists. The surface waves are now distinct from the body waves and can also exhibit Faraday rotation.

Reorienting the magnetic field so that it is $90^{\circ}$ with respect to the waveguide axis also results in propagation. The essential feature is a low frequency backward wave passband. A narrow forward wave passband also exists near the plasma frequency or cyclotron frequency depending on their relative magnitudes.

## IV. PLASMAGUIDE WAVES FOR ZERO D.C. MAGNETIC FIELD

If the magnetic field is reduced to zero for the plasma-filled waveguide, propagation is no longer possible; however, if the plasma only partially fills the waveguide, a surface wave mode of propagation which involves no charge bunching within the plasma is possible. In the absence of a d.c. magnetic field the plasma is a homogeneous isotropic dielectric and the propagation characteristics of these waves could be investigated using the complete Maxwell equations without becoming unduly complicated since mixed modes (i.e., both E and H modes simultaneously present) are not required to match the boundary conditions (11). However, in anticipation of slow wave solutions, the quasi-static approximation will again be used since the results appear in a somewhat simpler form and are correct to a good approximation when $k^2 \ll \beta^2$. Although the plasma-guide modes of propagation involve a mixture of surface rippling of the plasma column and charge accumulation in the interior region of the plasma for small d.c. magnetic fields $(\omega_c < \omega_p)$, enough interesting results are associated with the pure surface wave case $(\omega_c = 0)$ to warrant separate discussion.

For zero magnetic field the tensor permittivity for the plasma, equation III.9, reduces to

$$\epsilon = \epsilon_o \left(1 - \frac{\omega_p^2}{\omega^2}\right) \quad , \tag{IV.1}$$

and the equation which must be satisfied by the small signal potential is, from equation III.16,

$$\left(1 - \frac{\omega_p^2}{\omega^2}\right) \nabla^2 \phi_1 = 0 \quad . \tag{IV.2}$$

This equation has two solutions,

$$1 - \frac{\omega_p^2}{\omega^2} = 0 \qquad \text{(IV.3)}$$

$$\nabla^2 \phi_1 = 0 \quad . \qquad \text{(IV.4)}$$

The former solution represents plasma oscillations and in the case of a stationary plasma does not imply wave propagation since any disturbance would, in the absence of collisions or thermal velocities, persist indefinitely at the location of the disturbance. Assuming the exciting frequency to be different from the plasma frequency requires solutions of the latter type, i.e., the potential must satisfy Laplace's equation.

Assuming wave solutions (see III.19) leads to the modified Bessel's equation (III.20, with $\epsilon_{zz} = \epsilon_{rr} = 1$) and the solutions for the radial function inside and outside the plasma column are

$$R_i = A\, I_n(\beta r) \qquad \text{(IV.5)}$$

$$R_o = B\left[I_n(\beta r)\, K_n(\beta b) - I_n(\beta b)\, K_n(\beta r)\right] , \qquad \text{(IV.6)}$$

where the second solution of the modified Bessel's equation has been omitted inside the plasma since the fields on the axis must be finite. The solution outside has been chosen to satisfy the boundary condition of zero tangential electric field at the conducting boundary of the cylindrical waveguide containing the plasma column. Taking

$$A = \left[I_n(\beta a)\right]^{-1} \qquad \text{(IV.7)}$$

$$B = \left[I_n(\beta a)\, K_n(\beta b) - I_n(\beta b)\, K_n(\beta a)\right]^{-1} \qquad \text{(IV.8)}$$

satisfies the requirement that the tangential electric fields be continuous at $r = a$ . Applying the remaining boundary condition, continuity

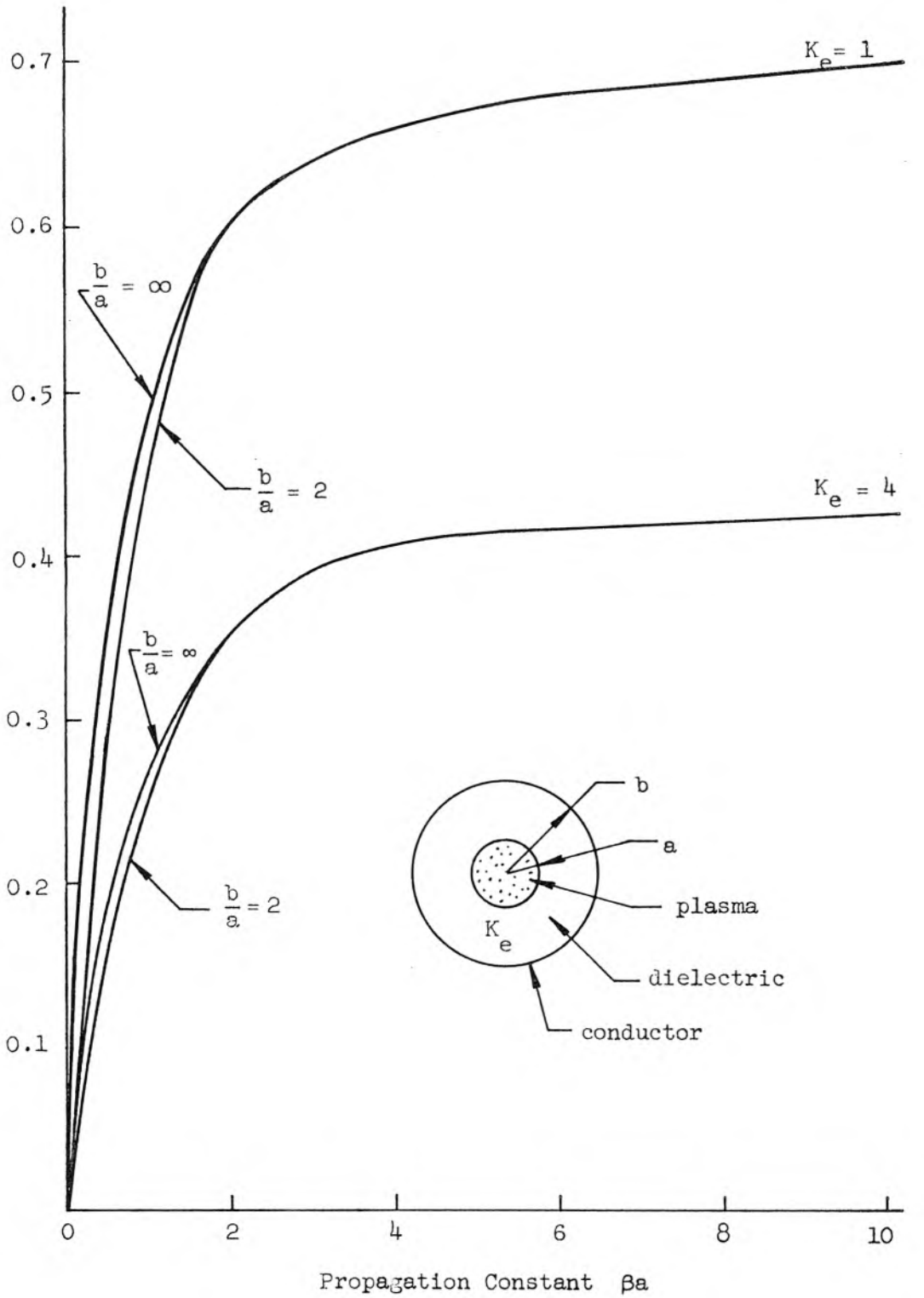


Figure 14. Phase Characteristics for Axially Symmetrical Surface Wave Mode .

of normal displacement leads to the determinantal equation for the propagation of waves

$$\left(1 - \frac{\omega_p^2}{\omega^2}\right) \frac{1}{K_e} = \left[\frac{I_n(\beta a)}{I_n'(\beta a)}\right] \left[\frac{I_n'(\beta a)\, K_n(\beta b) - I_n(\beta b)\, K_n'(\beta r)}{I_n(\beta a)\, K_n(\beta b) - I_n(\beta b)\, K_n(\beta a)}\right], \qquad \text{(IV.9)}$$

where $K_e$ is the dielectric constant of the region between the plasma and the conducting wall of the waveguide. The solution of this equation is shown in Figure 14 for the circularly symmetrical mode. Propagation is seen to exist from zero frequency up to the frequency

$$\omega = \frac{\omega_p}{\sqrt{1 + K_e}} . \qquad \text{(IV.10)}$$

This cutoff frequency is obtained by using the large argument approximations for the modified Bessel's functions and can be argued physically as follows. The potential variation in the plasma column and surrounding dielectric is as shown in Figure 15. For large $\beta a$ the potential is quite large at the plasma-dielectric interface and the fields extend only slightly into the plasma and dielectric. For this reason, the phase velocity of the waves at large $\beta a$ must depend only on the properties of the interface region. As will be shown later, this requirement can lead to backward waves in an isotropic homogeneous plasma filling a thin dielectric cylinder in free space. Since $K_e \geq 1$ for most dielectrics, the circularly symmetric surface waves cannot exist at frequencies above $\omega_p/\sqrt{2}$. The low frequency region is nondispersive for all finite $b/a$ values,

$$v_{ph}(\omega=0) = \left.\frac{\omega}{\beta}\right|_{\omega=0} = \left[\frac{\log \frac{b}{a}}{2K_e}\right]^{1/2} \omega_p a . \qquad \text{(IV.11)}$$

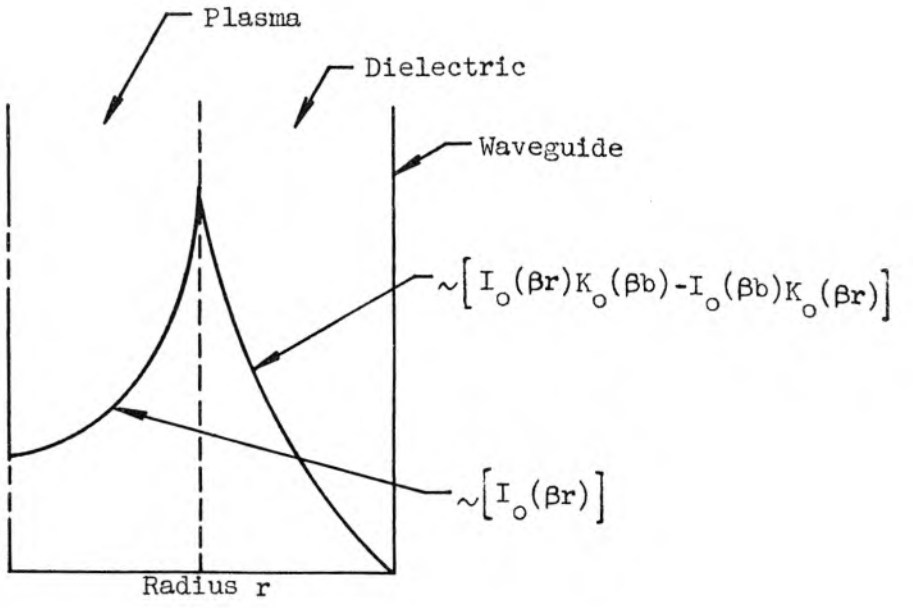


Figure 15. Potential Variation with Radius for Surface Waves on Plasma Column in a Dielectric Lined Cylindrical Waveguide.

When $b/a = \infty$, (i.e., for a plasma column in an infinite dielectric) the determinantal equation simplifies to

$$\left(1 - \frac{\omega_p^2}{\omega^2}\right) \frac{1}{K_e} = \frac{I_n(\beta a)\, K_n'(\beta a)}{I_n'(\beta a)\, K_n(\beta a)} \quad . \tag{IV.12}$$

The $\omega$-$\beta$ diagram for this case is also shown in Figure 14. As can be seen the cutoff frequency remains at $\omega_p/\sqrt{1 + K_e}$. The low frequency behavior is, however, not linear

$$v_{ph} = \omega/\beta = \left[0.116 + \log_e \frac{1}{\beta a}\right]^{1/2} \omega_p a \quad , \quad \omega^2 \ll \omega_p^2 \, , \; \beta a \ll 1 \qquad \text{(IV.13)}$$

and the system is dispersive in this region. That the dielectric space surrounding the plasma is essential to the existence of these waves can be understood by observing that making $b/a = 1$ leads to the degenerate case $\omega = 0$ for all $\beta$. That the dielectric space is essential, can also be argued by observing that the waves depend on surface charge accumulation, and the presence of a tight-fitting conducting cylinder prevents such accumulation. The rippling of the boundary of the plasma column is well described by the term "peristaltic". That is, one of the planes where the column has minimum diameter or is constricted, moves with the phase velocity of the wave. The perturbed shape of the plasma column and the electric field distribution is shown in Figure 16.

Simple Method for Obtaining Low Frequency Phase Velocities of Plasma Waves. The expression for the low frequency phase velocity, equation IV.11, was obtained by using the small argument approximations for the modified Bessel's functions. In matching the boundary conditions, the ratio of the normal displacement to the potential was made continuous across the boundary $r = a$. Passing to the limit of small $\beta a$ for this ratio using the functions in the region outside the plasma gives an expression which is independent of $\beta a$. It therefore seems appropriate to go directly to the solution of the differential equation with $\beta$ set equal to zero. The potential will be a solution of Laplace's equation,

$$\frac{1}{r}\frac{d}{dr}\left(r \frac{dR}{dr}\right) - \frac{n^2}{r^2} R = 0 \quad . \qquad \text{(IV.15)}$$

The solutions are

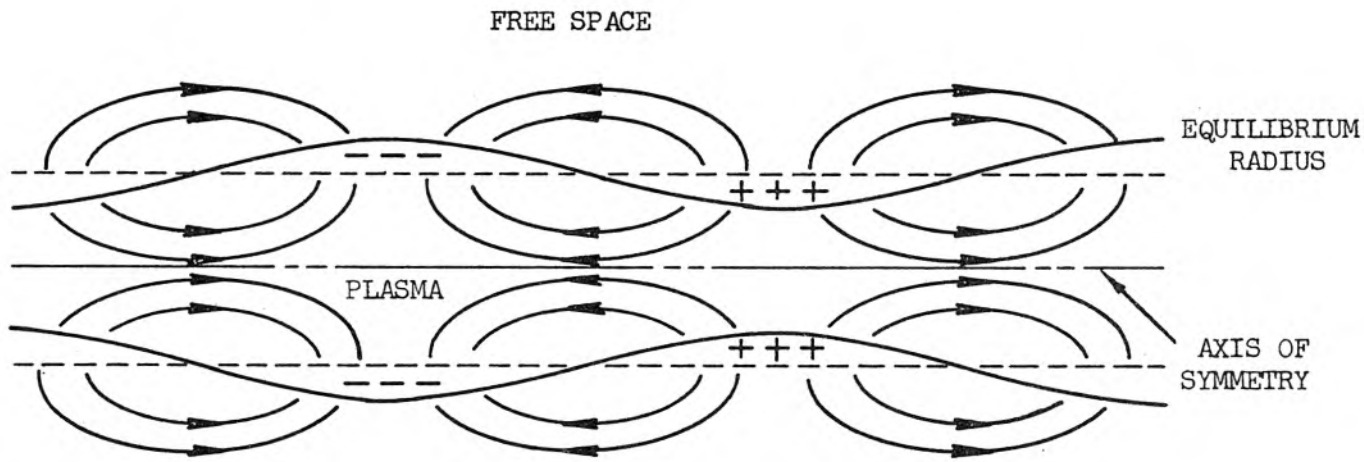


Figure 16. Field Distribution and Charge Perturbation for the Circularly Symmetric Surface Wave on an Isotropic Plasma Column.

$$R = A + B \log r \qquad \text{for} \quad n = 0 \tag{IV.16}$$

$$R = Ar^{n} + Br^{-n} \qquad \text{for} \quad n \neq 0 \quad . \tag{IV.17}$$

The application of the method involves writing the solutions in each of the regions outside the plasma, and starting with the most remote boundary (where the boundary condition is presumed to be known such as the conducting wall of the waveguide), transferring the solution to the next discontinuity, and requiring that the normal displacement-potential ratio be continuous across the boundary. This process is repeated until the surface of the plasma has been reached. At this point the normal displacement-potential ratio for the zero $\beta$ solution outside the plasma is equated to this ratio for the small argument ($\beta a$ approaching zero) solutions inside the plasma giving the desired solution. The reason that the zero $\beta$ solution is not used for the interior of the plasma is that the normal displacement-potential ratio does not approach a constant value for small $\beta$ , but rather goes to zero as $\beta^2$. Thus it would not be possible to realize a solution of the propagation equation IV.9 using the zero $\beta$ solution within the plasma.

This method is most useful in cases of complicated geometry or for investigating the higher order angular variation modes. To illustrate the method, however, only the simple two-region geometry considered here for the circularly symmetric case will be used. Other applications of the method will appear only as results. The zero $\beta$ solution of Laplace's equation for axial symmetry outside the plasma, is

$$R_o = A + B \log r \quad . \tag{IV.18}$$

The solution within the plasma is still given by IV.5 . Equating the

normal displacement-potential ratios

$$\left(1 - \frac{\omega_p^2}{\omega^2}\right) \frac{\partial R_i/\partial r}{R_i} = K_e \frac{\partial R_o/\partial r}{R_o} \quad , \tag{IV.19}$$

and evaluating at $r = a$ gives

$$\left(1 - \frac{\omega_p^2}{\omega^2}\right) \beta \frac{I_a'(\beta a)}{I_a(\beta a)} = K_e \frac{1/a}{\log \frac{a}{b}} \quad , \tag{IV.20}$$

where the small $\beta a$ forms of the modified Bessel's functions must now be used for the left hand side. This leads to the same result as given in IV.11.

Plasmaguide Surface Waves of One Angular Variation. For the $n = 1$ case, the behavior is as shown in Figure 17. The upper cutoff frequency remains at $\omega_p/\sqrt{1 + K_e}$. In contrast with the circularly symmetric mode, however, it is seen that the lower cutoff is not at zero frequency, but occurs at some frequency between zero and the upper cutoff. The lower frequency limit can be calculated using the small $\beta$ solution method just described. The result is

$$\omega_{co} = \left[1 + K_e \frac{b^2 + a^2}{b^2 - a^2}\right]^{-1/2} \omega_p \quad . \tag{IV.21}$$

The small $\beta a$ limit is in a region where the quasi-static approximation is not necessarily valid, and the result should be viewed with suspicion. This mode has oppositely-directed phase and group velocities for small $\beta a$ and large $b/a$, and is therefore a backward wave in this region. Examination of the differential equations reveals that $n$, the angular

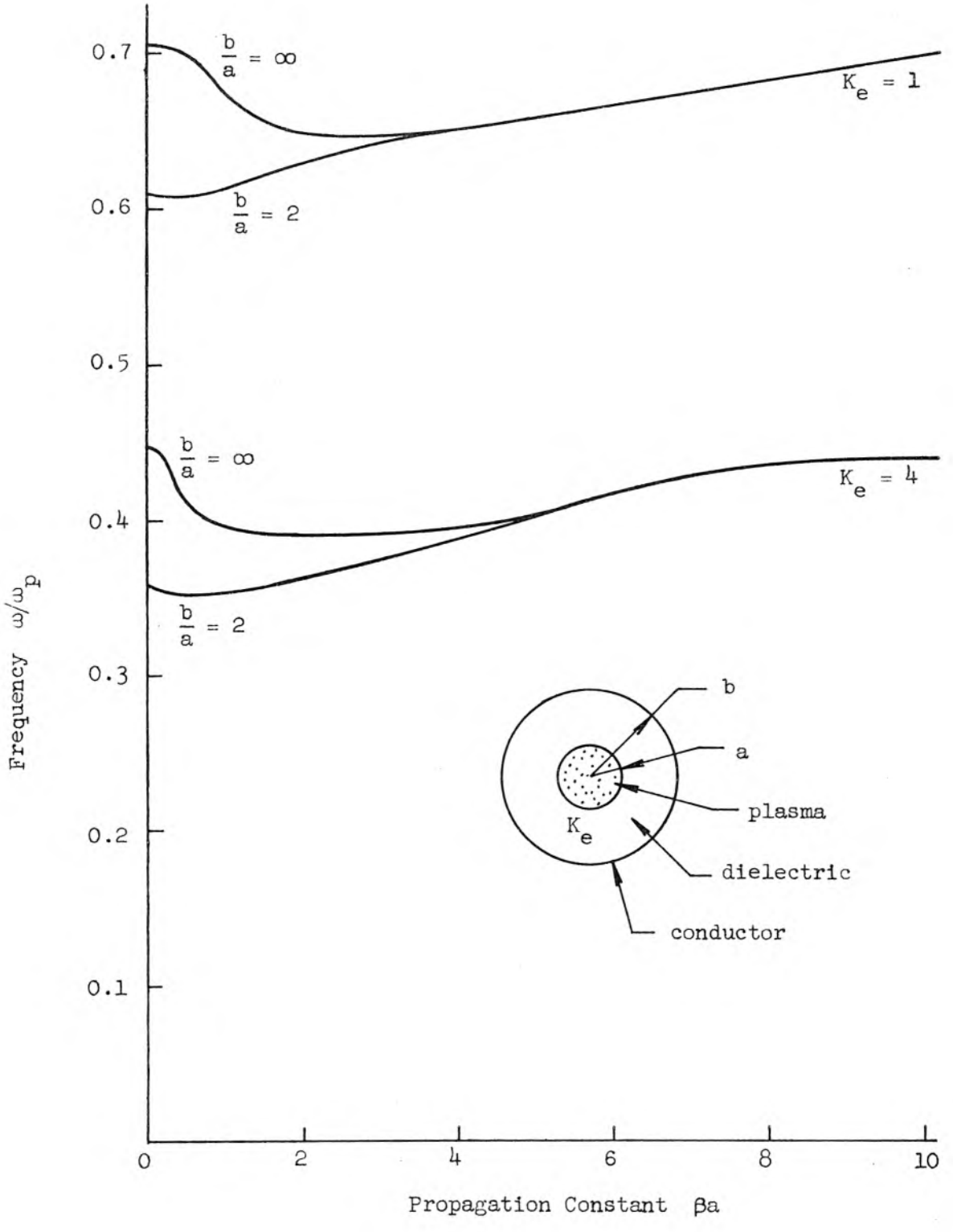


Figure 17. Phase Characteristics for Surface Wave Mode of One Angular Variation.

index, appears as a squared term only. Choosing the $n = -1$ solution would have, therefore, led to the same determinantal equation which is to say that degeneracy exists for the angular dependent modes of opposite index. The addition of an axial magnetic field removes this degeneracy.* For the $n = +1$ mode, the perturbation of the surface of the plasma column is such that, at any instant of time the column would be of a helical or serpentine shape; the reason being that in any one plane the electrons move together as a disk which executes a small circular motion at an angular rate equal to the exciting frequency. A linearly polarized wave (equal amplitudes $n = +1$ and $n = -1$ superposed) would perturb the plasma column to be sinusoidally scalloped, viewed at right angles to the plane of polarization and to be undisturbed when viewed along the polarization axis. The reason for this pattern is that the electrons in any one plane again move as a disk except now the disk moves sinusoidally in time, along the axis of polarization at the driving frequency.

Equivalent Electrical Transmission Line for Surface Waves. A qualitative description of the surface wave propagation can be given in terms of an equivalent electrical transmission line by the same arguments used in Chapter II. For the circularly symmetric modes on a plasma column only partially filling the waveguide, the transmission line is as given in Figure 18. The parallel L-C sections represent the transverse and longitudinal dielectric properties of the plasma, and the shunt capacitors represent the dielectric region between the plasma surface and the conducting waveguide. Examination of the total series and shunt reactances reveals (see Figure 18) that below the plasma frequency, the series reactance is inductive, and that at some slightly lower frequency

*See Chapter III Plasmaguide Modes of One Angular Variation in Finite Axial Magnetic Field.

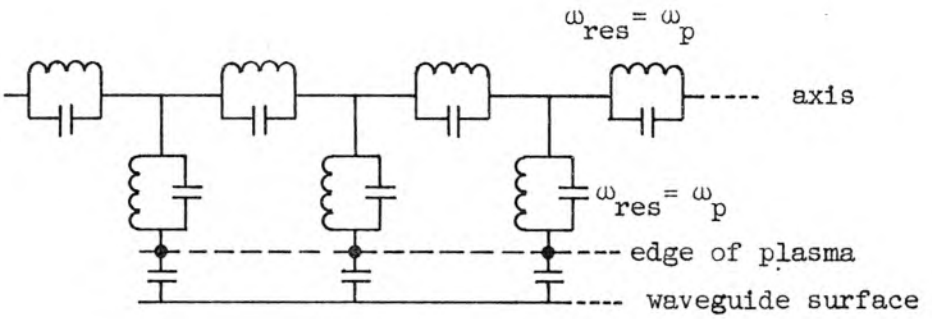


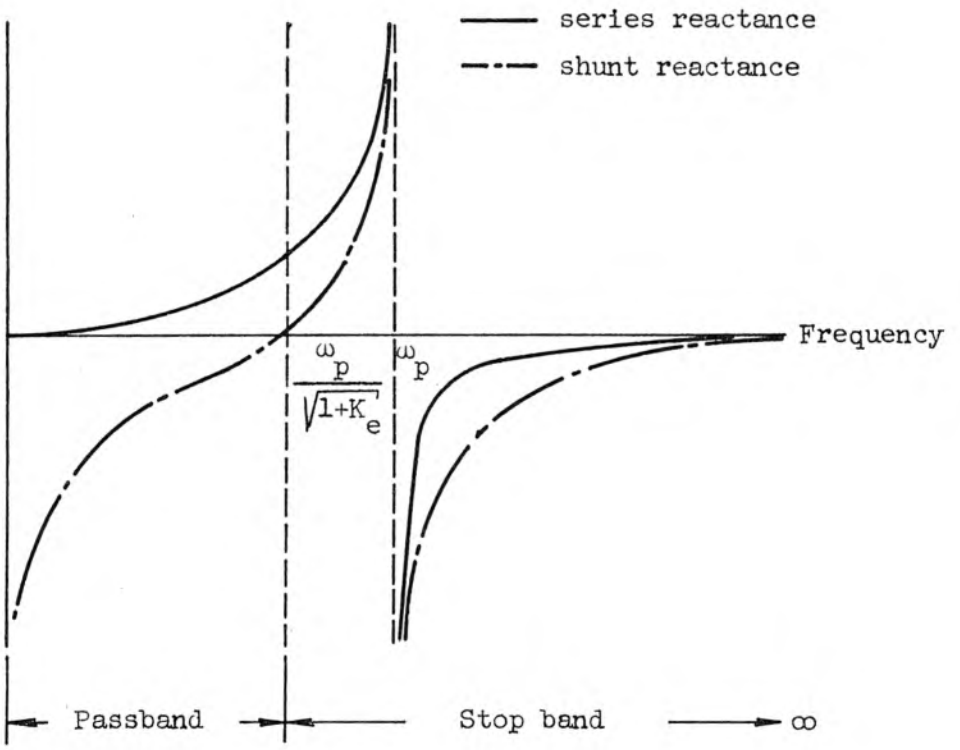


Figure 18. Equivalent electrical transmission line for Surface Waves on an Isotropic Plasma Column and Reactance Diagram Showing Passband.

the shunt reactance is capacitive. Below this latter frequency (shown in the previous section to be $\omega_p/\sqrt{1 + K_e}$, the transmission line has a passband down to zero frequency. That a dielectric region around the plasma is essential to the surface wave propagation can be seen by imagining the dotted line denoting the edge of the plasma in Figure 18 to be the conducting wall of the waveguide. For this case, the total series and shunt reactances can never be opposite in sign as required for a passband. That a plasma column in free space can also support a surface wave mode is understood by noting that removing the guide wall to infinity still presents a capacitance to the plasma column. Allowing the radius of the plasma column to extend to infinity, however, stops propagation since an infinite plasma column will have no dielectric region surrounding it and again the necessary condition of opposite signs for the total series and shunt reactances cannot be satisfied.

Backward Surface Waves on a Plasma Column. Consider now a plasma column of radius $a$ filling a dielectric cylinder (outer radius $b$ and relative dielectric constant $K_e$) in a conducting waveguide of radius $c$. The determinantal equation for the propagation of waves in this system is*

$$\left(1 - \frac{\omega_p^2}{\omega^2}\right) \frac{I_n'(\beta a)}{I_n\, \beta a} = \tag{IV.22}$$

$$K_e \frac{K_e\left[I_n'(\beta a)\, K_n'(\beta b) - I_n'(\beta b)\, K_n'(\beta a)\right] + \frac{Q(\beta b)}{\epsilon_o}\left[I_n(\beta b)\, K_n'(\beta b) - I_n'(\beta b) K_n(\beta b)\right]}{K_e\left[I_n(\beta a)\, K_n'(\beta b) - I_n'(\beta b)\, K_n(\beta a)\right] + \frac{Q(\beta b)}{\epsilon_o}\left[I_n(\beta b)\, K_n(\beta a) - I_n(\beta a) K_n(\beta b)\right]}$$

*The method used in obtaining this equation is outlined in Appendix II.

where

$$Q(\beta b;\beta c,\epsilon_o) = \epsilon_o \frac{I_n(\beta c)\, K_n'(\beta b) - I_n'(\beta b)\, K_n(\beta c)}{I_n(\beta c)\, K_n(\beta b) - I_n(\beta b)\, K_n(\beta c)} \quad .$$

Using the simple method described earlier in this chapter leads to the following expression for the low frequency phase velocity for the circularly symmetric mode:

$$v_{ph}(\omega = 0) = \left[\frac{\log \frac{b}{a} + K_e \log \frac{c}{b}}{2K_e}\right]^{1/2} \omega_p a \quad . \tag{IV.23}$$

The addition of an air space between the dielectric surrounding the plasma and the waveguide is seen to modify the low frequency phase velocity. This can be understood from the transmission line arguments by observing that at low frequencies the inductive reactance of the plasma is linear with frequency (constant inductance) and the phase velocity is determined by the effective inductance of the plasma and the shunt capacitance from the edge of the plasma to the waveguide. Changing this shunt capacitance by altering the dielectric configuration should then modify the low frequency phase velocity as shown in IV.23. Examination of the large $\beta a$ behavior reveals that

$$\omega = \omega_p / \sqrt{1 + K_e} \tag{IV.24}$$

when $\beta a$ goes to infinity. The physical reason for this is that, as with the case of the dielectric-lined plasma-filled waveguide discussed earlier in this chapter, the potential is a maximum at the plasma dielectric interface and fields extend only slightly into the two regions when $\beta a$ is large. Thus the asymptotic phase velocity should depend only on the properties of the plasma and the dielectric immediately surrounding it. For this case, however, the frequency given by IV.24 is not the maximum

frequency of transmission for the system. An $\omega$-$\beta$ diagram obtained from IV.22 is shown in Figure 19. Instead of monotonically approaching the large $\beta a$ limiting frequency, the $\omega$-$\beta$ curve rises to a maximum value above this limit and then approaches the large $\beta a$ solution. This behavior is best explained by considering two limiting cases. The first is that of a plasma column in free space and the second is a plasma column in an infinite medium of dielectric constant $K_e$. The $\omega$-$\beta$ diagrams for these two cases are shown in Figure 20. Imagine now the situation of a plasma column completely filling a thin dielectric cylinder which is in turn surrounded by free space. At low frequencies where $\beta a$ is small, the effect of the dielectric cylinder is slight because the waves extend well into the free-space region and the $\omega$-$\beta$ diagram will closely follow the upper curve in Figure 20. However, when $\beta$ is sufficiently large that $\beta t$ ($t$ is the thickness of the dielectric surrounding the plasma) is greater than unity, the fields will be confined largely to the dielectric shell and the phase velocity will be determined more by the dielectric and less by the free space surrounding it. In the limit of large $\beta a$ the solution will approach the lower curve of Figure 20. The maximum frequency of transmission will depend primarily on the relative thickness and dielectric constant of the dielectric surrounding the plasma column. An expression for the maximum frequency of transmission could be obtained by taking the derivative with respect to $\beta a$ in IV.22 and equating it to zero; however, such an expression lends nothing to the discussion and will, therefore, not be included.

A qualitative physical explanation can be given for the existence of this backward wave as follows. When $\beta t$ is the order of unity, the fields are confined primarily to the dielectric. The longitudinal displacement current in the dielectric leads the electric field by 90°

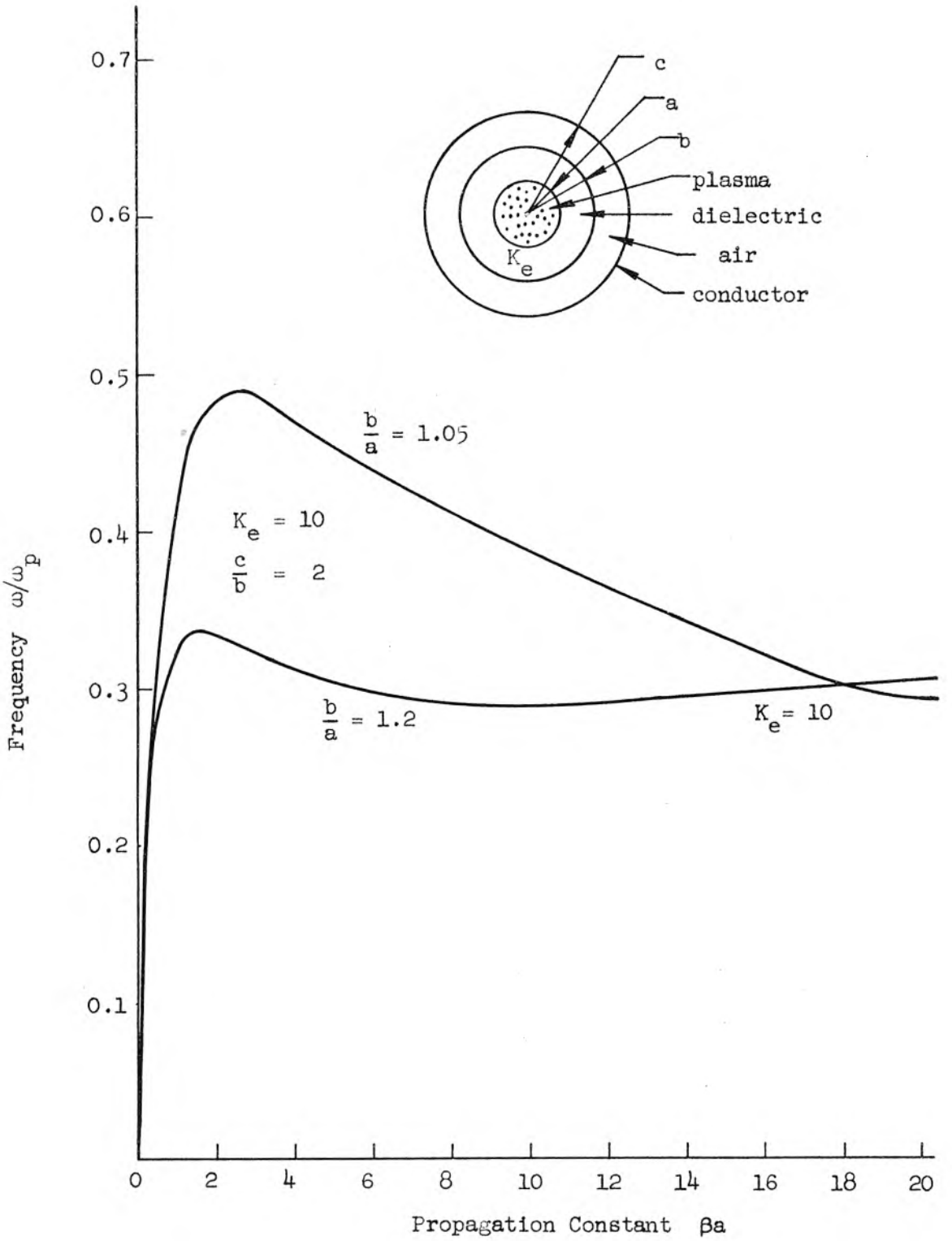


Figure 19. Phase Characteristics for Axially Symmetric Surface Wave on Plasma Column surrounded by Thin Dielectric Shell.

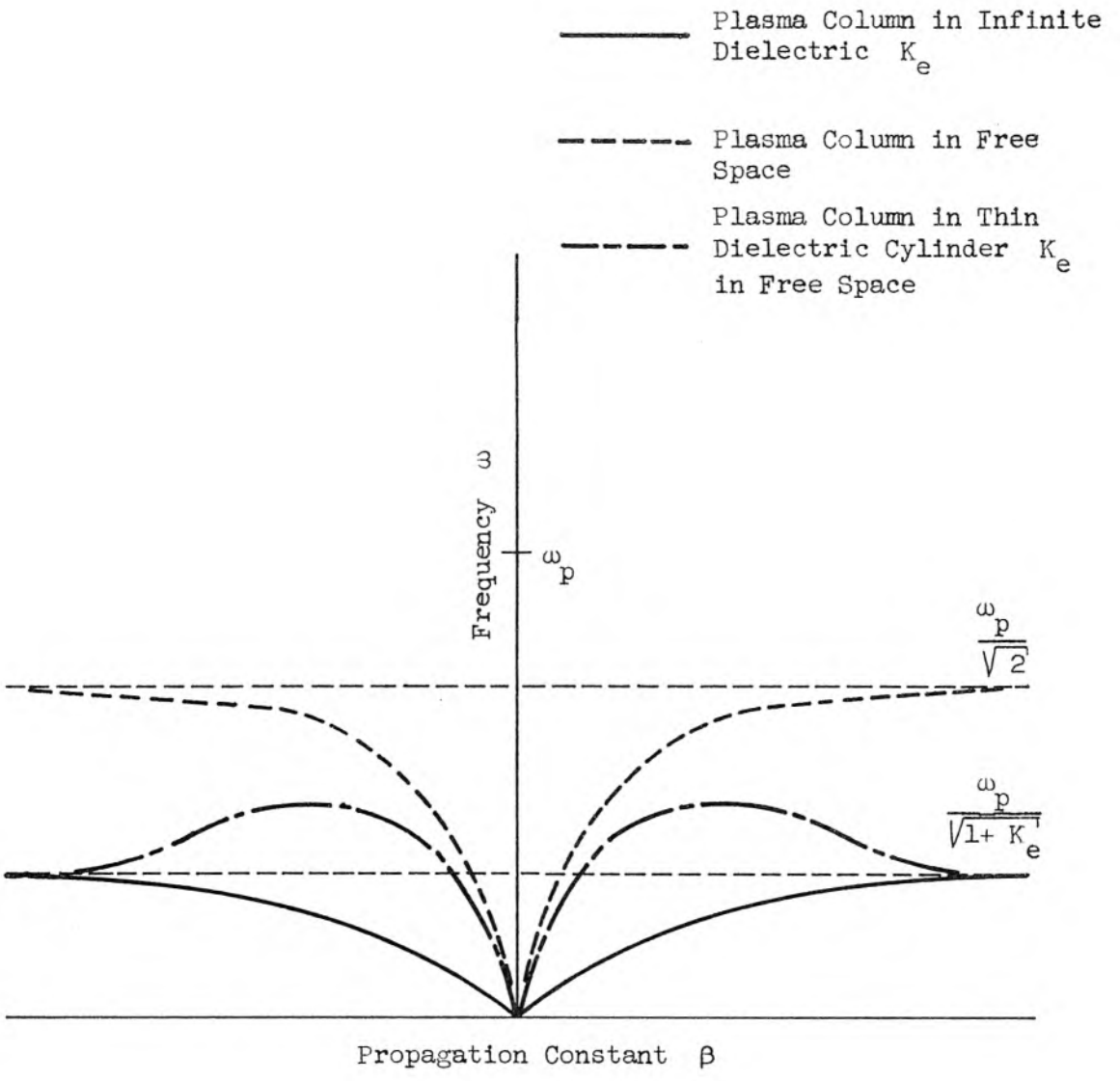


Figure 20. Phase characteristics for Axially Symmetric Mode on a Plasma Column Illustrating Reason for Backward Wave.

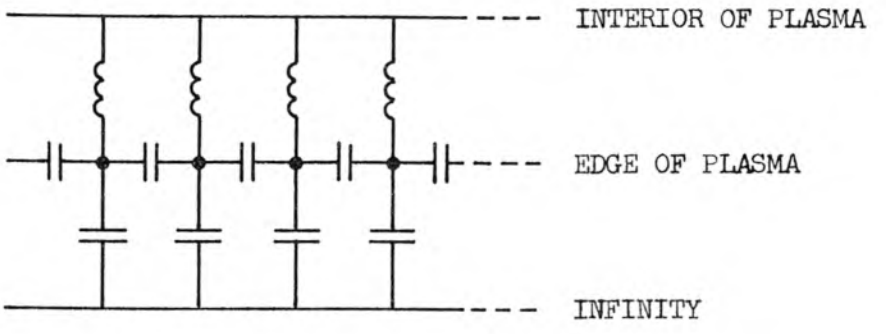


Figure 21. Approximate Equivalent Electrical Transmission Line for Backward Surface Waves on a Plasma Column.

(capacitive). Since the exciting frequency is less than the plasma frequency, the transverse displacement current into the plasma lags the electric field by $90^{\circ}$ (inductive). The transverse displacement current into the free-space region outside the dielectric will lead the electric field by $90^{\circ}$ (capacitive). Using the equivalent transmission line concept leads to the circuit shown in Figure 21. The backward wave region of such a circuit occurs when the transverse inductance predominates the transverse capacitance. Although the actual equivalent circuit is much more complex, the essential nature of the backward wave region is illustrated here and any attempt to include the other elements would only complicate the issue.

The backward wave described above can be enhanced by making the dielectric region thin and of a material of high relative dielectric

constant. Passing a directed electron beam along the axis of such a system at a velocity near the phase velocity of the backward wave region should result in interaction and growing waves. If the interaction region length and beam current are correctly chosen, the system should operate as a backward wave oscillator.*

The Effect of Radial Charge Density Variation on the Plasma Column Surface Waves. In the course of performing experiments to verify the various characteristics of the plasmaguide waves, it became evident that the variation in charge density with radius might play a significant role. Figure 22 shows a typical theoretical curve for a uniform plasma and some typical experimental points. The experimental points fall below the theoretical curve for values of $\beta a$ greater than unity and appear to be approaching different asymptotes. Since the large $\beta a$ behavior is determined by the properties of the plasma-dielectric interface region, the observed experimental asymptote could be attributed to a lower charge density at the edge of plasma column. To investigate such a possibility, the differential equation for the potential inside the plasma column was solved assuming a parabolic variation in charge density with radius. The solution obtained was then matched to the solution outside.

Consider a cylindrical isotropic plasma column of radius $a$ whose charge density is a function of radius only. Regarding the plasma as a spatially dependent dielectric requires the potential to be a solution of Laplace's equation for an inhomogeneous medium,

$$\nabla \cdot \epsilon(r) \nabla \phi_1 = 0 , \qquad \text{(IV.25)}$$

*The subject of interaction is treated in detail in Chapter V .

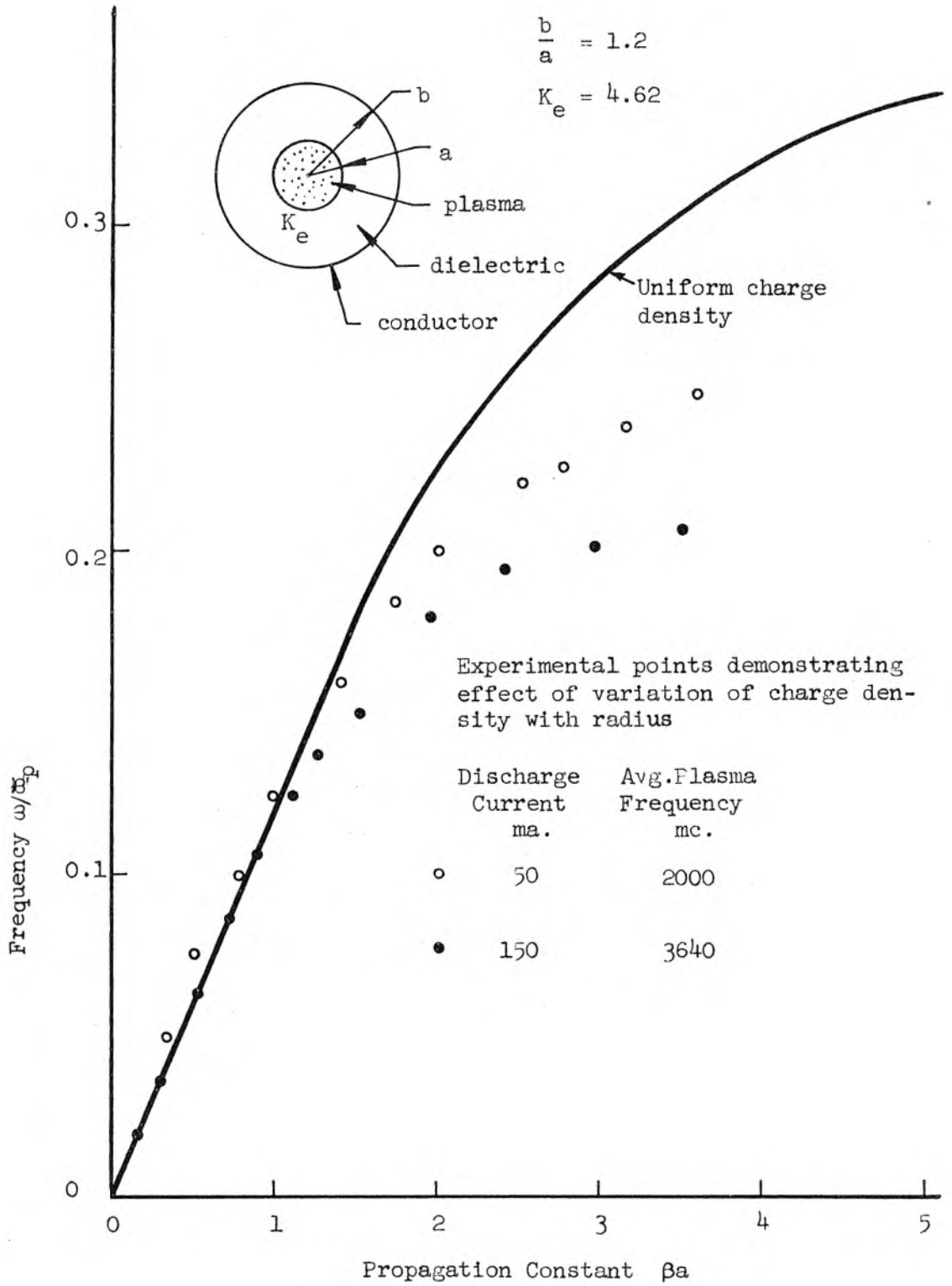


Figure 22. Theoretical Phase Characteristics for Surface Waves with Experimental Points.

if the quasi-static approximation is assumed. Assuming wave solutions of the form

$$\phi_1 = R(r)\, e^{-jn\theta}\, e^{-j\beta z} \tag{IV.26}$$

leads to the following differential equation for the radial function

$$\left\{\frac{d^2}{dr^2} + \left(\frac{1}{r} + \frac{1}{\epsilon}\frac{d\epsilon}{dr}\right)\frac{d}{dr} - \left(\beta^2 + \frac{n^2}{r^2}\right)\right\} R(r) = 0 . \tag{IV.27}$$

Let the radial charge density variation be given by

$$\rho(r) = \rho_a \left[1 - \alpha\left(\frac{r}{a}\right)^2\right] , \tag{IV.28}$$

where $\rho_a$ is the axis charge density and $\alpha$ is a parameter between zero and unity which determines the degree of radial charge variation. The permittivity for this parabolic charge density variation is

$$\epsilon(r) = \epsilon_o \left[1 - \frac{\omega_{pa}^2}{\omega^2}\left(1 - \alpha\frac{r^2}{a^2}\right)\right] , \tag{IV.29}$$

where $\omega_{pa}^2 = -\dfrac{\rho_a e}{\epsilon_o m}$ is the axis plasma frequency.

Defining a dimensionless independent variable $\xi = (\beta r)$ and a dimensionless frequency variable $f = \omega/\omega_{pa}$, the differential equation in the radial function becomes

$$\left\{\frac{d^2}{d\xi^2} + \left[\frac{1}{\xi} + \frac{2\xi}{\xi^2 - G}\right]\frac{d}{d\xi} - \left(1 - \frac{n^2}{\xi^2}\right)\right\} R(\xi) = 0 , \tag{IV.30}$$

where $G = (1 - f^2)(\beta a)^2/\alpha$. To solve this differential equation, multiply through by $\xi^2(\xi^2 - G)$ and assume a power series solution of the form* (only the $n = 0$ mode is considered)

*This differential equation has the origin as a regular point and the roots of the indicial equation are identical and zero.

$$R(\xi) = \sum_{i=0}^{\infty} C_i \xi^i \quad . \tag{IV.31}$$

The recursion relation obtained for the $C_i$'s is

$$C_{i+4} = \frac{1}{(i+4)^2}\left[\frac{(i+2)(i+4)\,C_{i+2} - C_i}{G} + C_{i+2}\right] \quad . \tag{IV.32}$$

Examination of power series which results from substituting IV.31 in the differential equation IV.30 reveals that the coefficient of the first power term $C_1$, must be zero for a solution. This in turn requires $C_3$ to be zero. By the recursion relation then all odd power terms in the series are zero. $C_0$ is arbitrary because it multiplies the indicial equation which is equal to zero. The second solution of the differential equation is singular at the origin and is therefore not of interest and will be excluded. The first few coefficients of the power series and the general term are

$$\begin{aligned}
C_2 &= \frac{C_o}{4} \\
C_4 &= \frac{C_o}{64} + \frac{C_o}{16G} \\
C_6 &= \frac{C_o}{2^6(3!)^2} + \left[\frac{1}{2^6\,G} + \frac{1}{24\,G^2}\right] C_o \\
C_8 &= \frac{C_o}{2^8(4!)^2} + \left[\frac{2}{2^6 \cdot 3G} + \frac{63}{2^{10}\,G^2} + \frac{1}{32\,G^3}\right] \\
C_{2i} &= \left[\frac{1}{2^{2\xi}(i!)^2} + \sum_{v=0}^{i-2} \frac{b_{vi}}{G^{v+1}}\right] C_o \quad .
\end{aligned} \tag{IV.33}$$

Setting $C_0 = 1$ and comparing the power series solution just obtained with power series for the modified Bessel's function of the first kind

reveals that the solution can be expressed as the Bessel's function plus a correction term

$$R_o(\xi) = I_o(\xi) + \sum_{i=0}^{\infty} \left[ \sum_{v=0}^{i} \frac{b_{v,2i}}{G^{v+1}} \right] \xi^{2(i+2)} \qquad \text{(IV.34)}$$

where the $b_{vi}$'s are determined from the recursion relation.

To examine how the radial charge variation affects the propagation of waves, it is necessary to consider a specific geometry. For the case of the plasma column filling a dielectric-lined waveguide of radius $b$, the solutions are

$$\left.\begin{aligned} \phi_{1i} &= A \frac{R_o(\xi)}{R_o(\beta a)} && r < a \qquad \text{(IV.35)} \\ \phi_{1o} &= A \frac{I_o(\xi)\, K_o(\beta b) - K_o(\xi)\, I_o(\beta b)}{I_o(\beta a)\, K_o(\beta b) - K_o(\beta a)\, I_o(\beta b)} && a < r < b \qquad \text{(IV.36)} \end{aligned}\right\} e^{j(\omega t - \beta z)}$$

where subscripts $o$ and $i$ denote the dielectric and plasma regions respectively and the boundary condition on the tangential electric field has already been satisfied. Requiring the normal displacement to be continuous leads to the following propagation equation:

$$\left[1 - \frac{1}{f^2}(1-\alpha)\right] \frac{I_1(\beta a) + \sum_{i=0}^{\infty} \left( \sum_{v=0}^{i} \frac{b_{v,2i+4}}{(1-f^2)^{v+1}} \right) (2i+4)(\beta a)^{2i+3}}{I_o(\beta a) + \sum_{i=0}^{\infty} \left( \sum_{v=0}^{i} \frac{b_{v,2i+4}}{(1-f^2)^{v+1}} \frac{\alpha^{v+1}}{(\beta a)^{2v+2}} \right) \beta a^{2i+4}} =$$

$$K_e \frac{I_1(\beta a)\, K_o(\beta b) + I_o(\beta b)\, K_1(\beta a)}{I_o(\beta a)\, K_o(\beta b) - I_o(\beta b)\, K_o(\beta a)} \qquad \text{(IV.37)}$$

An $\omega$-$\beta$ curve obtained from IV.37 showing the effect of charge density variation with radius is given in Figure 23. As can be seen, the $\omega$-$\beta$ curves break away from the uniform charge density $\omega$-$\beta$ curve for $\beta a$ greater than unity. The reason for this is that for $\beta a > 1$, the phase velocity of the waves depends more on the edge charge density than on the average charge density.

It is now of interest to examine the solutions for two limiting cases, $\beta a = 0$ and $\beta a = \infty$. From IV.28 and the definition of plasma frequency,

$$\omega_{pe} = \sqrt{1 - \alpha}\ \omega_p a \quad , \tag{IV.38}$$

where $\omega_{pe}$ is the edge plasma frequency. Since the phase velocity of the waves at large $\beta a$ depends only on the plasma-dielectric interface properties,

$$\omega(\beta a = \infty) = \frac{\sqrt{1 - \alpha}}{\sqrt{1 + K_e}}\ \omega_{pa} \quad . \tag{IV.39}$$

To obtain the low frequency phase velocity, it is necessary to examine the radial functions inside the plasma for small $\beta a$. Keeping first order terms in $\beta a$ for the correction term to the modified Bessel's function (see IV.31) gives

$$\lim_{\beta a \to 0} F(\beta a) = \frac{(\beta a)^2}{8} \sum_{i=0}^{\infty} \frac{1}{(i+2)} \left(\frac{\alpha}{1 - f^2}\right)^{i+1} \quad , \tag{IV.40}$$

where $F$ denotes the correction term,

$$R_o(\xi) = I_o(\xi) + F(\xi; G) \quad . \tag{IV.41}$$

Letting $r = \alpha/1 - f^2$, the series in IV.40 can be written

$$S = \sum_{n=0}^{\infty} \frac{r^{n+1}}{n+2} = \frac{r}{2} + \frac{r^2}{3} + \frac{r^3}{4} + \cdots \quad . \tag{IV.42}$$

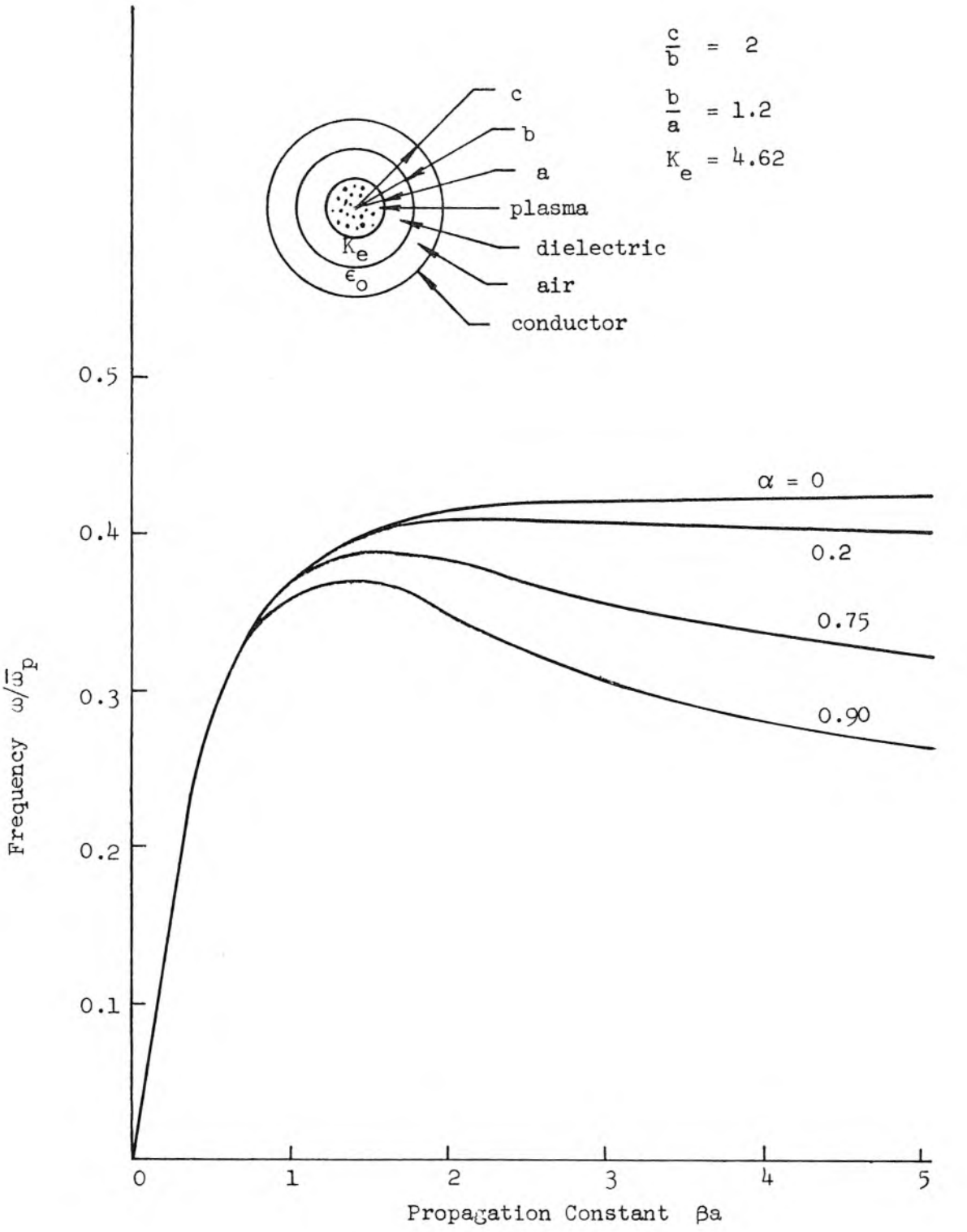


Figure 23. Phase Characteristics of Surface Waves Showing the Effect of Variation of Charge Density with Radius.

The sum of this series is

$$S = \frac{1}{r} \log \frac{1}{1 - r} - 1 \quad . \tag{IV.43}$$

This series is convergent for all $r^2 < 1$ . The condition for convergence will be satisfied at $f = 0$ by requiring $\alpha$ to be less than unity. Thus the solutions obtained will be good at $f = 0$ for all cases except that of zero edge charge density. Since $F$ is of order $(\beta a)^2$ and $I_o$ is of order $(\beta a)^0$, the radial function approaches unity in the limit of small $\beta a$ when the series $S$, is convergent. Keeping the first order terms in $\beta a$ for the derivative of the correction term gives

$$\mathrm{Lm} \left. \frac{dF(\beta r)}{dr} \right|_{r = a} = \beta \left(\frac{\beta a}{4}\right) \sum_{i = 0}^{\infty} \left(\frac{\alpha}{1 - f^2}\right)^{i+1} = \beta \frac{\beta a}{4} \frac{\left(\frac{\alpha}{1 - f^2}\right)}{\left(1 - \frac{\alpha}{1 - f^2}\right)} \quad , \tag{IV.44}$$

which, as before, is valid for all $(\alpha/1\text{-}f^2)^2 < 1$ and the arguments about range of validity of the $f = 0$ solution also apply here.

Using the small $\beta a$ approximations for the modified Bessel's functions and the results for the small $\beta a$ behavior of the radial functions within the plasma obtained above gives for the zero frequency phase velocity,

$$v_{ph}(\omega = 0) = \left[\frac{\log \frac{b}{a}}{2K_e}\right]^{1/2} \sqrt{1 - \frac{\alpha}{2}} \; \omega_p a \quad . \tag{IV.45}$$

Since the average value of the parabolic distribution is

$$\bar{\rho} = \frac{1}{\pi a^2} \int_0^a \int_0^{2\pi} \rho(r) \; r \, dr \, d\theta = \rho_a \left(1 - \frac{\alpha}{2}\right) \quad , \tag{IV.46}$$

the expression for the phase velocity becomes

$$v_{ph}(\omega = 0) = \left[\frac{\log \frac{b}{a}}{2K_e}\right]^{\frac{1}{2}} \bar{\omega}_p a \quad , \tag{IV.47}$$

where $\bar{\omega}_p^2 = -\frac{\bar{\rho}\, e}{\epsilon_o m}$ is the average plasma frequency. The low frequency phase velocity is thus seen to be constant; i.e., the system is nondispersive and depends only on the average charge density while the large $\beta a$ behavior is determined primarily by the edge plasma frequency.

A potentially useful plasma diagnostic tool is indicated here in that two measurements should in principle determine the axis charge density and the best parabolic fit to the actual charge density. These two measurements are the low frequency phase velocity and the frequency for which $\beta a = \infty$ . The former of these two gives directly the average plasma frequency for the column as a whole. Unfortunately, however, an experimental measurement of the frequency for which $\beta a$ is infinite is difficult. The reason for the difficulty is that at large $\beta a$ the group velocity of the waves is high, the losses* are large and the large $\beta a$ frequency is not always the maximum frequency** of transmission. An alternate method of measuring the variation in radial charge density which avoids the above difficulties is to obtain a family of $\omega$-$\beta$ diagrams in the parameter $\alpha$ and then compare the experimental results with theoretical curves and select the value of $\alpha$ which gives best agreement.***

Power Flow Associated with Surface Waves on a Plasma Column. In Chapter V, where the subject of interaction of moving electron beams and the plasmaguide modes of propagation is treated, it will be necessary to

*Losses are treated in Chapter V.

**The arguments concerning backward waves and the maximum frequency of transmission for the three-region problem given in the previous section apply here.

***This work is being extended and will appear in a separate paper (25).

have expressions for the power flow associated with the various plasma-guide modes. The expressions for the power flow in plasma-filled waveguides given in the previous two chapters are not satisfactory since there is no power flow at zero magnetic field for the cases examined (i.e., when $b = a$).

Consider a homogeneous isotropic plasma column of radius $a$ in free space. For the circularly symmetric mode, the potential and electric field components are

$$\left.\begin{aligned} \phi_{1i}(r,z,t) &= A \frac{I_o(\beta r)}{I_o(\beta a)} \\ E_{1zi}(r,z,t) &= j\,\beta A \frac{I_o(\beta r)}{I_o(\beta a)} \\ E_{1ri}(r,z,t) &= A \frac{I_o(\beta r)}{I_o(\beta a)} \end{aligned}\right\} \quad e^{j(\omega t - \beta z)} \qquad r < a \qquad \text{(IV.48)}$$

$$\left.\begin{aligned} \phi_{1o}(r,z,t) &= A \frac{K_o(\beta r)}{K_o(\beta a)} \\ E_{1zo}(r,z,t) &= j\beta A \frac{K_o(\beta r)}{K_o(\beta a)} \\ E_{1ro}(r,z,t) &= +\beta A \frac{K_1(\beta r)}{K_o(\beta a)} \end{aligned}\right\} \quad e^{j(\omega t - \beta r)} \qquad a < r < \infty \qquad \text{(IV.49)}$$

where $\beta$ is a solution of IV.21 with $n$ set equal to zero. The a.c. magnetic fields were set equal to zero in the determination of the propagation characteristics using the quasi-static approximation. A first order estimate of their value which is consistent with this approximation is obtained with the aid of one of the Maxwell equations, II.2 . The result is

$$H_{1\theta i}(r,z,t) = \frac{\omega}{\beta} \epsilon_o \left(1 - \frac{\omega_p^2}{\omega^2}\right) E_{1ri}(r,z,t) \qquad r < a \qquad \text{(IV.50)}$$

$$H_{1\theta o}(r,z,t) = \frac{\omega}{\beta} \epsilon_o E_{1ro}(r,z,t) \qquad a < r < \infty \qquad \text{(IV.51)}$$

The time average power flow is from II.33

$$\overline{P}_z = A^2 \pi \epsilon_o \frac{\omega}{\beta} \left[ \left(1 - \frac{\omega_p^2}{\omega^2}\right) \int_0^{\beta a} \left[\frac{I_1(\beta r)}{I_0(\beta a)}\right]^2 (\beta r)\, d(\beta r) + \int_{\beta a}^{\infty} \left[\frac{K_1(\beta r)}{K_0(\beta a)}\right]^2 (\beta r) d(\beta r) \right] \qquad \text{(IV.52)}$$

$$= A^2 \frac{(\beta a)^2}{2} \pi \epsilon_o \frac{\omega}{\beta} \left[ \left(1 - \frac{\omega_p^2}{\omega^2}\right) \left[ \frac{I_1^2(\beta a) - I_o(\beta a)\, I_2(\beta a)}{I_o^2(\beta a)} \right] - \left[ \frac{K_1^2(\beta a) - K_o(\beta a) K_2(\beta a)}{K_o^2(\beta a)} \right] \right]$$

The power flow is seen to be zero at both zero frequency and at the upper cutoff frequency and presumably has a maximum value between these limits. The power flow calculated above using the approximate a.c. magnetic field is in agreement with a calculation of power flow made by multiplying the time average stored energy per unit length by the group velocity of the waves.*

Review of the Features of Plasmaguide Propagation for Zero D.C. Magnetic Field. In the absence of an axial magnetic field or drifting motion, a homogeneous isotropic, plasma column only partially filling a waveguide can support a slow surface wave, electromechanical mode of propagation. The fields associated with this mode are strongest at the surface of the plasma and decay exponentially with radius from the plasma surface. The surface is perturbed when the plasma column is driven at some frequency within the passband, and the time dependent shape of the

---

* See Chapter V, Power Conservation for Plasmaguide Waves.

plasma column is peristaltic. All of the surface waves for two-region geometry have an upper frequency cutoff which depends only on the dielectric properties just outside the plasma column and the charge density just within the plasma column. The circularly symmetric mode is non-dispersive at low frequencies; the phase velocity depends on the average charge density of the plasma column and the capacitance presented to the column by its surroundings. Backward waves can exist for the circularly symmetric mode when the plasma column in free space is surrounded by a thin dielectric shell. The linearly polarized mode of one angular variation also exhibits a backward wave property and has a non-zero lower frequency limit. It is also dispersive over the entire passband. The plane of polarization is not rotated as the wave travels down the guide because of degeneracy of the right- and left-hand circularly polarized components.

Perhaps the most useful feature associated with the surface wave propagation is that of plasma diagnostics. Comparison of theory and experiment provides a means of determining such properties as the average plasma frequency and the charge density distribution.

## V. INTERACTION OF AN ELECTRON BEAM WITH THE PLASMAGUIDE MODES

The electromechanical modes of propagation in plasma columns discussed in the preceding chapters usually can have phase velocities much less than the velocity of light. For instance, the phase velocity of the waves in a plasma-filled waveguide is $v_{ph} = \omega_p a / p_{n\nu}$ and can be made quite small if the waveguide radius or plasma frequency is made small, i.e., $\omega_p a / p_{n\nu} \ll c$ . Since almost any circuit capable of supporting a slow wave can be used to interact with the space charge waves of a moving electron beam, it seems reasonable to expect that the plasmaguide modes could be used as such a circuit. Of particular interest is the possibility of allowing an electron beam to interact with any of the backward wave plasmaguide modes described earlier (chapters III and IV) making a "structureless" backward wave oscillator. Such a backward wave oscillator might be useful in generating very high microwave frequencies. The problem of achieving millimeter waves would be shifted from fabrication of very small and delicate slow wave circuits to that of obtaining high electron densities or large magnetic fields. Knowledge of the electron beam characteristics (velocity, etc.) and the resulting frequency of oscillation gives a good measure of the plasma frequency, thus providing a plasma diagnostic tool.

The rate of growth for the interaction of an electron beam with the plasmaguide modes is obtained by two methods. The first is a field analysis which is exact to within the approximation of the quasi-static analysis used in this paper. The second method uses the notion of an interaction impedance (15) and calculates the traveling wave tube interaction parameter $C$ for several cases including the backward wave. The difficulty of solving the resultant transcendental obtained in the field

analysis necessarily restricts the solution to a simple case which will be used to check the validity of the approximate method for the same case.

Field Analysis of Electron-Beam Plasmaguide-Interaction. Consider a smooth, perfectly conducting cylindrical waveguide of radius b containing an electron beam of radius a and completely filled with a stationary ideal plasma, and let there be a finite axial magnetic field $B_o$. The tensor dielectric constant within the moving beam ($r < a$) is easily obtained from the tensor dielectric constant given in Chapter III, equation II.9, by adding the susceptance of an additional charge column which has been modified by a coordinate transformation.* Using the same notation for the components of the tensor dielectric as in III.4, the components for the beam-plasma region are

$$\epsilon_{rr} = \epsilon_{\theta\theta} = 1 + \frac{\omega_p^2}{\omega_c^2 - \omega^2} + \frac{\omega_{pb}^2}{\left[\omega_c^2 - (\omega - \beta u_o)^2\right]} \tag{V.1}$$

$$\epsilon_{r\theta} = \epsilon_{\theta r} = \frac{\omega_c}{\omega} \frac{\omega_p^2}{(\omega_c^2 - \omega^2)} + \frac{\omega_c}{(\omega - \beta u_o)} \frac{\omega_{pb}^2}{\left[\omega_c - (\omega - \beta u_o)^2\right]} \tag{V.2}$$

$$\epsilon_{zz} = 1 - \frac{\omega_p^2}{\omega^2} - \frac{\omega_{pb}^2}{\left[\omega_c - (\omega - \beta u_o)^2\right]} \tag{V.3}$$

where

$\omega_p^2 = -\frac{\rho_o e}{\epsilon_o m}$ "plasma" plasma frequency

$\omega_{pb}^2 = -\frac{\rho_{ob}}{\epsilon_o}\frac{e}{m}$ beam plasma frequency

$\omega_c = \frac{e}{m} B_o$ cyclotron frequency

$u_o = \left[\frac{2e}{m} V_o\right]^{\frac{1}{2}}$ d.c. beam velocity

*See Chapter VI.

The dielectric constant without the beam is obtained by setting $\omega_{pb}$ equal to zero, thus giving III.9.

To study the propagation and possible growth of waves in this system, the quasi-static approximation will again be used. The differential equation which must be satisfied by the radial function is obtained directly from Chapter III, equation III.20,

$$\frac{1}{r}\frac{d}{dr}\left(r\frac{dR}{dr}\right) - \frac{n^2}{r^2}R + T_{1,2}^2 R = 0 , \tag{V.4}$$

where inside the beam

$$T_1^2 = -\beta^2 \frac{\epsilon_{zz1}}{\epsilon_{rr1}} = -\beta^2 \frac{\left[1 - \frac{\omega_p^2}{\omega^2} - \frac{\omega_{pb}^2}{(\omega - \beta u_o)^2}\right]}{\left[1 + \frac{\omega_p^2}{\omega_c^2 - \omega^2} + \frac{\omega_{pb}^2}{(\omega - \beta u_o)^2}\right]} \tag{V.5}$$

and outside the beam

$$T_2^2 = -\beta^2 \frac{\epsilon_{zz2}}{\epsilon_{rr2}} = -\beta^2 \left[\frac{1 - \frac{\omega_p^2}{\omega^2}}{1 + \frac{\omega_p^2}{\omega_c^2 - \omega^2}}\right] . \tag{V.6}$$

Suitable solutions in the two regions are

$$R_1(r) = A\, J_n(T_1 r) \quad \text{inside the beam} \quad (a < r) \tag{V.7}$$

$$R_2(r) = G\left[J_n(T_2 r)\, N_n(T_2 b) - J_n(T_2 b)\, N_n(T_2 r)\right]$$

$$\text{outside the beam} \quad (a < r < b) . \tag{V.8}$$

Matching the ratio of normal displacement to tangential electric field at the beam-plasma interface $(r = a)$ leads to the following determinantal

equation

$$\epsilon_{rr1}(T_1a)\ \frac{J_n'(T_1a)}{J_n(T_1a)} + n\,\epsilon_{r\theta 1} =$$

$$\epsilon_{rr2}(T_2a)\left[\frac{J_n'(T_2a)\,N_n(T_2b) - J_n(T_2b)\,N_n'(T_2a)}{J_n(T_2a)\,N_n(T_2b) - J_n(T_2b)\,N_n(T_2a)}\right] + n\,\epsilon_{r\theta 2} \quad . \qquad (V.9)$$

This equation, V.9, and the equations defining the radial separation constants, V.5 and V.6, must be solved for complex values of $Ta$ in order to examine growing wave solutions. A systematic examination of the solutions of such an equation would be a formidable task and is not undertaken here. The equation was derived only for completeness and to serve as a convenient point of departure for the work to follow.

By allowing the beam to also fill the waveguide $a = b$, the complexity of the problem is reduced considerably. Considering the axially symmetric mode $(n = 0)$ for this restricted case reduces V.9 to

$$J_o(T_1b) = 0\ , \qquad T_1b = p_{o\nu}\ , \qquad (V.10)$$

where the $p_{o\nu}$'s are the $\nu$ roots of the Bessel function. Using the definition of $T_1b$ ,

$$p_{o\nu}^2 = -\beta b\ \frac{\left[1 - \frac{\omega_p^2}{\omega^2} - \frac{(\beta_{pb}b)^2}{(\beta_e b - \beta b)^2}\right]}{\left[1 + \frac{\omega_p^2}{\omega_c^2 - \omega^2} + \frac{(\beta_{pb}b)^2}{(\beta_c b)^2 - (\beta_e b - \beta b)^2}\right]}\ , \qquad (V.11)$$

where

$\beta_e b = \omega_b / u_o$ is the electronic or beam wave number

$\beta_c b = \omega_c b / u_o$ is the cyclotron wave number

$\beta_{pb}b = \omega_{pb}b/u_o$ is the beam plasma wave number.

A limited number of solutions of V.11 have been obtained for typical values of the parameters. The rate of growth $\alpha b$, obtained from these solutions is plotted as a function of the electronic phase constant $\omega b/u_o$ in Figure 24 for the first two circularly symmetric modes ($\nu = 1,2$). The perveance ($P = |I_o/V_o^{3/2}|$, where $I_o$ is the d.c. beam current) and the ratio of operating to plasma frequency is held constant. The fact that $\beta_e b$ less than a certain value for a given axially symmetric mode does not result in gain is explained by considering the sketched $\omega$-$\beta$ diagrams for the first two modes (Figure 25), and recognizing that the phase velocity of the waves in the plasma must be nearly in synchronism with the electron beam velocity for interaction to take place. Shown on this diagram is a curve representing the electron beam velocity $u_o$. As can be seen, increasing $u_o$ above the value which corresponds to the phase velocity of the waves ($u_o > \omega_{pb}/p_{o\nu}$ for the plasma-filled waveguide in an infinite axial magnetic field) at low frequencies results in no intersections of the $\omega$-$\beta$ curve and the electron beam velocity as required for interaction. This corresponds to the minimum value of $\beta_e b$ of Figure 24. On the other hand, decreasing the beam velocity will result in interaction with higher order modes since there will be intersections of the d.c. beam velocity curve and the $\omega$-$\beta$ curve for these higher modes. Increasing the plasma frequency will also result in interaction with higher order modes for a fixed beam velocity. This is understood by observing that the points on the $\omega$-$\beta$ curves for the plasmaguide waves are scaled upward when the plasma frequency is increased, thus resulting in an intersection of the $\omega$-$\beta$ curve

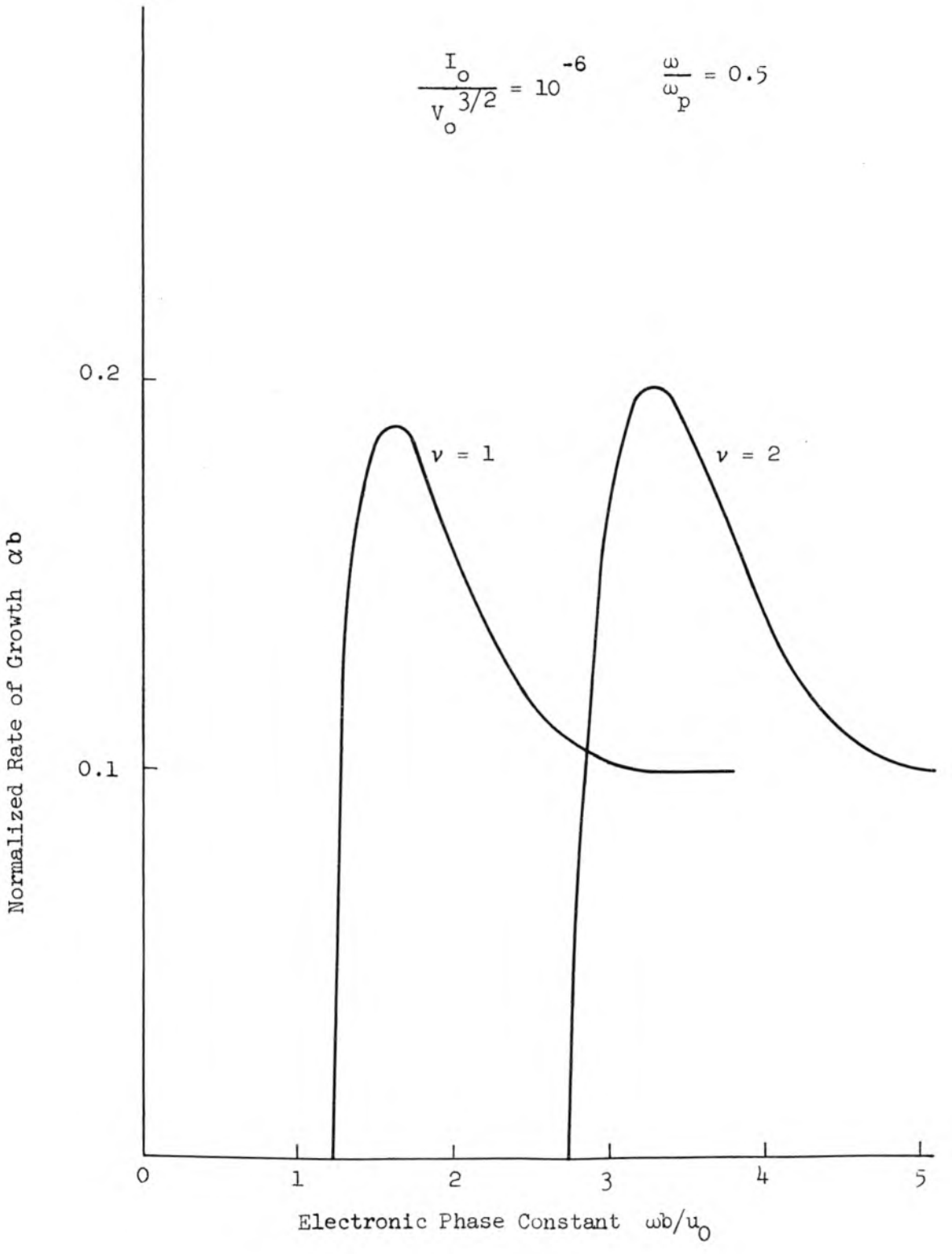


Figure 24. Rate of Growth for the First Two Axially Symmetric Modes for Interaction of an Electron Beam with a Stationary Plasma Column. Plasma and Beam Both Filling a Cylindrical Wave-Guide in an Infinite Axial Magnetic Field.

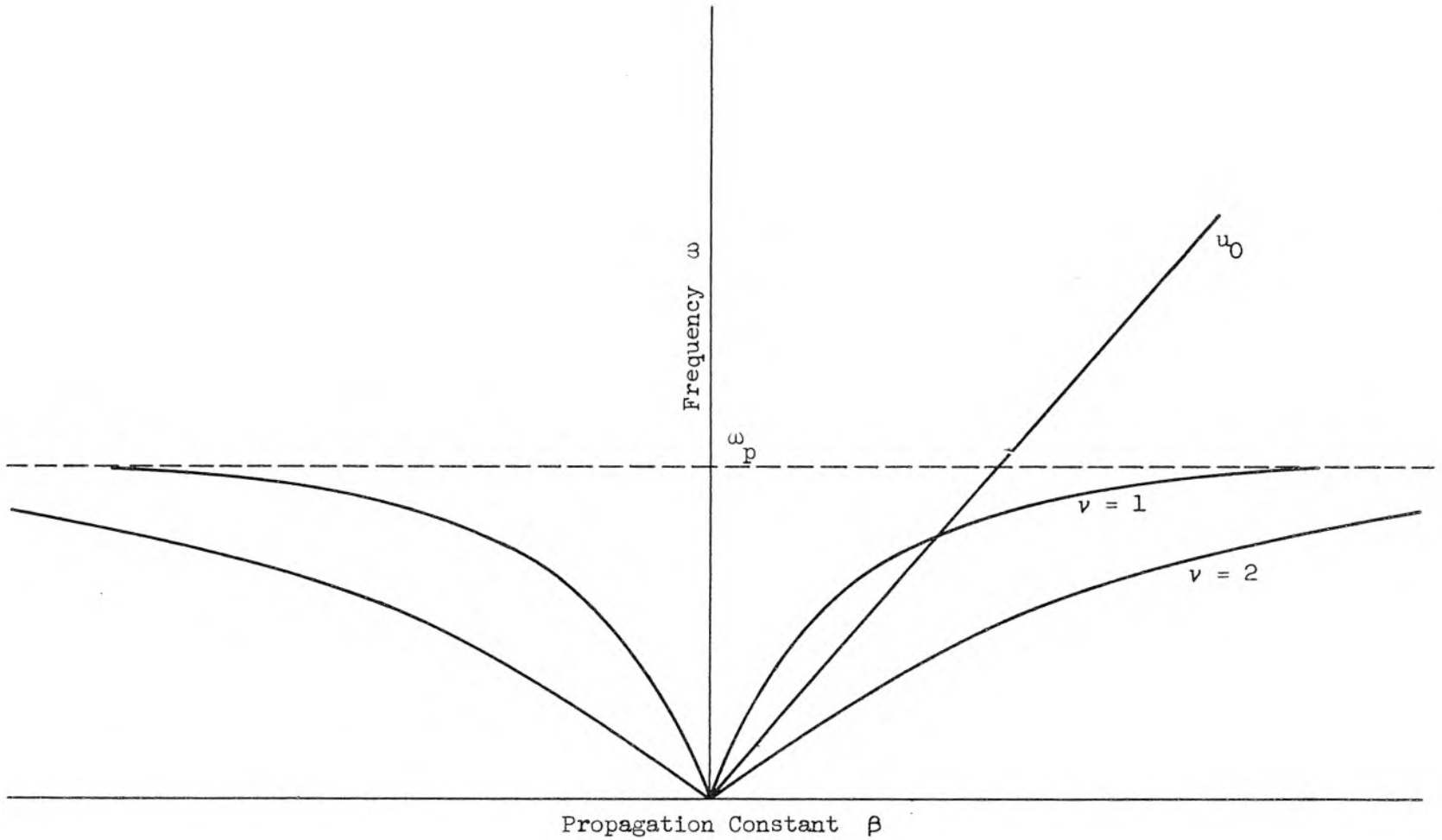


Figure 25. Sketch of Phase Characteristics for Plasma-Filled Waveguide in an Infinite Axial Magnetic Field.

and the d.c. beam velocity curve.

Approximate Analysis of Electron Beam - Plasmaguide Interaction.

Pierce (14) shows that the rate of growth for the waves on an electron beam in the presence of a slow wave circuit can be calculated approximately in terms of an interaction impedance which is a measure of the electric field available to act on the electrons for a given power flow on the circuit. Such an analysis can include the effects of the space charge of the electron beam. The effects of space charge will be neglected in this analysis and the electron beam will be assumed to be concentrated on the axis of symmetry. This simplified analysis is usually referred to as a "thin beam" theory.

Regarding the plasmaguides as slow wave circuits permits the calculation of an interaction impedance which can then be used to evaluate the traveling wave tube interaction parameter (14). The interaction impedance

$$K = \frac{E_{1z}^2(0)}{2\beta^2 \bar{P}_z} \quad , \tag{V.12}$$

enters in the traveling wave tube interaction parameter $C$ by

$$C^3 = \frac{KI_o}{4V_o} \quad . \tag{V.13}$$

$\bar{P}_z$ is the time average z-directed power flow associated with the plasmaguide waves. Using the expression for power flow in Chapter III, equation III.48, the interaction impedance on the axis for a plasma-filled waveguide in a finite magnetic field is given by

$$K = \frac{1}{\pi \epsilon_o a} \left[ \frac{(\omega_c^2 - \omega^2)}{(\omega_p^2 + \omega_c^2 - \omega^2)(\omega_p^2 - \omega^2)} \right]^{1/2} \frac{1}{p_{ov} J_1^2(p_{ov})} \quad . \qquad (V.14)$$

This expression is plotted in Figure 26 as a function of frequency. The impedance is seen to be zero when $\omega = \omega_c$ (except when $\omega_p = \omega_c$), and infinite when $\omega = \omega_p$ or $\omega = [\omega_p^2 + \omega_c^2]^{1/2}$ .

It is of interest to compare the rate of growth as predicted by the interaction impedance calculation with that predicted by the field analysis. Consider the following operating conditions:

| | | |
|---|---|---|
| Plasma frequency | = | 300 mc |
| Operating frequency | = | 150 mc |
| Beam voltage | = | 130 volts |
| Beam current | = | 1.0 ma. |
| Cyclotron frequency | = | $\infty$ |
| Radius of plasma | = | 1.0 cm. |
| Radius of waveguide | = | 1.0 cm. |

The interaction parameter C and the corresponding rate of growth in db/cm as calculated by the two methods are given below:

| | Field Analysis | Interaction Impedance Analysis |
|---|---|---|
| | C = 0.166 | C = 0.187 |
| Rate of Growth | 1.73 db/cm | 1.95 db/cm |

The two methods are thus seen to be in reasonable agreement. The discrepancy might be attributed to the fact that the interaction impedance analysis is based on the assumption that electron beam is concentrated on the axis where the electric field is a maximum $E_z(r) = E_z(0) J_o(\beta r)$. This gives a higher rate of growth than if the electron beam were spread uniformly over the entire cross section. An estimate of the

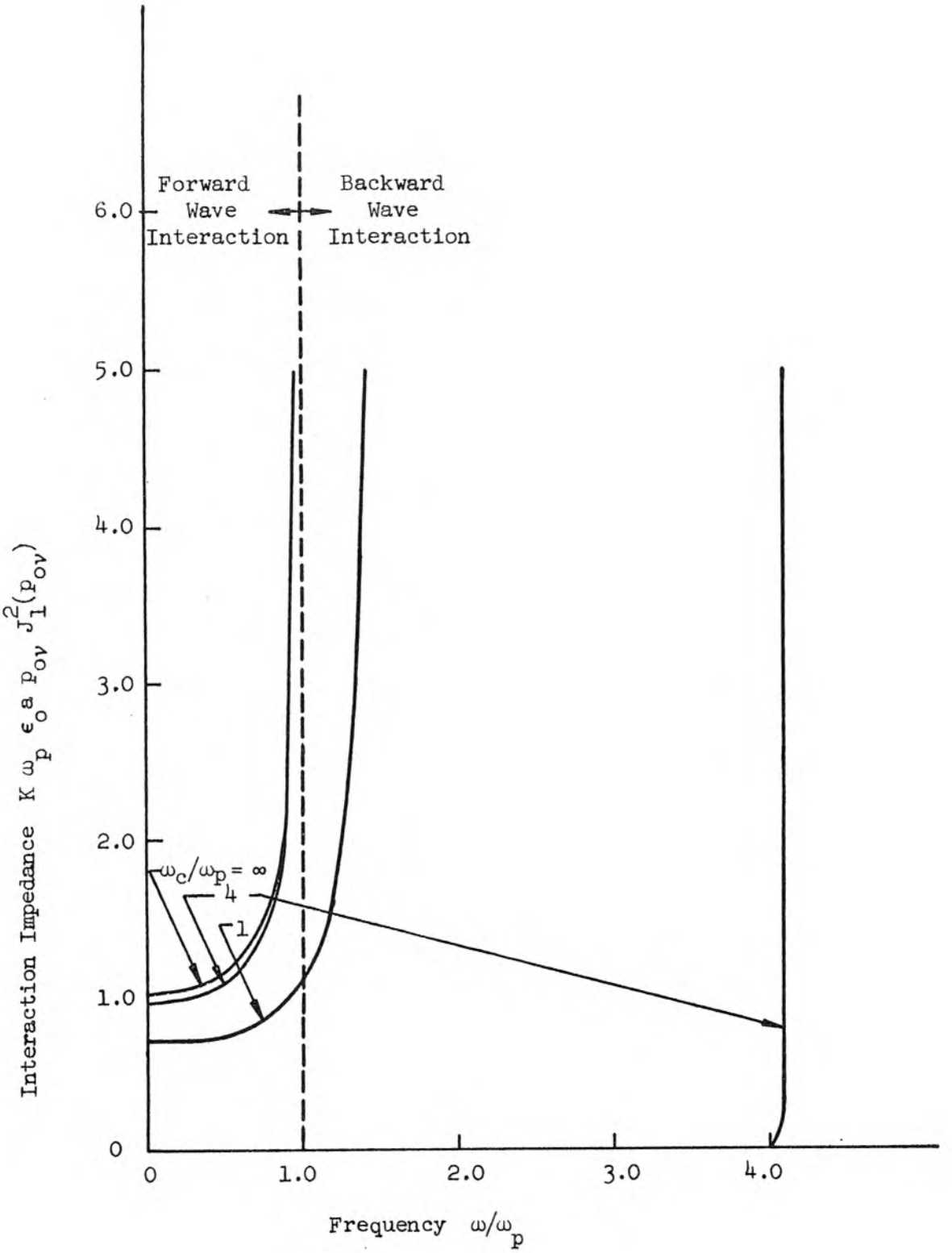


Figure 26. Interaction Impedance for Plasma-Filled Waveguide.

reduction in the rate of growth calculated by the interaction impedance method is obtained by using the mean square z-directed electric field to compute the interaction impedance rather than the square of the electric field on the axis. The value of $C$ obtained using this approximate reduction factor is $0.134$ .

Figure 27 shows the gain per unit length as a function of frequency for a plasma-filled waveguide of 1 cm diameter in an infinite axial magnetic field with a 0.5 ma. electron beam on the axis. The plasma frequency is 1000 megacycles, and the electron beam velocity has been taken to be the phase velocity of the slow waves in the plasma, i.e., the electron beam and slow wave are in synchronism. This rate of growth has been calculated using the interaction impedance method where the electron beam has been assumed to be concentrated on the axis.

Although backward wave interaction between an electron beam and a plasma has not been observed as yet in the laboratory, it is presumed that the possibility of realizing a backward wave oscillation exists for this interaction process much in the same way as for a helix or other backward wave circuit. The essential difference is that this backward wave interaction process is "structureless" and does not depend on a spatial harmonic of a periodic structure, such as a disk-loaded waveguide. Taking a simple point of view and using the start oscillation conditions for backward wave oscillation (26)

$$(CN)_{start} = 0.314 \quad , \tag{V.15}$$

where $N = L\, f/u_0$ is the length of the interaction region in electronic wavelengths ($L$ is the length in meters, $f$ is the driving frequency in

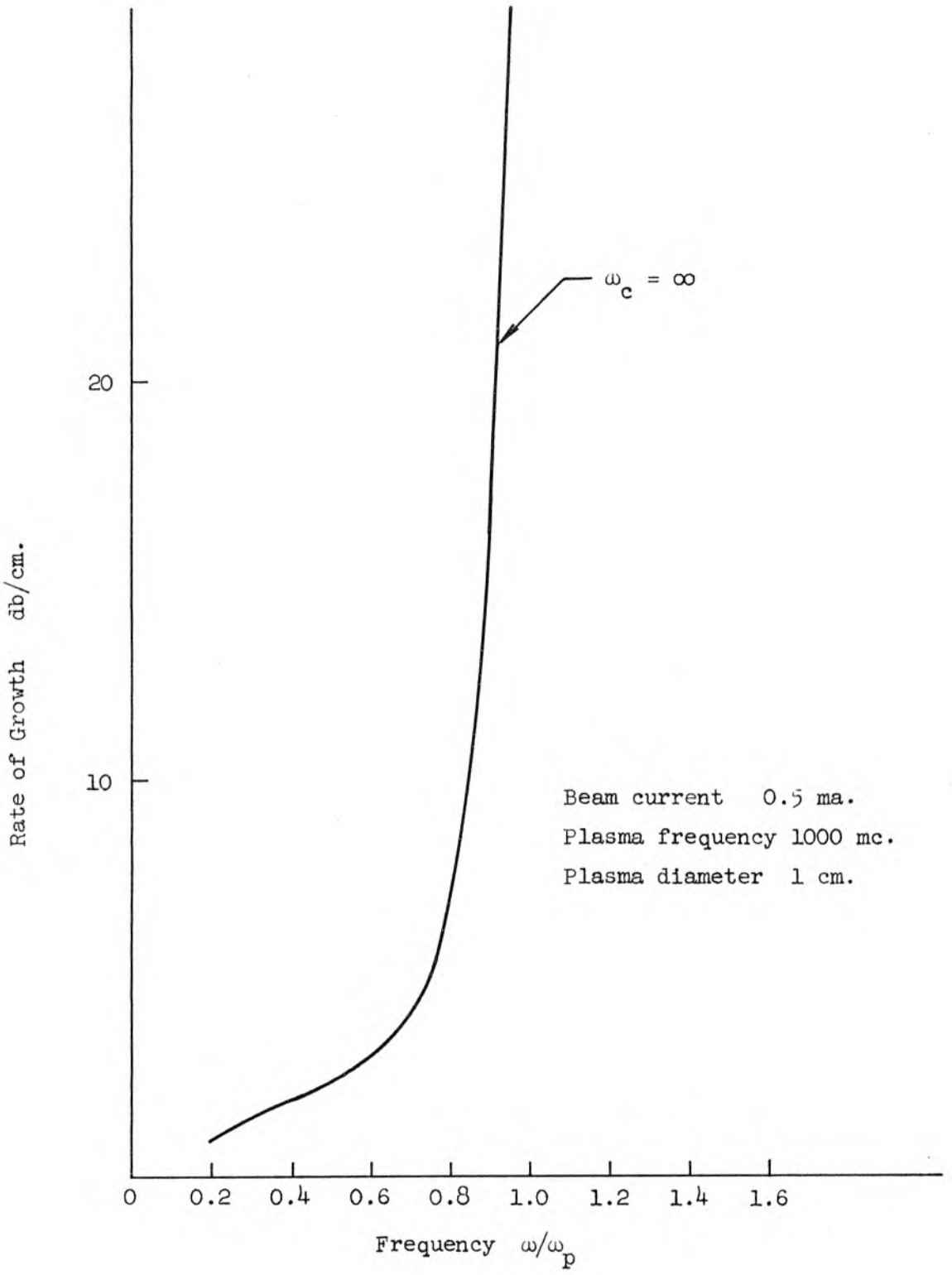


Figure 27. Rate of Growth for an Electron Beam in a Plasma-Filled Waveguide in an Infinite Axial Mangetic Field. Electron Beam Velocity is Synchronous with Phase Velocity of the Waves.

cycles per second, and $u_0$ is the electron beam velocity in meters per second) it will be possible to evaluate the start oscillation current for the electron beam. For a 10 cm. interaction region of plasma-filled waveguide (diameter 1 cm., $\omega_p = \omega_c = 2\pi \times 10^9$), the start oscillation current as a function of frequency is as shown in Figure 28. The other backward waves in plasmas described in this paper could also be used, in principle, to interact with a moving electron beam; however, their behavior is not essentially different and will therefore not be examined here.

The expression for the interaction impedance V.15 is not suitable to examine the interaction of an electron beam with the surface waves (see Chapter IV) since that expression is for a plasma-filled waveguide where there is no surface wave propagation. Although the case of a plasma only partially filling a waveguide in a finite magnetic field could be examined for surface wave electron beam interaction, it is simplier and no less instructive to consider a plasma column in free space. The interaction impedance V.12 is evaluated using the expression for power flow IV.52

$$K = \frac{1}{\omega_p \epsilon_o \pi a} \left\{ \left(\frac{\omega}{\omega_p}\right)(\beta a) \left(1 - \frac{\omega_p^2}{\omega^2}\right) \left[ \frac{I_1^2}{I_o^2} - \frac{I_2}{I_0} \right] - \left[ \frac{K_1^2}{K_0^2} - \frac{K_2}{K_0} \right] \right\}^{-1} \qquad \text{(V.16)}$$

where the modified Bessel functions are of argument $\beta a$ . The dimensionless interaction impedance from V.16 is plotted in Figure 29 as a function of $\omega/\omega_p$ . The gain in db/cm for the same operating conditions (beam current, 0.5 ma; plasma diameter, 1 cm; plasma frequency, 1000 mc; cyclotron frequency, zero; electron beam velocity and phase velocity appropriate to operating frequency), used in the infinite magnetic

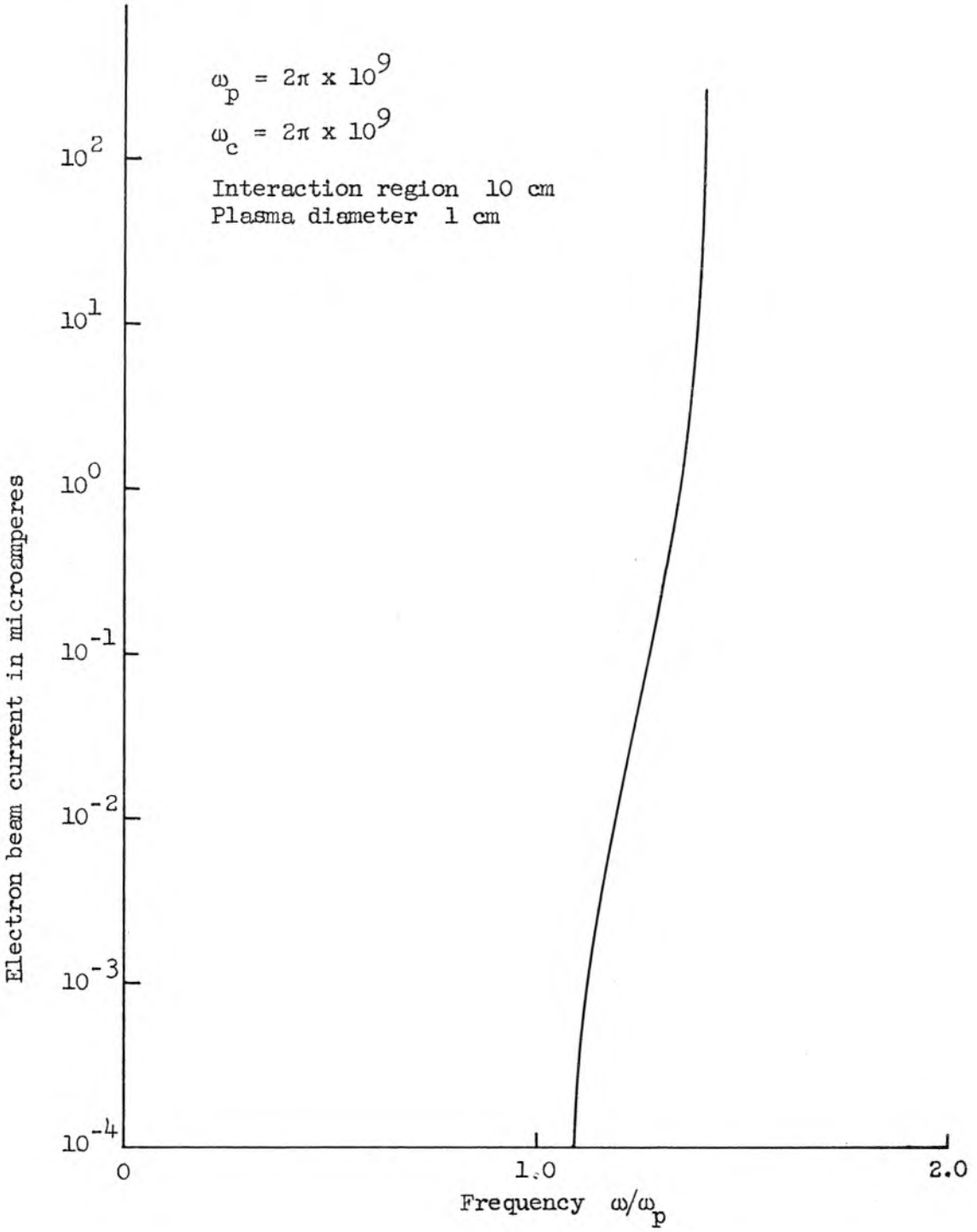


Figure 28. Start Oscillation Current for Plasma-Filled Cylindrical Waveguide. Cyclotron Frequency Equal to Plasma Frequency.

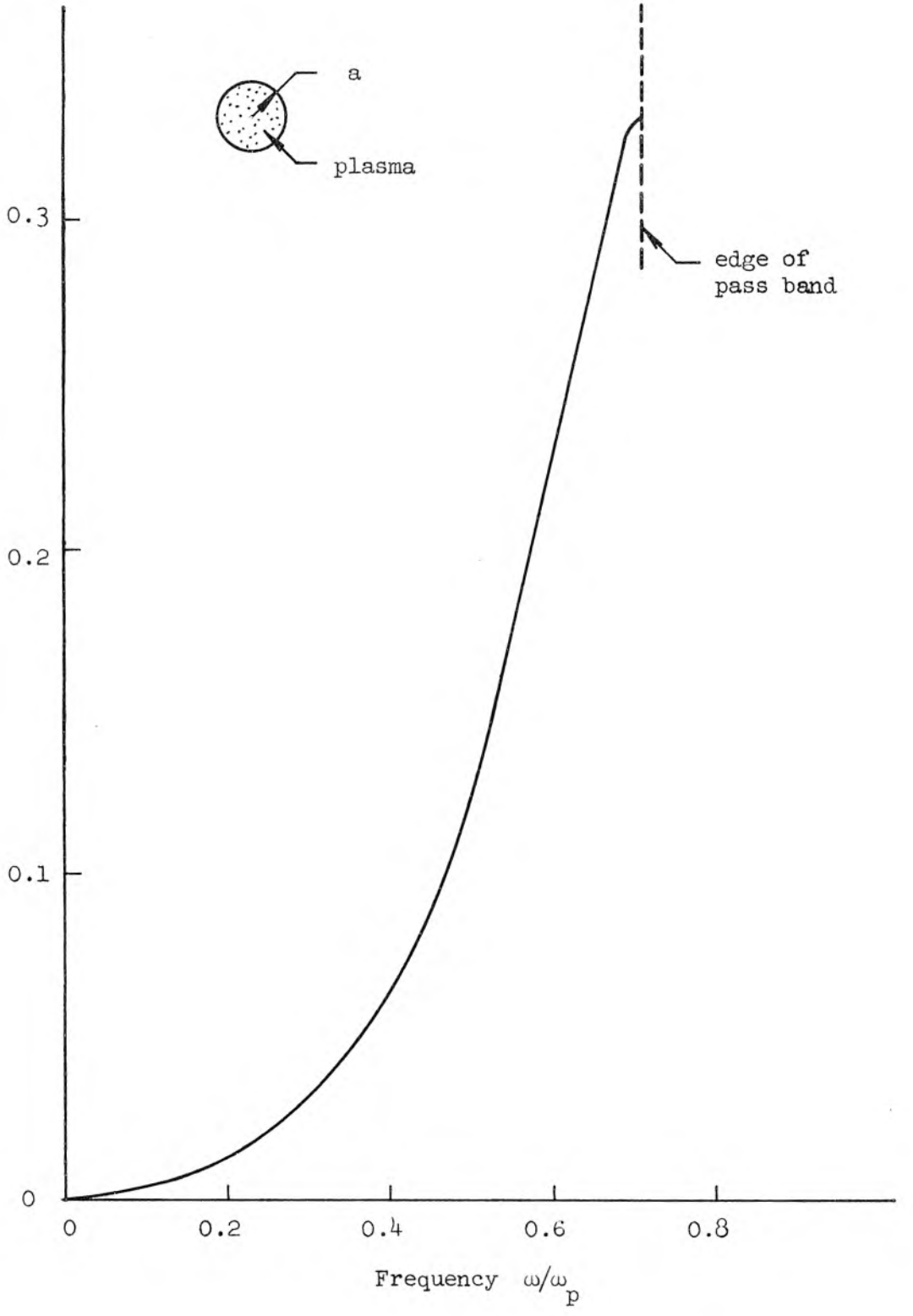


Figure 29. Interaction Impedance for a Plasma Column in Free Space.

field gain calculation is used shown in Figure 30 as a function of frequency.

This analysis is not intended to be a complete study of interaction of electron beams with stationary plasmas, but rather was included to demonstrate that the slow waves which propagate on a plasma column may interact with an electron beam to produce growing waves, and to show that this interaction can be achieved with plasmas and electron beams which are available in the laboratory. The most important implication of this analysis is that the backward wave interaction could be used to generate frequencies in the millimeter range or to investigate the properties of plasmas whose densities correspond to plasma frequencies in the millimeter range. The usefulness of these calculations is primarily that of demonstrating the method of obtaining quantitative results for plasma-beam interactions by regarding the plasma as a slow wave circuit and evaluating the interaction impedance.

Energy Conservation in Plasmaguide Waves. To obtain the propagation characteristics of the plasmaguide modes, it was assumed that the a.c. magnetic field could be neglected. To obtain an estimate of the a.c. magnetic fields for power flow calculations, it was assumed that they were not zero and that they were given by $\nabla \times H = j\omega \underline{\underline{\epsilon}} \cdot \underline{E}$. A demonstration that the power flow thus obtained is consistent with the initial approximation can be given by computing the time average total stored energy in the plasmaguide and multiplying by the rate at which energy propagates in the system (group velocity).

An expression for the total stored energy can be derived starting with the differential form of Poynting's theorem

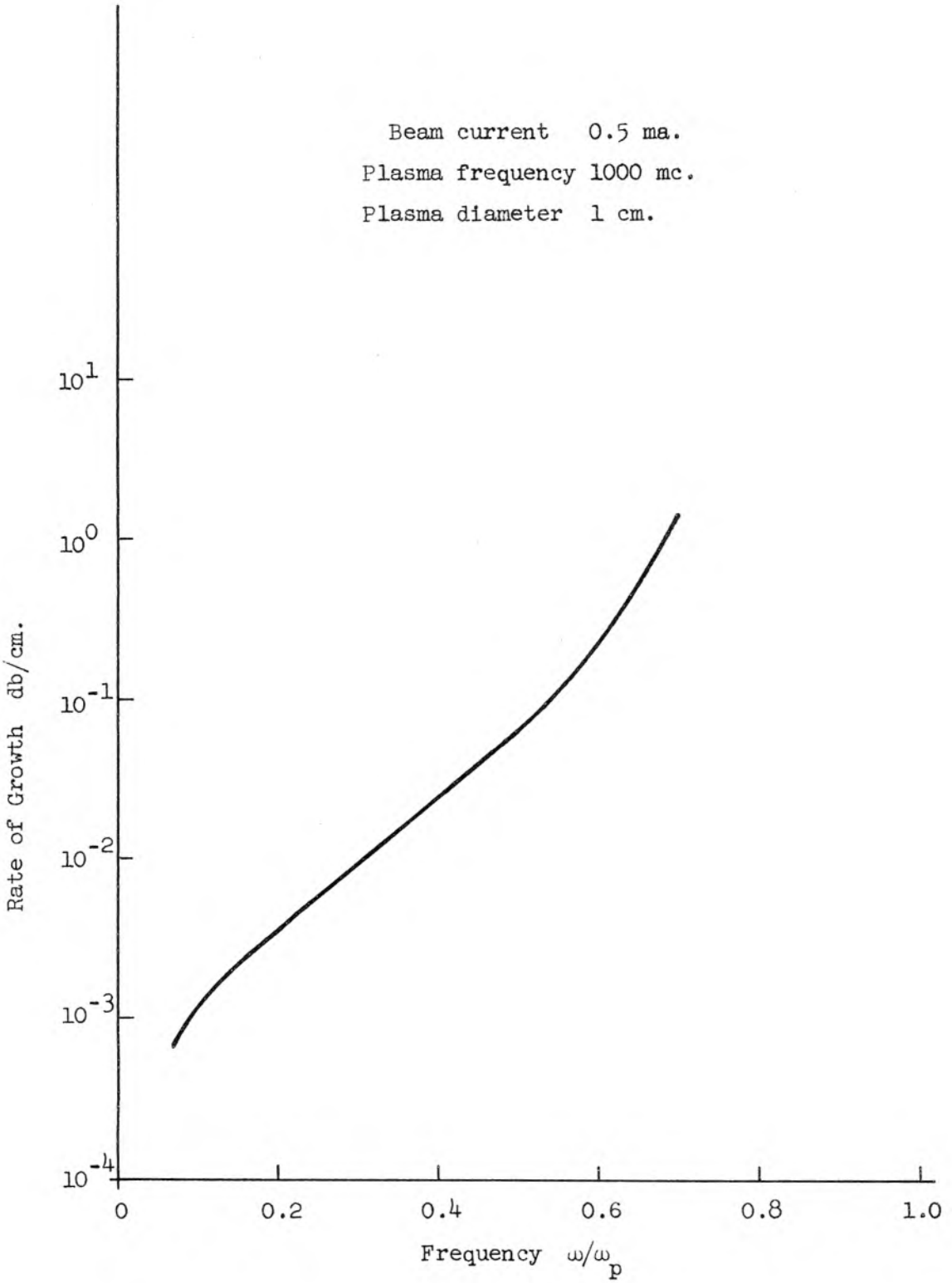


Figure 30. Rate of Growth for an Electron Beam Interacting with the Surface Waves on a Plasma Column. Beam Velocity is Equal to the Phase Velocity of the Waves.

$$\nabla \cdot (\underline{E}_1 \times \underline{H}_1) + \frac{\partial}{\partial t} \left(\frac{\epsilon_o}{2} E_1^2 + \frac{\mu_o}{2} H_1^2\right) + \underline{E}_1 \cdot \underline{J}_1 = 0 \ , \tag{V.17}$$

where $\underline{E}_1 \times \underline{H}_1$ is the Poynting vector and $\frac{\epsilon_o}{2} E_1^2$ and $\frac{\mu_o}{2} H_1^2$ are respectively the electric and magnetic energy densities, and $\underline{E}_1 \cdot \underline{J}_1$ is the rate at which the electrons extract energy from the field. $\underline{E}_1 \cdot \underline{J}_1$ is evaluated from the equation of motion

$$\frac{\partial \underline{v}_1}{\partial t} = - \frac{e}{m} \underline{E}_1 \ , \tag{V.18}$$

where either infinite or zero magnetic field has been assumed, and the current $\underline{J}_1 = \rho_o \underline{v}_1$ , thus

$$\underline{E}_1 \cdot \underline{J}_1 = \left(\frac{m}{e}\right)^2 \left(\frac{\epsilon_o}{2}\right) \omega_p^2 \frac{\partial}{\partial t} v_1^2 \ . \tag{V.19}$$

The kinetic power flow is zero and the kinetic energy density is

$$W_k = \left(\frac{m}{e}\right)^2 \left(\frac{\epsilon_o}{2}\right) \omega_p^2 v_1^2 \ . \tag{V.20}$$

Neglecting the magnetic energy density, the time average total stored energy per unit length is

$$\overline{W}_T = \frac{\epsilon_o}{4} \ \mathrm{Re} \int_S \left(E_1^2 + \left(\frac{m}{e}\right)^2 \omega_p^2 v_1^2\right) ds \ , \tag{V.21}$$

where S is the guide cross section. When the d.c. axial magnetic field is infinite, V.21 becomes for the plasma-filled guide of radius a, using the field components given in Chapter III

$$\overline{W}_T = \frac{\pi \epsilon_o}{2} A^2 (Ta)^2 J_1^2(Ta) \frac{\omega_p^2 / \omega^2}{\left(\frac{\omega_p^2}{\omega^2} - 1\right)} \ , \tag{V.22}$$

where $A$ is the excitation amplitude. The time average power flow is given by

$$\overline{P}_z = v_g \overline{W}_T \quad , \tag{V.23}$$

where

$$v_g = \frac{\omega^2}{\omega_p^2} \frac{\omega}{\beta} \left(\frac{\omega_p^2}{\omega^2} - 1\right) \tag{V.24}$$

is the group velocity. Thus,

$$\overline{P}_z = \frac{\epsilon_o \pi A^2}{2} \frac{\omega}{\beta} (Ta)^2 J_1^2(Ta) \quad , \tag{V.25}$$

which is the same as the power flow calculated by integrating Poynting's vector over the guide cross section, III.48. The agreement of these two methods indicates that the approximate values for the a.c. magnetic field obtained with the quasi-static approximation are probably close to the actual magnetic field.

Attenuation of Plasmaguide Waves. When the plasma electrons are produced by an electrical discharge in a gas, attenuation may arise because of collisions of the electrons with neutral gas molecules, positive ions, or the wall of the discharge tube. These collisions interrupt interaction with the wave and remove energy from it. An approximate way of including this effect is to define an average electron collision frequency $\nu_c$ and replace $\omega$ by $\omega - j\nu_c$ in the preceding equations. An approximate solution to these equations is obtained by writing

$$\alpha(\omega,\nu_v) + j\beta(\omega,\nu_c) = j\beta(\omega,0) + j \frac{d\beta(\omega,0)}{d\omega} (-j\nu_c) + \cdots . \tag{V.26}$$

When $\nu_c$ is small the first two terms give a satisfactory approximation

$$\alpha(\omega,\nu_c) = \frac{d\beta}{d\omega}\,\nu_c \qquad (V.27)$$

$$\beta(\omega,\nu_c) = \beta(\omega,0) \quad . \qquad (V.28)$$

Thus to a first approximation the phase velocity is unaffected by collisions and the attenuation is proportional to the collision frequency and inversely proportional to group velocity, $d\omega/d\beta$ .

# VI. RELATION OF PLASMAGUIDE MODES TO SPACE CHARGE WAVES ON DRIFTING ELECTRON BEAMS

It is usually assumed that a drifting motion is essential to the propagation of energy by space charge waves. Actually this is true only for the case of a one-dimensional electron beam and does not apply for finite electron beams. The term "plasmaguide" has been used in this paper to denote the various electromechanical modes of propagation in stationary ion-neutralized plasma columns of finite cross section. These modes of propagation are the same as space charge waves as seen by an observer in a coordinate system moving with the electron beam. A knowledge of the propagation characteristics in a system where the electrons are at rest can be used to investigate the properties of space charge waves on a moving electron beam by means of a coordinate transformation. If $\omega$ and $\beta$ are the frequency and propagation constants in the coordinate system where the electrons are at rest, the frequency $\omega'$ and propagation constant $\beta'$ in the coordinate system where the electrons drift with velocity $u_o$ are

$$\omega' = \omega + \beta u_o \tag{VI.1}$$

$$\beta' = \beta \quad . \tag{VI.2}$$

The wavelengths are the same, and $\omega'$ is just the Doppler shifted frequency. Although each of the plasmaguide solutions given in the previous chapters can be easily modified to include a drift velocity, only the plasma-filled guide in an infinite magnetic field will be considered here. A typical $\omega$-$\beta$ diagram constructed from Figure 1 with the aid of VI.1 and VI.2 is shown in Figure 31. The slanted dashed lines are the

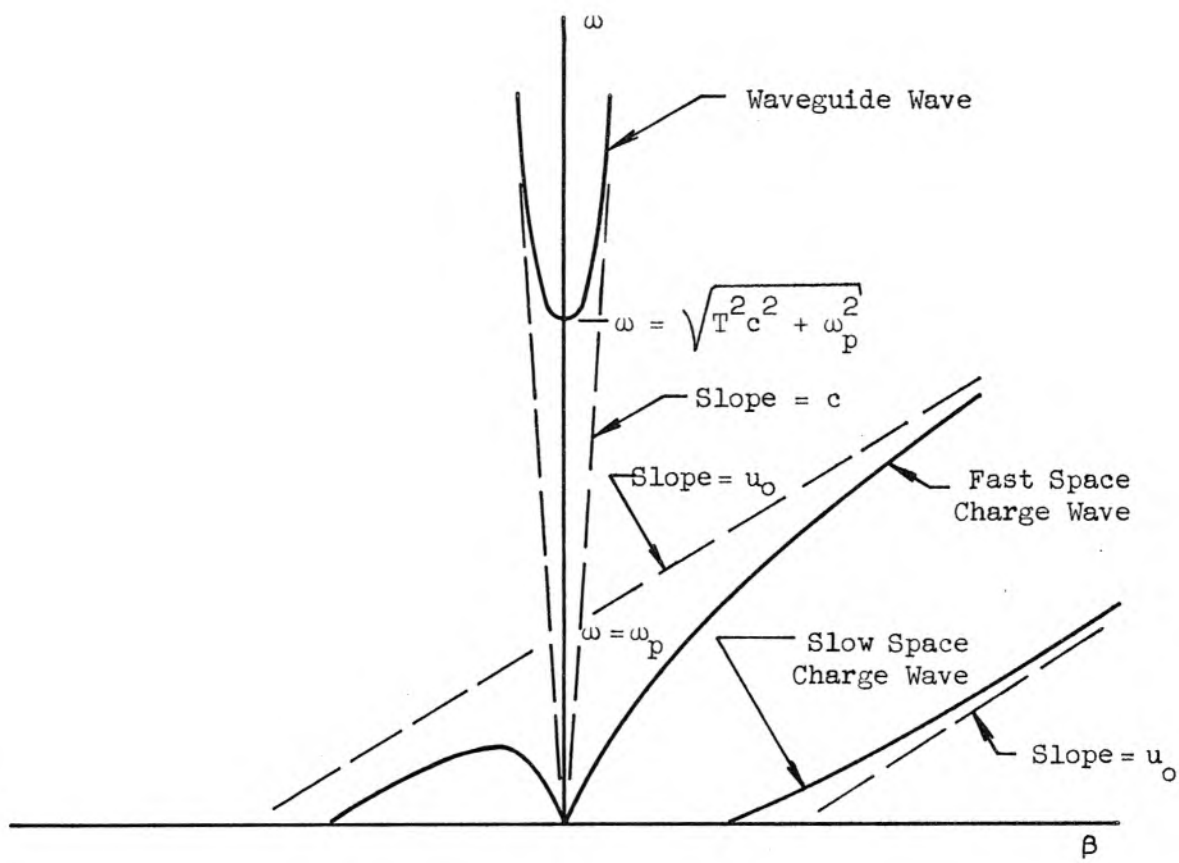


Figure 31. Phase Characteristics of Waves in an Electron Beam of Velocity $u_o$ in an Infinite Magnetic Field.

phase characteristics of the one-dimensional or beam-of-infinite-radius space charge wave solutions (see I.6 and I.7). The departure from the one-dimensional solution when the beam is small can be explained as follows. When the electron beam is of infinite radius, all the electric fields from the electrons terminate on positive ions and the natural frequency of oscillation is just the plasma frequency appropriate to the average charge density; however, when the electron beam has a finite radius, the electric fields of electrons do not all terminate on other positive ions, but rather terminate on induced wall charges when the beam is in a conducting tube. The restoring force on a displaced electron is therefore reduced, and the net effect is to reduce the plasma frequency of the system. The amount by which the plasma frequency is lowered, due to finite geometry is called the reduction factor. The lower curve of Figure 1 is just the reduction factor as a function of the propagation constant. This is easily shown by considering the propagation equation which would have resulted in the analysis of Chapter II if the plasma or electron beam had been allowed to have a drift velocity $u_o$ along the axis of symmetry $(\omega = \omega' - \beta u_o)$

$$\left(\frac{p_{n\nu}}{a}\right)^2 = -\beta^2 \left[1 - \frac{\omega_p^2}{(\omega' - \beta u)^2}\right] \quad , \tag{VI.3}$$

where $k^2$ has been neglected as compared with $\beta^2$. This equation may be expressed

$$\beta = \frac{\omega'}{u_o} \pm \frac{1}{\sqrt{1 + \left(\frac{p_{n\nu}}{\beta a}\right)^2}} \frac{\omega_p}{u_o} \quad . \tag{VI.4}$$

Comparing this with I.7 it is seen that the reduction factor is

$$R = \frac{1}{\left[1 + \left(\frac{p_{n\nu}}{\beta a}\right)^2\right]^{1/2}} \qquad \text{(VI.5)}$$

which when solved for $\beta/T$ $(T = p_{n\nu}/a)$,

$$\frac{\beta}{T} = \left[\frac{1}{R^2} - 1\right]^{-1/2} . \qquad \text{(VI.6)}$$

By identifying $R$ with $\omega/\omega_p$ and comparing this equation with the propagation equation obtained in Chapter II, equation II.29, it is apparent that the $\omega$-$\beta$ diagram for the propagation of space charge disturbances in coordinate systems where the electrons are at rest is just the space charge reduction factor curve (provided the ordinate is measured in units of $\omega/\omega_p$ ). A simple graphical method (27) for obtaining the reduction factors of the fast and slow space charge waves in terms of $\beta_e a = \omega a/u_o$ can be given by plotting

$$\beta a = \beta_e a \pm R_{\pm}\, \beta_p a \qquad \text{(VI.7)}$$

on the plasmaguide $\omega$-$\beta$ diagram when it is plotted as $\omega/\omega_p$ as a function of $\beta a$ . This is done in Figure 32. The intersections of the $\omega$-$\beta$ curve and the curves of VI.7 represent the solutions, the value of $\omega/\omega_p$ being just the reduction factor for a beam in that geometry having the value of $\beta_e a$ selected to plot VI.7 . Considering many values of $\beta_e a$ allows the fast and slow space charge wave reduction factors, $R_+$ and $R_-$ respectively to be plotted as a function of the beam propagation constant, $\beta_e a$. The curves thus obtained do not include the usual approximation made in investigating space charge waves, namely that $\omega_p \ll \omega$ . A typical reduction factor curve obtained from this method is shown in Figure 33.

This section shows the relation of plasmaguide waves to the space

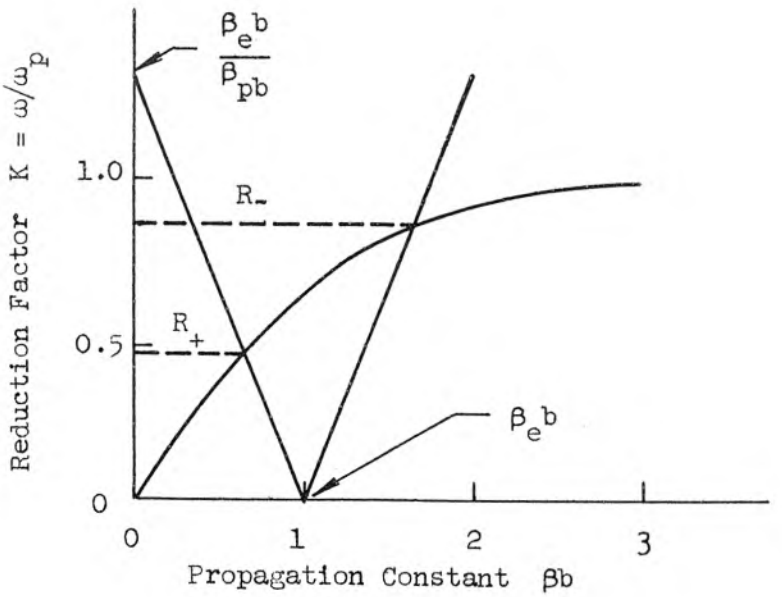


Figure 32. Diagram Showing Method for Obtaining Fast and Slow Space Charge Waves from Plasma Mode Phase Characteristics.

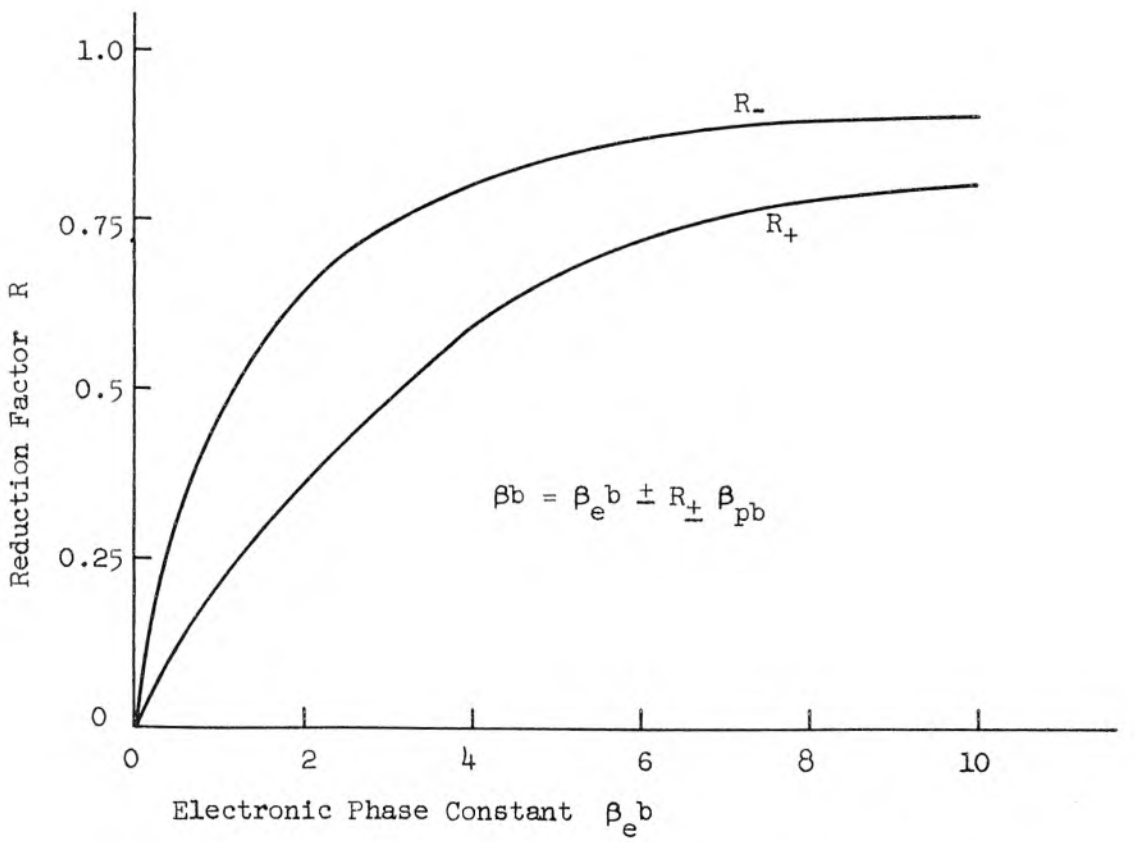


Figure 33. Fast and Slow Space Charge Wave Reduction Factors for Ion Neutralized Electron Beam Filling a Drift Tube. Cyclotron Frequency Equal to Plasma Frequency ($\beta_{pb} = 1$).

charge waves on a drifting electron beam. The method of obtaining the moving beam reduction factors described here is much simpler than that of solving the field equations including the drifting motion of the electron beam. Thus the properties of space charge waves for many cases can be determined by solving Poisson's equation in a system where the electrons do not have a drift velocity and transferring to a coordinate system where the electrons have the desired drift velocity.

## VII. SLOW WAVE PROPAGATION IN FERRITE WAVEGUIDES

In Chapter III it was shown that for a plasma-filled waveguide in a finite axial d.c. magnetic field the necessary condition for propagation was that the ratio of the zz-component of the dielectric tensor for the plasma to the rr-component be negative

$$T^2 = -\beta^2 \frac{\epsilon_{zz}}{\epsilon_{rr}} \tag{III.21}$$

for the reason that $T^2$ is greater than zero and for propagating waves $\beta^2$ must be positive. For a ferrite-filled waveguide in a finite axial magnetic field there exists a region where the zz-component and the rr-component of the permeability tensor are of opposite sign, and it seems quite likely that there should exist a "magnetic dual" to the plasmaguide waves.

Ferrite Rod in a Cylindrical Waveguide. Consider a perfectly conducting cylindrical waveguide of radius $b$ containing a homogeneous lossless ferrite rod of radius $a$, and let there be a finite axial magnetic field $B_o$. The ferrite will be treated as an anisotropic medium of tensor permeability (11)

$$\underline{\underline{\mu}} = \mu_o \begin{Vmatrix} \mu_{rr} & -j\mu_{r\theta} & 0 \\ +j\mu_{\theta r} & \mu_{\theta\theta} & 0 \\ 0 & 0 & \mu_{zz} \end{Vmatrix} \tag{VII.1}$$

where

$$\mu_{rr} = \mu_{\theta\theta} = 1 - \frac{\sigma P}{1 - \sigma^2} \tag{VII.2}$$

$$\mu_{r\theta} = \mu_{\theta r} = \frac{P}{1 - \sigma^2} \tag{VII.3}$$

$$\mu_{zz} = 1 \tag{VII.4}$$

and

$$P = |\gamma| \frac{M_o}{\mu_o} \frac{1}{\omega} \tag{VII.5}$$

$$\sigma = |\gamma| H_o \frac{1}{\omega} \tag{VII.6}$$

$M_o$ is the d.c. magnetization, $H_o$ is the d.c. magnetic intensity and $\gamma$ is the gyromagnetic ratio for the electron. A sketch showing the variation of components of the permeability tensor is given in Figure 34.*

To study the propagation characteristics of this system the quasi-static approximation will again be used. In this case, however, it will be the a.c. electric field which will be neglected. Unfortunately a situation analogous to the infinite magnetic field case for the plasma filled guide (Chapter II) which can be treated simply and rigorously does not seem to exist. The validity of the approximation here will have to rest on making a test of the solutions to see if the a.c. electric field components are negligible. Setting the a.c. electric field to zero in the curl B Maxwell equation

$$\nabla \times \underline{H}_1 = j \omega \epsilon \underline{E}_1 \tag{VII.7}$$

permits the magnetic intensity to be derived from a scalar potential

$$\underline{H}_1 = - \nabla \phi_1 \tag{VII.8}$$

where the differential equation which must be satisfied by $\phi_1$ comes from the requirement

$$\nabla \cdot \underline{B}_1 = \nabla \cdot (\underline{\underline{\mu}} \cdot \underline{H}_1) = 0 \quad . \tag{VII.9}$$

---

*This sketch is taken from reference 11.

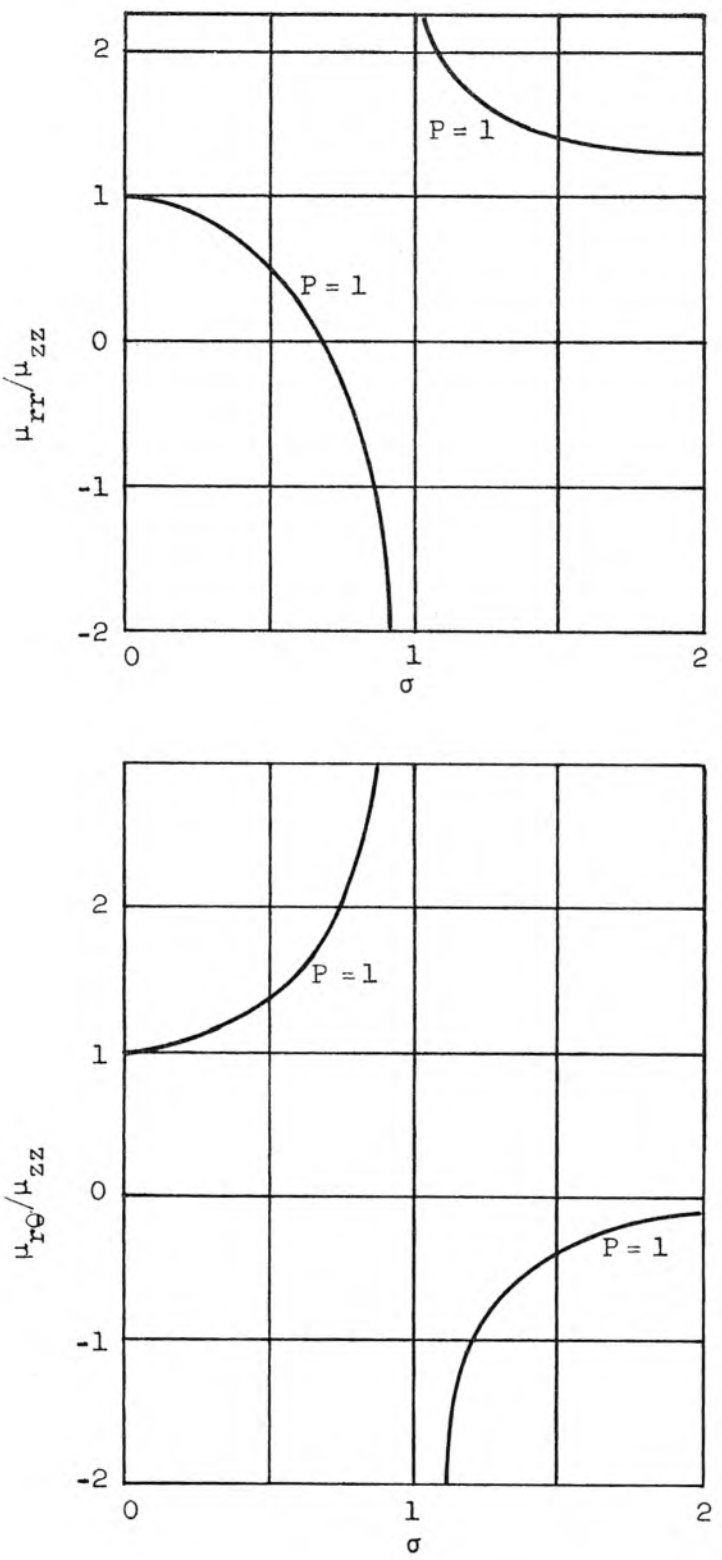


Figure 34. Relative Radial and Angular Permeabilities for Ferrite Rod in an Axial Magnetic Field.

Using the tensor permeability given in VII.1 leads to the following partial differential equation,

$$\frac{1}{r}\frac{\partial}{\partial r}\left[r\,\mu_{rr}\,H_{1r} - j\mu_{r\theta}\,H_{1\theta}\right] + \frac{1}{r}\frac{\partial}{\partial\theta}\left[j\,\mu_{\theta r}\,H_{1r} + \mu_{\theta\theta}\,H_{1\theta}\right] + \frac{\partial}{\partial z}\left[\mu_{zz}\,H_{1z}\right] = 0 . \tag{VII.10}$$

The partial differential equation in the magnetostatic potential is

$$\frac{1}{r}\frac{\partial}{\partial r}\left(r\frac{\partial}{\partial r}\phi_1\right) + \frac{1}{r^2}\frac{\partial^2\phi_1}{\partial\theta^2} + \frac{\mu_{zz}}{\mu_{rr}}\frac{\partial^2\phi_1}{\partial z^2} = 0 \quad . \tag{VII.11}$$

Assume wave solutions,

$$\phi_1 = K(r)\, e^{-jn\theta}\, e^{-j\beta z} \tag{VII.12}$$

leads to the following differential equation which must be satisfied by the radial function,

$$\frac{1}{r}\frac{d}{dr}\left(r\frac{dR}{dr}\right) - \frac{n^2}{r^2}R - \beta^2\frac{\mu_{zz}}{\mu_{rr}}R = 0 \quad . \tag{VII.13}$$

Letting

$$T^2 = -\beta^2\frac{\mu_{zz}}{\mu_{rr}} \quad , \tag{VII.14}$$

the solutions of the Bessel's differential equation VII.19 are

$$R(r) = A\,J_n(Tr) + B\,N_n(Tr) \quad . \tag{VII.15}$$

Omitting the second solution which is singular at the origin, a suitable solution for the potential inside the ferrite and the associated field components are:

$$\left.\begin{aligned}
\phi_{1i}(r,\theta,z,t) &= A\, J_n(Tr) && \text{(VII.16)}\\
H_{1r}(r,\theta,z,t) &= -A\, T\, J_n'(Tr) && \text{(VII.17)}\\
H_{1\theta}(r,\theta,z,t) &= A\, \frac{jn}{r}\, J_n(Tr) && \text{(VII.18)}\\
H_{1z}(r,\theta,z,t) &= A\, j\beta\, J_n(Tr) && \text{(VII.19)}
\end{aligned}\right\} e^{j(\omega t - n\theta - \beta z)},\ r < a\ .$$

The solution outside the ferrite is obtained by setting $\mu_{rr} = \mu_{zz} = 1$ in VII.13 ,

$$\phi = C\left[I_n(\beta r)\, K_n'(\beta b) - I_n'(\beta b)\, K_n(\beta r)\right] \qquad e^{j(\omega t - n\theta - \beta z)} \qquad \text{(VII.20)}$$

$$a < r < b\ .$$

This solution satisfies the boundary condition that the normal component of the a.c. magnetic induction vanish at the conducting waveguide. One of the boundary conditions at the surface of the ferrite rod, i.e., that the tangential component of the a.c. magnetic intensity be continuous, is satisfied by taking

$$A = \left[J_n(Ta)\right]^{-1} \qquad \text{(VII.21)}$$

$$B = \left[I_n(\beta a)\, K_n'(\beta b) - I_n'(\beta b)\, K_n(\beta a)\right]^{-1} \ . \qquad \text{(VII.22)}$$

The other boundary condition, that the normal component of the a.c. magnetic induction be continuous, leads to the equation for propagation of waves in this system,

$$\mu_{rr}(Ta)\, \frac{J_n'(Ta)}{J_n(Ta)} + n\, \mu_{r\theta} = (\beta a)\, \frac{\left[I_n'(\beta a)\, K_n'(\beta b) - I_n'(\beta b)\, K_n'(\beta a)\right]}{\left[I_n(\beta a)\, K_n'(\beta b) - I_n'(\beta b)\, K_n(\beta a)\right]} \ . \qquad \text{(VII.23)}$$

As discussed in Chapter III the fact that VII.23 is an odd function of $n$ indicates that the value of $\beta$ for $+n$ is different from $-n$ ,

resulting in the rotation of the plane of polarization of a linearly polarized wave (for this case slow wave Faraday rotation). Since this paper is primarily concerned with wave propagation in plasma-filled waveguides, a systematic examination of the properties of slow wave propagation in ferrites will not be given; however, it is of interest to examine at least one case and obtain the $\omega$-$\beta$ diagram.

Ferrite Filled Waveguide in Finite Axial D.C. Magnetic Field. When the ferrite fills the guide $(b = a)$, the numerator of the right side of VII.32 vanishes and the propagation equation is

$$(Ta) \quad \frac{J_n'(Ta)}{J_n(Ta)} = -n \frac{\mu_{r\theta}}{\mu_{rr}} \quad . \tag{VII.24}$$

In contrast with the plasma-filled guide, the ferrite-filled guide can produce a rotation of the plane of polarization of the higher order modes $(n > 0)$. Again, the higher order modes undoubtedly have interesting properties which could be systematically investigated; however, interest will be confined in this paper to the case of axially symmetric modes $(n = 0)$.

For the circularly symmetric mode $(n = 0)$,

$$J_1(Ta) = 0 \quad , \quad Ta = p_{1\nu} \tag{VII.25}$$

where $p_{1\nu}$ are the $\nu$ roots of the Bessel function of order unity. The normalized propagation constant can then be expressed

$$\left(\frac{\beta}{T}\right)^2 = - \frac{\mu_{rr}}{\mu_{zz}} \quad . \tag{VII.26}$$

Examining Figure 34 reveals that there is a narrow frequency band just above the precession resonance where the quantity $(\mu_{zz}/\mu_{rr})$ on the

right side of VII.26 is negative. The $\omega$-$\beta$ diagram for this pass band is shown in Figure 35 and as can be seen, the waves are of a backward wave nature.

A possible use of the ferrite modes would be that of measuring the properties of the ferrite. The technique would be similar to that described in Chapter VII for plasma diagnostics, i.e., by measuring the attenuation, it should be possible to deduce the losses in the ferrite, and by measuring the phase velocity versus frequency, it should be possible to establish the permeability tensor components.

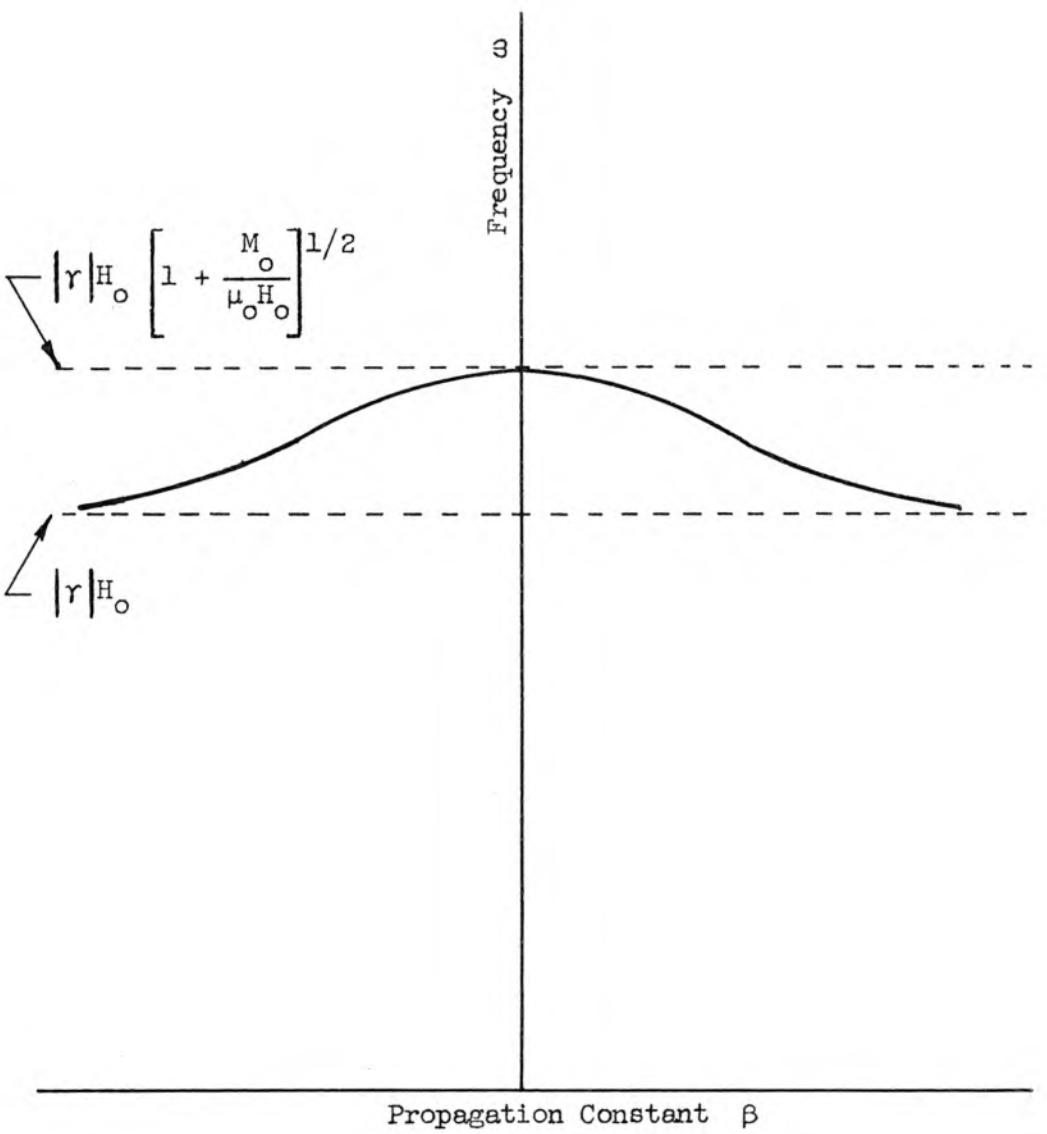


Figure 35. Phase Characteristics for Slow Wave Propagation in a Ferrite-Filled Cylindrical Waveguide in an Axial Magnetic Field $H_o$. Axially Symmetric Mode.

# VIII. EXPERIMENTAL RESULTS

Most of the analysis given in the preceding chapters was made either to explain results which had been observed experimentally or to predict in advance what results to expect in a given experiment. The experiment is quite simple and involves nothing more than exciting a wave, such as described in earlier chapters, on an ion-neutral plasma column and measuring the wavelength in the plasma waveguide. By measuring the wavelength for a particular frequency of excitation and a given geometry, it is possible to calculate the propagation constant ($\beta = 2\pi/\lambda$). Repeating this measurement at various frequencies within the passband gives an experimental curve of the phase characteristics of the waves ($\omega$ versus $\beta$). Such measurements were made and in each case the agreement between theory and experiment is quite good. The experimental results will be presented in relation to the analysis which is being verified.

Description of Experiment. A schematic diagram of the apparatus used to investigate the properties of the various modes of propagation is shown in Figure 36. The plasma is the positive column of a mercury arc discharge that is maintained by applying a d.c. voltage (through a large external resistor which limits the discharge current) between the thermionic cathode and the anode. The anode is a disk whose diameter is slightly less than the diameter of the glass cylinder which contains the plasma. The oxide-coated cathode is a conventional type taken from a commercially available mercury arc rectifier tube. To excite the waves in this system, a radio frequency signal is coupled to the plasma through the discharge anode. This is accomplished by operating the anode

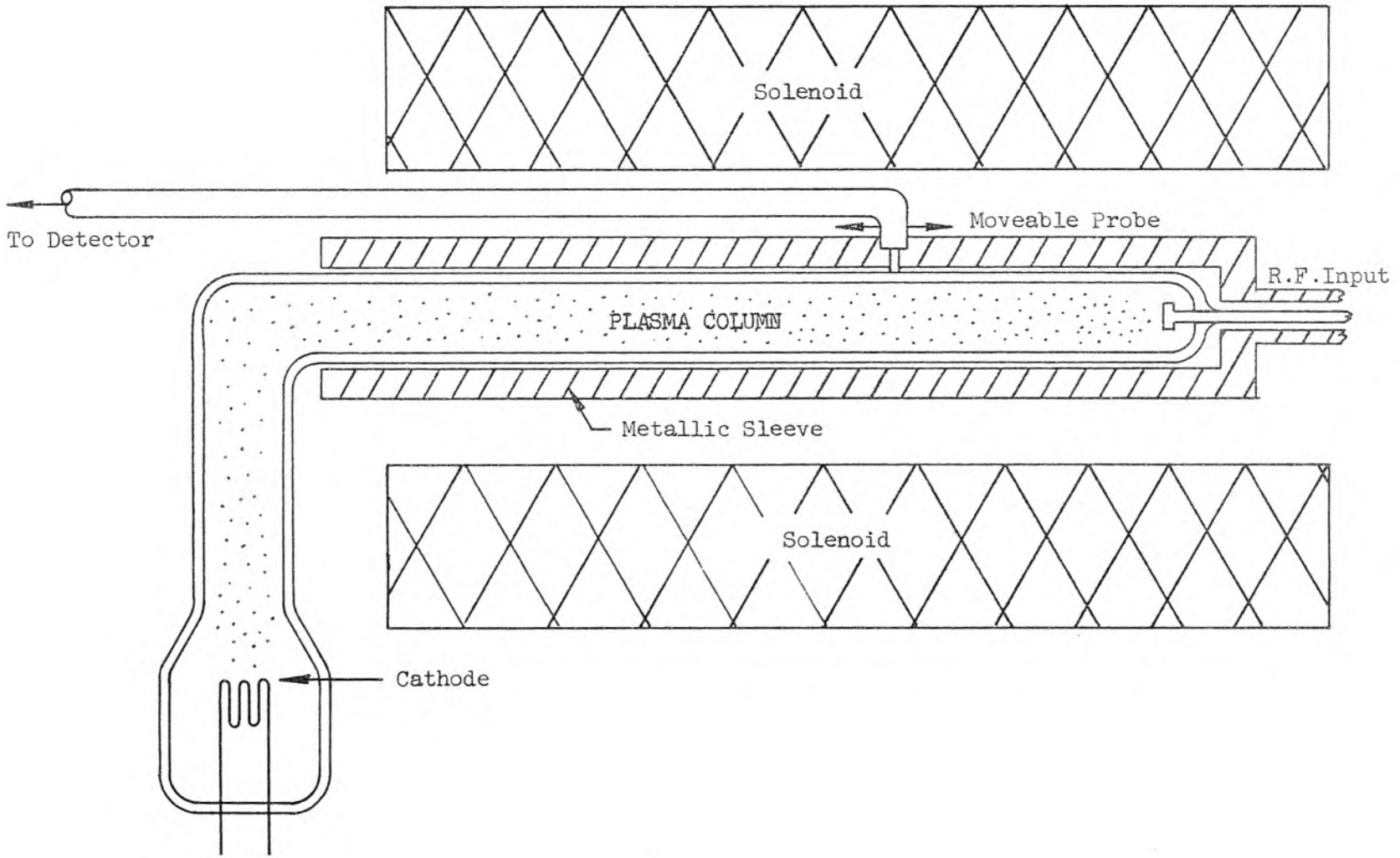


Figure 36. Schematic Drawing of Apparatus for Measuring Wavelengths and Attenuation in a Plasma-Filled Waveguide.

at zero d.c. potential and the cathode at a negative voltage and by bringing the r.f. signal to the anode along a coaxial conductor. The d.c. path for the current is provided by placing a length of shorted coaxial conductor in parallel with the line supplying the r.f. Actually, several of these shorted sections (usually referred to as stub tuners) of line were strategically located so as to provide a better impedance match between the 50 ohm output of the signal generator and the plasma (the r.f. input impedance of the plasma waveguide has been estimated to be on the order of 1000 ohms). The signal along the plasma column is sampled by means of a moveable probe as schematically indicated in Figure 36. The guide wavelengths are measured in two ways. The first is to measure the standing waves which result from the reflected energy at the unterminated end of the plasma waveguide. This method was useful when the loss was low and the wavelengths were long (10 cm). The length of the plasma column is about 25 cm. thus making it possible to conveniently measure 15 cm. wavelengths. Using the standing wave method it is therefore possible to measure guide wavelengths up to 30 cm. since the guide wavelength is twice the measured wavelength. When the losses become rather high and the wavelengths short (one or two cm.) little or no energy is reflected from the unterminated end of the plasma column and no standing waves are observed. To measure the wavelength under these circumstances, a second method was used. This method involves adding some signal from the generator to the signal coming from the probe. As the probe is moved along the plasma column, the phase of the probe signal goes through $2\pi$ radians every guide wavelength. For some probe position, the constant phase of the signal from the generator is

$180^{\circ}$ out of phase with respect to the probe signal, and the two signals partially cancel. By adjusting the amplitude of the added signal, it is possible in principle to make the two signals cancel completely. Thus as the probe is moved along the plasma column, the combined output will have a minimum at points which are separated by one guide wavelength. The attenuation of the signal with distance away from the input was measured by observing the probe signal amplitude as a function of probe position.

The pressure of the mercury within the tube is controlled by regulating the temperature of a mercury well which is attached to the glass envelope at a point near the cathode (not shown in the schematic). The temperature is held between $26.7^{\circ}C$ and $26.9^{\circ}C$ (about $300^{\circ}K$), and the corresponding pressure is a few microns. For this pressure, the mean free path of the plasma electrons (a few centimeters) is long compared with the diameter of the discharge (0.328 inches). To make accurate quantitative measurements, it would be essential to immerse the entire discharge tube in a thermostatic bath. This would be difficult from a practical standpoint and was not done because the experiments were not performed to provide accurate quantitative results, but rather were performed to verify the gross features of the waves reported in the analysis. In spite of only regulating the temperature of the mercury well, the results are quite reproducible, and it would seem that the most serious consequence of only partial immersion is to place all the results in error by a small but constant amount.

Propagation was investigated from 10 megacycles to 4000 megacycles. The cyclotron and plasma frequency are variable over about the same range. The axial d.c. magnetic field is provided by a solenoid. The

diameter of the plasma is 0.328 inches, and the outer diameter of the glass cylinder containing the plasma is 0.410 inches. One of the cylindrical waveguides in which the plasma column is placed closely fits the glass cylinder, and the other waveguide which is used in the experiment is 0.750 inches in diameter. When empty, the cutoff frequencies for these waveguides is in the tens of kilomegacycles so that the frequencies used in the experiment are all well below cutoff. The frequency range over which propagation was investigated was determined by the equipment available in the laboratory and does not represent any fundamental limitation.

Plasma Column in a Cylindrical Waveguide. Finite Magnetic Field.

In Chapter III it was shown that the propagation characteristics depend on the strength of the axial d.c. magnetic field. In addition to forward wave pass bands, there are backward wave pass bands near the cyclotron or plasma frequency depending on which is larger. Figure 37 is a theoretical $\omega$-$\beta$ diagram for a plasma column in a glass cylinder which tightly fits a cylindrical waveguide. Experimental points for several discharge currents and magnetic fields are shown. As can be seen the experimental points are in agreement with the theoretical phase characteristics. Notice that in contrast with the presentation of the phase characteristics in the theory sections of this paper, the operating frequency is normalized to the cyclotron frequency rather than the plasma frequency. The reason for this is that the cyclotron frequency is known and until a comparison with the theory is made, the plasma frequency is unknown. The backward wave pass bands are not indicated in this diagram for the reason that using the cyclotron frequency as a normalizing frequency causes the backward wave pass bands to cross the forward wave pass bands,

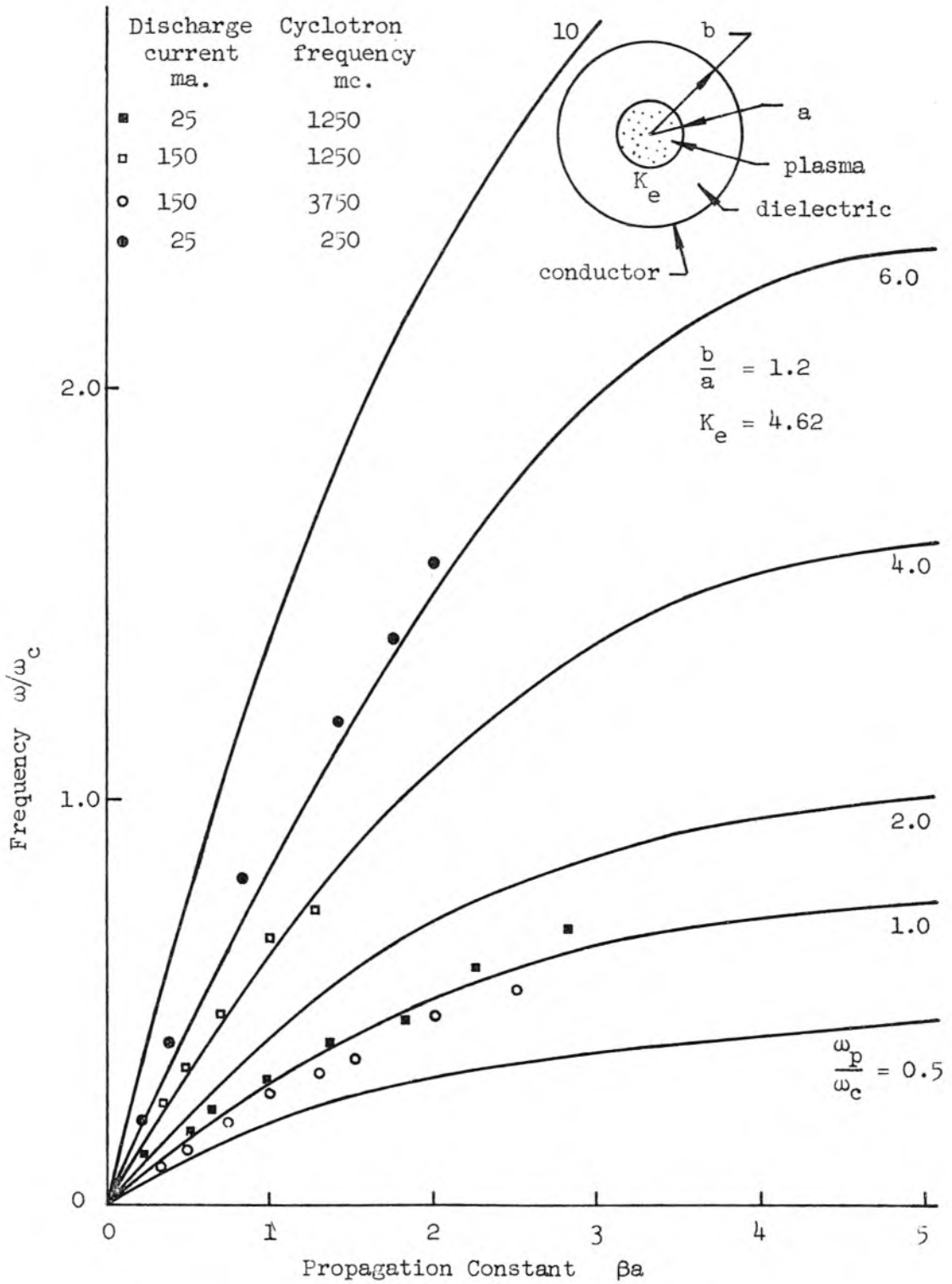


Figure 37. Theoretical Phase Characteristics for a Plasma Column in a Waveguide for a Finite Axial Magnetic Field and Experimental Points.

creating a confusing diagram. Another reason is that no backward waves were observed for this geometry of a tightly fitting metallic sleeve. The inability to observe the backward waves is probably a result of high attenuation, bad input mismatch, and poor probe coupling to the r.f. fields. The poor probe coupling results from the fact that the probe is in a narrow slot cut in the sleeve and can at most touch the glass cylinder containing the plasma. Another factor which contributed to difficulty in observing backward waves was a rather high noise level. This noise was distributed rather uniformly over the entire frequency range investigated. The source of this noise, which seemed to be a function of the r.f. signal level, is not known. A more complete description of this noise spectrum is given in the next chapter. To remedy the poor probe coupling, a second geometry was considered. This geometry allows for an air space between the glass cylinder and metallic sleeve thus permitting better coupling between the probe and the r.f. field. For this geometry, transmission was observed in regions where backward wave pass bands are predicted theoretically; however, the high attenuation made phase velocity measurements virtually impossible. Figure 38 shows the regions of propagation for this geometry as a function of the cyclotron frequency. The range over which propagation was experimentally observed is seen to be in reasonable agreement with the theory. The reason that points in the backward wave region were not taken at higher frequencies is due to the lack of suitable signal generators in the frequency range where the pass bands occur. Limited phase velocity measurements in the backward wave region were made. These are shown in Figure 39 along with measurements made in the forward wave pass band for the same operating conditions. The backward

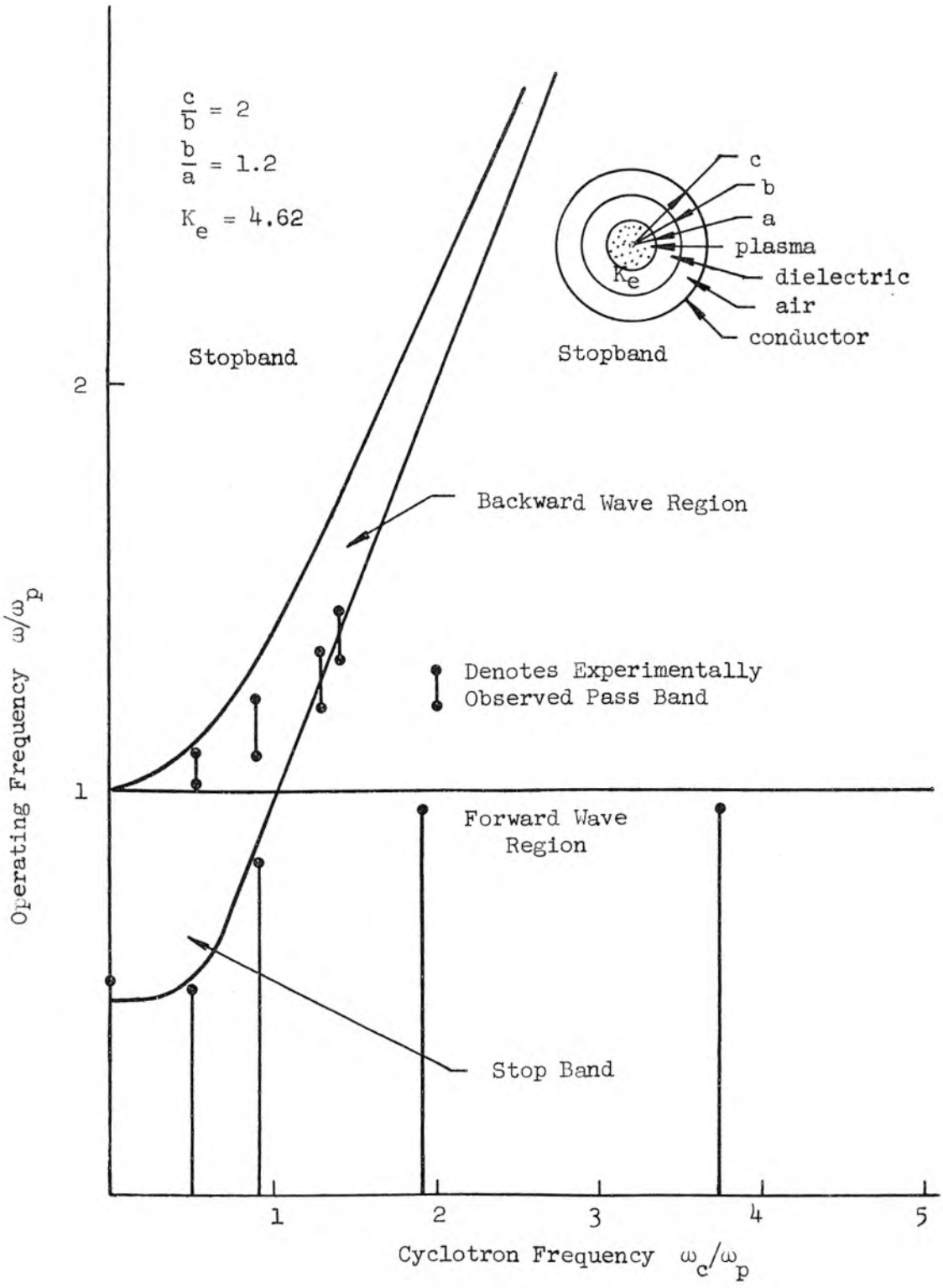


Figure 38. Diagram Showing Pass Bands Expected Theoretically and Regions where Transmission was Observed Experimentally.

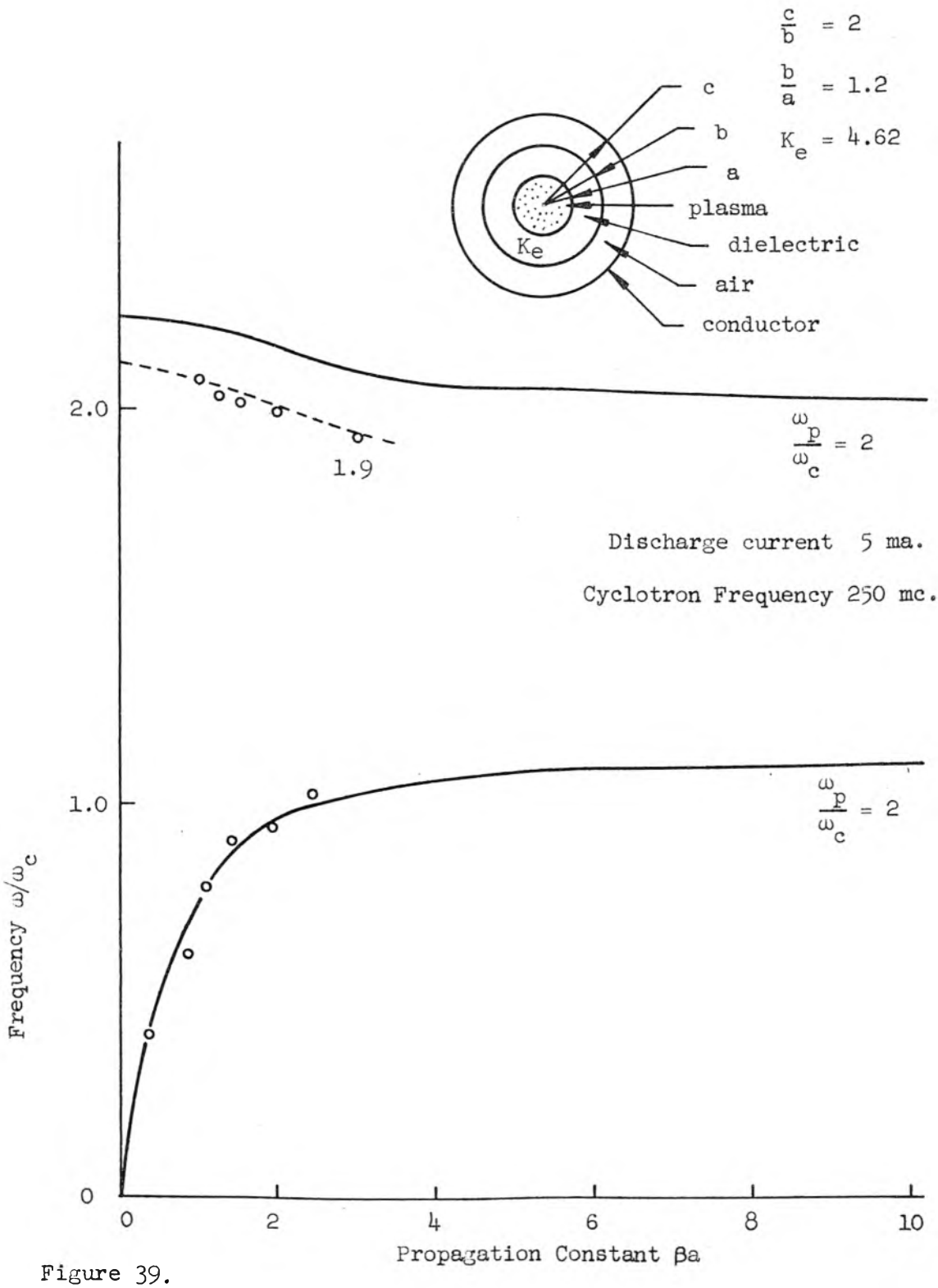


Figure 39.

Theoretical Phase Characteristics for Forward and Backward Wave Passbands and Experimental Points Corresponding Approximately to the Case Shown.

wave passband is quite sensitive to the choice of either cyclotron or plasma frequency and the forward wave pass bands are quite insensitive to small changes in these quantities. The dashed phase characteristics curve which best fits the experimental backward wave data is for $\omega_p/\omega_c = 1.9$ . As can be seen this is rather far from the $\omega_p/\omega_c = 2$ curve for the backward wave pass band. For the forward wave pass band, however, the $\omega_p/\omega_c = 1.9$ curve is very close to the $\omega_p/\omega_c = 2.0$ curve so that both would fit the data equally well. For this reason, $\omega_p/\omega_c = 1.9$ is probably the best value. Thus the plasma frequency for this discharge current (5 ma.) is 475 megacycles.

Plasma Column in a Cylindrical Waveguide. Zero Magnetic Field. In Chapter IV, the surface waves which propagate on an isotropic plasma column are discussed. To verify the features of these modes, the same experimental set up and technique described earlier was used. The magnetic field of the solenoid was reduced to zero. Figure 40 shows the theoretical phase characteristics (for the geometry used in the experiment) which would result if the charge density were uniform over the cross section of the tube. In Chapter IV it was shown that if the charge density was a function of radius (maximum on the axis and minimum at the edge) the phase characteristics would be modified. As can be seen from Figure 40, the experimental points for $\beta a > 1$ are below the uniform charge density curve, which is as expected from the analysis. The experimental points are normalized to the average charge density of the plasma column so that they all have the same behavior at low frequencies. The fact that their low frequency phase velocity depends only on the average charge density is explained in Chapter IV. The experimental points for the larger of the two discharge currents are the lowest on

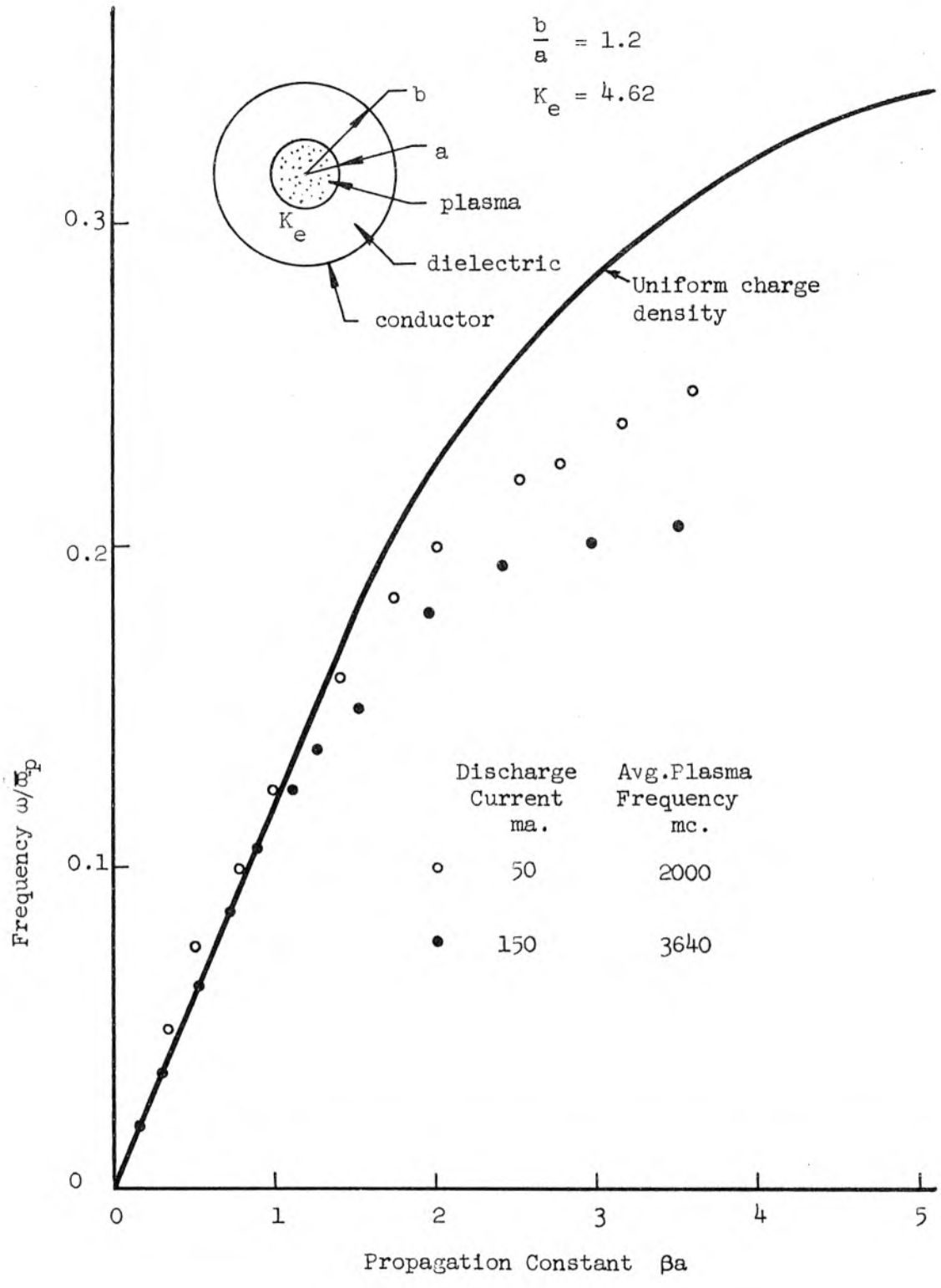


Figure 40. Theoretical Phase Characteristics for Surface Waves with Experimental Points.

the diagram. From the analysis of Chapter IV, this would indicate that the edge charge density is lower relative to the axis charge density for higher discharge currents. Such behavior can be explained qualitatively by noting that the rate of production of plasma electrons increases with increasing discharge current and by assuming that the radial diffusion constant is not a function of discharge current; this means that the curvature of the distribution, which is proportional to the rate of production-diffusion constant ratio, increases with discharge current. The value of the parameter $\alpha$ used in Chapter IV to denote the parabolicity of the radial charge distribution, has been calculated for a few cases; however, the values are at best crude estimates for reasons cited in Chapter IV and will therefore not be given as results.

Plasma Diagnostics. It was shown in Chapter IV in the section involving the effect of variation of charge density with radius, that the phase velocity at low frequencies is asymptotic to a constant velocity which depends on the average charge density and the geometry. A measurement of this low frequency phase velocity therefore provides a measure of the average plasma frequency. This was shown only for the surface waves which exist in the absence of an axial magnetic field. It is assumed, without proof, that the low frequency phase velocity of waves which propagate in the presence of an axial magnetic field also depends only on the average charge density. Figure 41 shows curves of the plasma frequency squared (proportional to average charge density) as a function of the axial magnetic field for several discharge currents. As the magnetic field is increased from zero, there is a sharp enhancement of the average charge density. This is explained by observing that the plasma electrons go from a regime at zero magnetic field where

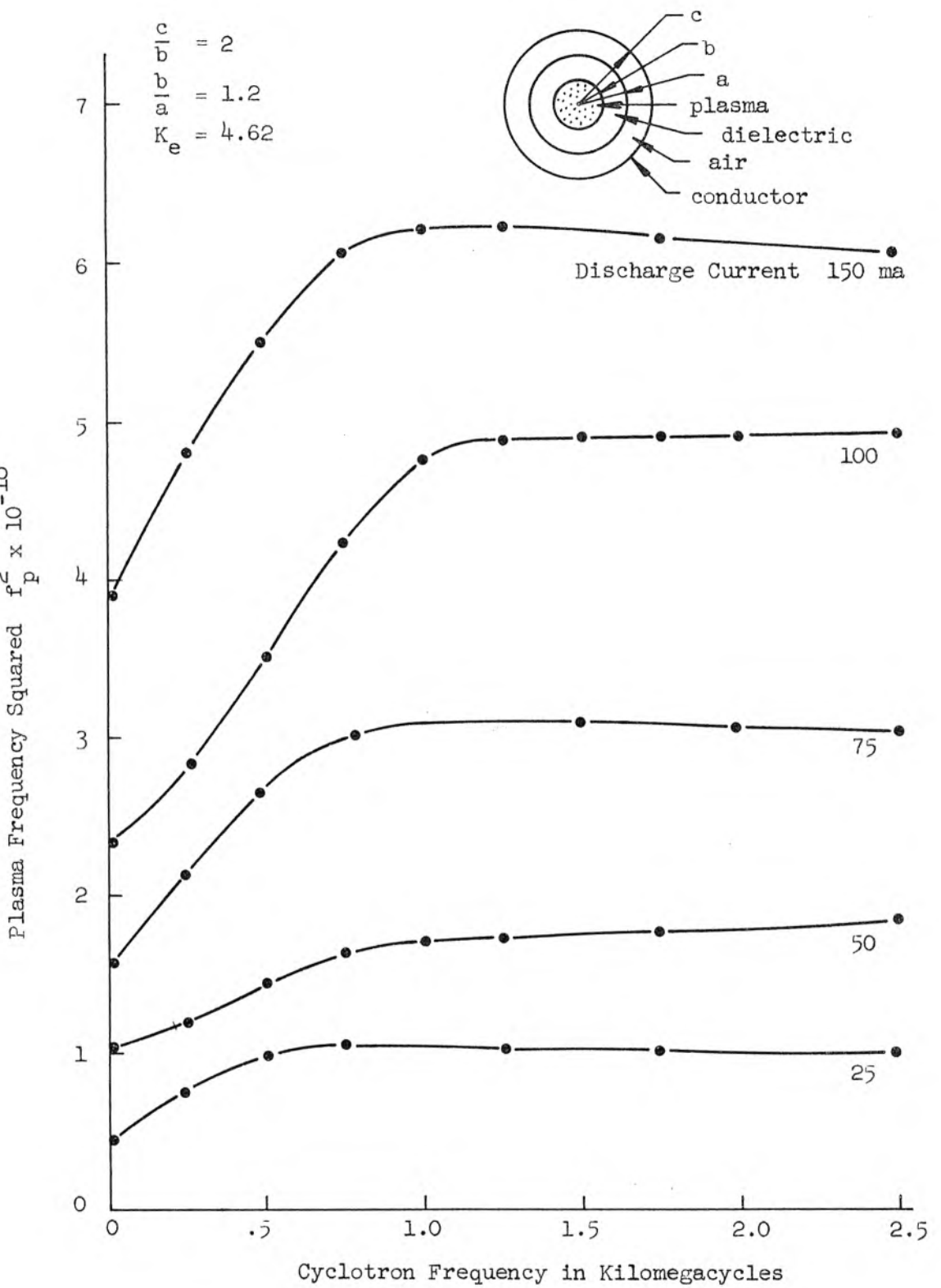


Figure 41. Plasma Frequency as a Function of Magnetic Field for Several Discharge Currents.

wall collision (the mean free path of plasma electrons is several times the diameter of the glass cylinder containing the plasma) is the primary loss mechanism to a regime where only a few electrons collide with the wall because their cyclotron radius is much less than the diameter of the plasma column. Thus at a magnetic field greater than the value required for a cyclotron radius equal to the plasma column diameter for few volt electrons, the plasma electrons should drift along the axis of symmetry spending a longer time in the plasma thus resulting in a higher average charge density. It would be expected that once the cyclotron radius was much less than the diameter of the plasma column that a further increase of the magnetic field would produce no further enhancement of the charge density. As seen in Figure 41, this is in agreement with the experimental observation.

Equation V.33 relates the average collision frequency of plasma electrons to the wave attenuation and wave group velocity. A measurement of the wave attenuation along the plasma column and simultaneous evaluation of the group velocity therefore provides a measure of the collision frequency. Figure 42 is a plot of the collision frequency as a function of discharge current for zero axial magnetic field. The measured collision frequency is in agreement with a calculation based on a few volts energy for plasma electrons and a mean free path long compared with the one centimeter diameter (the calculated collision frequency is the order of 100 megacycles). Attenuation measurements in the presence of an axial magnetic field have been made. The loss was in most cases low and reflected energy from the end of the plasma column prevented accurate measurements. The results are questionable and will not be included.

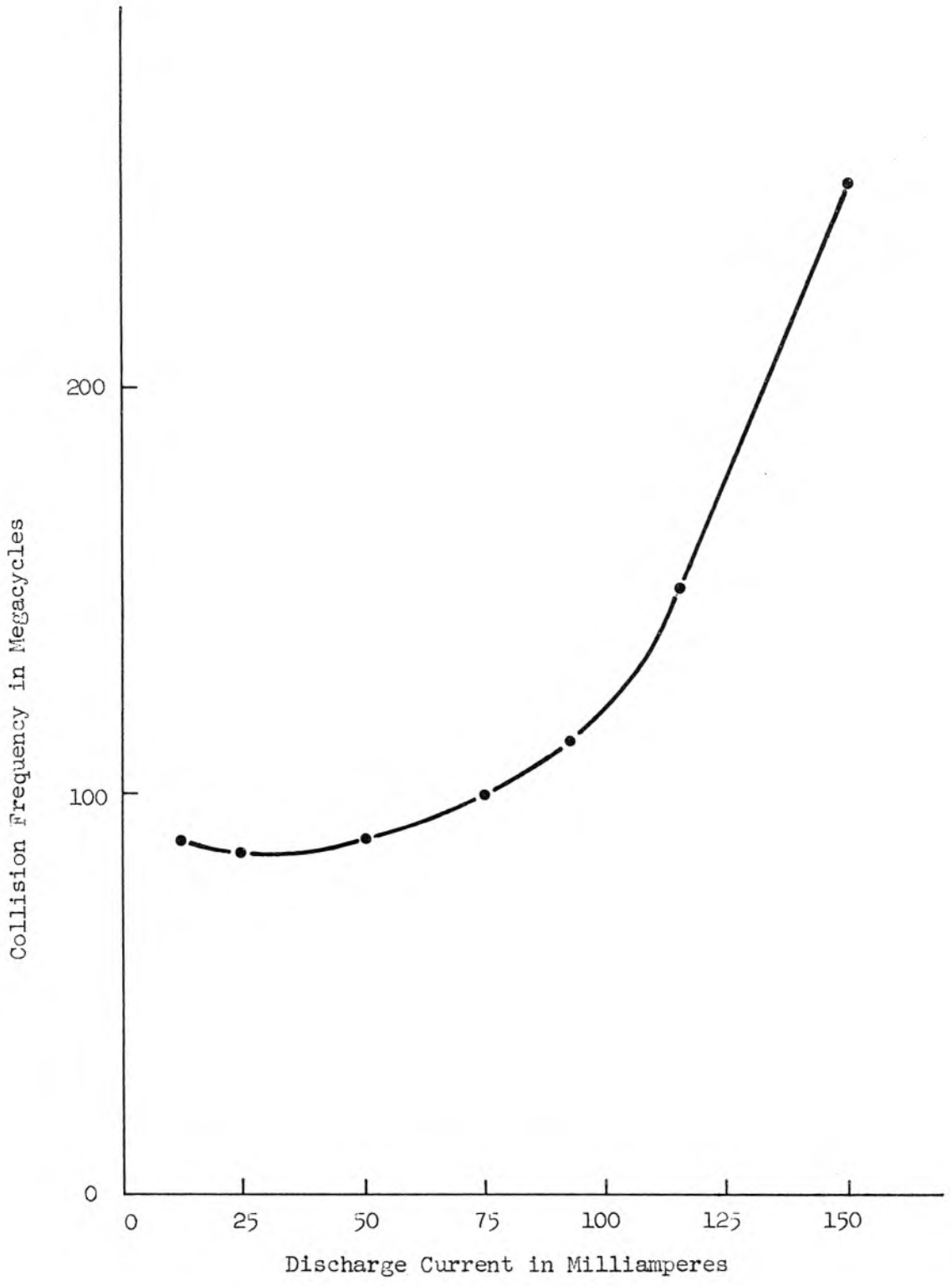


Figure 42. Experimental Values of Collision Frequency from Attenuation Measurements. Zero Axial Magnetic Field.

# IX. SUMMARY AND CONCLUSIONS

Some of the features of slow electromechanical modes of wave propagation in a stationary plasma of finite transverse cross section have been examined by considering the plasma to be a dielectric and solving the field equations. It has been shown that there exist two basic types of propagation, both of which have phase velocities that are generally much less than the velocity of light. The first might be described as a body wave since it involves a perturbation in the average charge density of the plasma; the presence of a d.c. magnetic field is essential to the existence of body waves. The second is a surface wave which involves a perturbation or "rippling" of the plasma surface but no charge accumulation within the plasma; this type exists for either zero or small d.c. magnetic fields and does not exist when the plasma completely fills a conducting waveguide. Each of these types of propagation has modes which can exist down to zero frequency and modes which for certain conditions are backward waves. Backward waves usually exist as a spatial harmonic on a periodic circuit and not as separate and distinct modes as observed here. Five distinct backward waves are reported and the possibility of interacting an electron beam with one of them is considered briefly. The interaction of an electron beam with this "structureless" backward wave has potential application in the generation of very high microwave frequencies since the emphasis would be shifted from the fabrication of delicate slow wave structures to that of obtaining very high charge density plasmas. Faraday rotation of the plane of polarization was an important consideration in the perturbation of the electromagnetic waveguide modes by

the introduction of a plasma into the waveguide system. Significant Faraday rotation is shown to exist for the angular dependent slow wave modes in a plasma column partially filling a conducting waveguide in a finite axial d.c. magnetic field. It is shown that it is not essential for the d.c. magnetic field to be coaxial with the waveguide system for propagation to exist by considering the problem of a plasma-filled rectangular waveguide with a d.c. magnetic field perpendicular to one of the guide surfaces. The mode types which result are a backward wave which propagates down to zero frequency and a narrow pass band forward wave near the plasma frequency.

The surface waves which involve no charge accumulation within the plasma are quite sensitive to the radial charge density variation of the plasma column near the edge of the pass band. At low frequencies, however, the phase velocity of the waves depend only on the average charge density. The effects of the radial charge density on the propagation characteristic are examined and experimental methods for obtaining a measure of the radial charge variation and the average charge density are described. It seems likely that one of the most useful applications of surface wave propagation is that of plasma diagnostics since the frequencies required are much less than the plasma frequency. This is of particular interest where the charge densities correspond to millimeter wavelength plasma frequencies and signal generation is rather difficult. A measurement of the attenuation of the wave amplitude is shown to provide a measure of the average collision frequency in the plasma. This method could be quite useful in obtaining the collision frequency in regimes where an analytical solution would be quite difficult.

Each of the modes described are closely related to space charge waves associated with drifting electron beams. A method for obtaining the properties of drifting electron beam space charge waves by a coordinate transformation is described. The space charge wave reduction factor for drifting beams is easily obtained from the stationary plasma phase characteristics by a simple graphical construction. This results in a considerable lessening in the labor of obtaining the space charge wave reduction factor as well as providing a better understanding of the nature of space charge waves in general.

Slow wave magnetostatic modes of propagation in ferrite waveguides which are essentially the magnetic dual of the waves in a stationary plasma are examined briefly. These modes do not appear to be of much usefulness at the present time except for purposes of ferrite diagnostics. The electric fields associated with these modes are small and the possibility of interaction of electron beams with these modes seems unlikely. For an axial magnetic field there is one slow backward wave passband near the precession resonance frequency, and for a transverse magnetic field a forward wave passband in the same vicinity.

Many of the features of the plasma modes have been verified experimentally by measuring the phase velocity on a mercury arc discharge column. These measurements have yielded estimates of charge density which are in essential agreement with other methods of obtaining charge density.

The analytical and experimental work reported in this paper does not pretend to be exhaustive; in fact, more problems were uncovered which remain to be solved than were solved. One of the more interesting of these problems is the nature of the noise which seriously hampered

efforts to obtain precise experimental data. This noise is present both with and without magnetic fields. With magnetic fields there was a more or less continuous spectrum with several discrete prominences for which the amplitude of successive peaks was lessened as the frequency was increased. For some operating conditions, the amplitude of the noise was a function of position along the guide. It is not known whether these signals were growing or decaying since their origin is not known. For other conditions, there were definite standing waves of noise voltage along the mercury discharge column. In most cases the level of noise voltage at any plane along the discharge column appeared to be related to the level of the incident signal (the noise increased as the signal level was raised.) One of the types of noise which is known to exist in discharge columns is that of moving striations, although it is not known to be the mechanism in this case.

Another interesting problem is that of slow wave propagation in discharges of the thermonuclear type. The primary differences should come from the rather large circumferential magnetic field which results from the large currents carried by the discharge. A knowledge of the properties of these waves and experimental procedures similar to those described in this paper should permit the diagnostics of such discharges.

The possibility of interacting an electron beam with any of the backward waves described to make a "structureless" backward wave oscillator is particularly intriguing. Although interaction of an electron beam with one of the forward wave modes has been observed, the results were entirely too preliminary to be reported in a systematic way. Work is being continued in the hope that backward wave interaction will be found.

Certain deviations from the theoretical surface wave behavior which were not reported in the chapter on experimental work can probably be attributed to the variation in charge density near the edge of the plasma column.

The primary conclusion to be drawn from this analysis is that a drifting motion of a plasma is not essential to the propagation of space charge wave disturbances provided that the plasma is of finite transverse cross section. The most important result of the analysis is that of describing methods whereby the properties of plasmas can be investigated by rather simple experimental techniques involving frequencies which are much less than the plasma frequency. Also of interest is the conclusion or implication that the propagation of noise disturbances near the potential minimum of a diode may be considerably different from that predicted by one-dimensional space charge wave theory when the plasma frequency is of the same order as the frequency of interest. Finally, it seems likely that an understanding of these slow wave modes of propagation may be useful in studying the radiation or reception of radio signals in guided missiles since the hot exhaust gases are a low frequency propagating structure, and the antenna pattern might be modified by the exhaust gas column which r.f.-wise is part of the missile.

BIBLIOGRAPHY

1. Spangenberg, K. R., Vacuum Tubes, (1948), 475-526.

2. Heil, A. A., and O. Heil, "Eine neue Method zur Erzeugung kurzer ungedampfungter electromagnetischen Wellen von Grosser Intensitat" (A New Method of Generating Short Undamped Electromagnetic Waves of High Intensity), Zeit. fur Phys., (July 1935), 95, 752-773.

3. Varian, R. H. and S. F. Varian, "A High Frequency Oscillator and Amplifier", Jour. Appl. Phys., (May 1939), 10, 321-327.

4. Webster, D. L., "Theory of Klystron Oscillations", Jour. Appl. Phys. (December 1939), 10, 864-872.

5. Hahn, W. C., "Small Signal Theory of Velocity-Modulated Electron Beams", Gen. Elec. Rev., (June 1939), 33, 591-596.

6. Ramo, S. "Space Charge Waves and Field Waves in an Electron Beam", Phys. Rev. (1939), 56, 276.

7. Rigrod, W. W., and J. A. Lewis, "Wave Propagation along a Magnetically Focused Cylindrical Electron Beam", B.S.T.S. (March 1954), 33, 399-416.

8. Brillioun, L. "A Theorem of Larmor and Its Importance for Electrons in Magnetic Fields", Phys. Rev., (1945), 67, 260.

9. Brewer, G. R., "Some Effects of Magnetic Field Strength on Space-Charge Wave Propagation", Proc. I.R.E., (July 1956), 44, 896-903.

10. Labus, J. "Space Charge Waves along Magnetically Focused Electron Beam", Proc. I.R.E., (June 1957), 45, 854-861.

11. Suhl, H. and L. R. Walker, "Topics in Guided Wave Propagation through Gyromagnetic Media", B.S.T.S., (1954), 33; Part I 579-659, Part II 939-986, Part III 1133-1194.

12. Gamo, H., "The Faraday Rotation of Waves in a Circular Waveguide", Jour. Phys. Soc. Japan, (1953), 8, 176-182.

13. Van Trier, A. A. Th. M., "Guided Electromagnetic Waves in Anisotropic Media", Appl. Sci. Res. (1954), B3, 305.

14. Pierce, J. R., Traveling-Wave Tubes, D. Van Nostrand (1950)

15. Pierce, J. R. and W. E. Danielson, "Minimum Noise Figure of Traveling-Wave Tubes with Uniform Helices", Jour.Appl.Phys. (1954), 25,1163-1165.

16. Bloom, S. and R. W. Peter, "A Minimum Noise Figure for the Traveling-Wave Tube", RCA Review, (1954), 15, 252-267.

17. Robinson, F.N.H.,"Microwave Shot Noise in Electron Beams and the Minimum Noise Factor of Traveling-Wave Tubes and Klystrons", Jour.British Inst. Radio Engineers, (1954), 42, 79-86.

18. Watkins, D. A., "Noise Reduction in Beam Type Amplifiers", Proc. I.R.E. (1952), 40, 65 .

19. Pierce, J. R., "General Sources of Noise in Vacuum Tubes", Trans. of the I.R.E., P.G.E.D., (1954) 135-167.

20. Trivelpiece, A. W., R. W. Gould, and L. M. Field, "Low Noise Preamplifiers for Radio Astronomy Observation", California Institute of Technology Vacuum Tube Research Project, Quarterly Status Report No. 15 (October 1956) Study IV.

21. Trivelpiece, A. W., R. W. Gould, and L. M. Field, "Low Noise Preamplifiers for Radio Astronomy Observation", California Inst. of Technology Vacuum Tube Research Project, Quarterly Report No. 18, (July 1957), Study III.

22. Smullin, L. D., and P. Chorney, "Electron-Stimulated Ion Oscillators", Massachusetts Inst. of Technology, Quarterly Progress Report (October 1957).

23. Smythe, W. R., Static and Dynamic Electricity, McGraw-Hill, (1950) 519.

24. Slater, J. C., Microwave Electronics, D. Van Nostrand (1954) 169-187.

25. Trivelpiece, A. W., R. W. Gould, and R. K. Cooper, "Electromechanical Modes of Propagation in Plasma Waveguides and their Application to Measurement of Electron Density in a Cylindrical Plasma Column", California Inst. of Technology Vacuum Tube Research Project, Technical Report No. 8 (to be published.)

26. Johnson, H. R., "Backward-Wave Oscillators", Proc. I.R.E., (June 1955), 43, 684.

27. Gould, R. W., Course Notes on Physical Electronics, California Inst. of Technology, 1956-57.

28. Birdsall, C. K., "A Simple Method for Obtaining Phase Velocity, Attenuation, and Impedance of a Sheath Helix in Arbitrary Surroundings" Memorandum for File ETL-12, (July 1, 1953), Hughes Research and Development Laboratories, Culver City, California.

## APPENDIX I. ONE-DIMENSIONAL SPACE CHARGE WAVES

Consider an ion-neutralized, drifting electron stream of average velocity $u_{oz}$ and average charge density $\rho_o$. A simple derivation for the space charge waves which propagate in this system begins by assuming the total velocity and charge density to be the average value plus a small, harmonic time-dependent perturbation,

$$v(z,t) = u_{oz} + v_{1z}\, e^{j(\omega t - \beta z)} \tag{AI.1}$$

$$\rho(z,t) = \rho_o + \rho_1\, e^{j(\omega t - \beta z)} \quad . \tag{AI.2}$$

The total convection current density $J = \rho v$ passing a given plane is also assumed to have an average value plus a small perturbation,

$$J(z,t) = J_{oz} + J_{1z}(z,t) = \rho_o\, u_{oz} + (u_{oz}\, \rho_1 + \rho_o\, v_{1z})\, e^{j(\omega t - \beta z)} \quad , \tag{AI.3}$$

where the term $\rho_1\, v_{1z}$ has been neglected since it is the product of perturbation quantities and is of second order. For the assumed time and space dependence, the a.c. current and a.c. charge density are related by the equation of continuity II.8

$$J_{1z} - \frac{\omega}{\beta}\, \rho_1 = 0 \quad . \tag{AI.4}$$

The a.c. electric field is related to the a.c. charge density by the divergence relation II.3

$$j\beta\, E_{1z} + \frac{\rho_1}{\epsilon_o} = 0 \quad . \tag{AI.5}$$

The a.c. velocity and a.c. electric field are related by the equation of motion II.7

$$(\omega - \beta u_{oz})\, v_{1z} - j \frac{e}{m} E_{1z} = 0 \qquad \text{(AI.6)}$$

where

$$\frac{dv}{dt} = \frac{\partial v}{\partial t} + \frac{\partial v}{\partial z}\frac{dz}{dt} \approx \frac{\partial v}{\partial t} + u_{oz}\frac{\partial v}{\partial t}$$

since $v$ is a function of both $z$ and $t$. Taking $dz/dt = u_{oz}$ assumes the drift velocity to be much larger than the a.c. velocity. The a.c. convection current density from AI.3 can be written

$$J_{1z} - u_{oz}\rho_1 - \rho_o v_{1z} = 0 \quad . \qquad \text{(AI.7)}$$

The equations AI.4 through AI.7 constitute a set of homogeneous algebraic equations which relate the a.c. velocity, charge density, current, and electric field. To have a non-trivial solution, the determinant of the coefficients associated with these variables must vanish. The interesting solution

$$\omega_p^2 - (\omega - \beta u_{oz})^2 = 0 \quad , \qquad \text{(AI.8)}$$

is the propagation equation for the space charge waves associated with the drifting motion of the electron stream. $\omega_p^2 = -\frac{\rho_o e}{\epsilon_o m}$ is the electron plasma frequency. The implications of this equation are examined in the introduction (see I.1).

## APPENDIX II. ADMITTANCE TRANSFORMATION

The characteristic equation for the propagation of waves in multi-region systems can be obtained by calculating the surface admittance (ratio of tangential H to tangential E when surface currents are absent) in two adjoining regions and equating them at the boundary. Birdsall (28) shows that the surface admittance at a plane (or as in the case considered here, at some cylindrical surface) can be easily calculated by means of cutoff guide admittance transformation if the admittance is known at some other plane such as at the conducting wall of a waveguide. This method need only be modified slightly to be used with the quasi-static approximation to obtain the propagation equation of a multi-region system containing a plasma column.

The boundary condition for the quasi-static approximation is continuity of the normal displacement-tangential electric field ratio at each discontinuity. This ratio is presumed known at the conducting surface of the waveguide and can be transformed to the surface of the plasma column by successive application of the transformation through each region between the waveguide wall and the plasma surface. In each region outside the plasma, the phasor potential is

$$\phi_1 = A\, I_n(\beta r) + B\, K_n\, \beta r \quad . \tag{AII.1}$$

The normal displacement and tangential electric field are

$$\epsilon\, E_{1r} = -\epsilon \frac{\partial \phi_1}{\partial r} = -\epsilon\, \beta \left[ A\, I_n'(\beta r) + B\, K_n'(\beta r) \right] \tag{AII.2}$$

$$E_{1z} = -\frac{\partial \phi_1}{\partial z} = +\, j\beta \left[ A\, I_n(\beta r) + B\, K_n(\beta r) \right] \quad . \tag{AII.3}$$

Defining a surface admittance

$$\epsilon \frac{E_{1r}}{E_{1z}} \equiv j\, Q(x) = -\frac{1}{j}\,\epsilon\, \frac{A\, I_n'(x) + B\, K_n'(x)}{A\, I_n(x) + B\, K_n(x)} \qquad \text{(AII.4)}$$

where the notation $x = \beta r$ has been used. At some other radius $(\beta r' = y)$,

$$Q(y) = \epsilon\, \frac{\frac{A}{B}\, I_n'(y) + K_n'(y)}{\frac{A}{B}\, I_n(y) + K_n(y)} \quad . \qquad \text{(AII.5)}$$

Solving AII.4 for the ratio of $A/B$ and substituting in AII.5,

$$Q(y) = \epsilon\, \frac{\epsilon\left[I_n'(y)\, K_n'(x) - I_n'(x)\, K_n'(y)\right] + Q(x)\left[I_n(x)\, K_n'(y) - I_n'(y)\, K_n(x)\right]}{\epsilon\left[I_n(y)\, K_n'(x) - I_n'(x)\, K_n(y)\right] + Q(x)\left[I_n(x)\, K_n(y) - I_n(y)\, K_n(x)\right]} \quad .$$

(AII.6)

This equation allows the evaluation of $Q(y)$ given $Q(x)$ and the values of $x, y$ and the dielectric constant $\epsilon$.

As an example, consider the three-region problem (i.e., plasma column of radius $a$ filling a dielectric cylinder of outer radius $b$ in a waveguide of radius $c$. $Q(\beta c)$ is infinite, and $Q(\beta b)$ $(\beta b < \beta c)$ is given by

$$Q(\beta b; \beta c, \epsilon_o) = \epsilon_o\, \frac{\left[I_n(\beta c)\, K_n'(\beta b) - I_n'(\beta b)\, K_n(\beta c)\right]}{\left[I_n(\beta c)\, K_n(\beta b) - I_n(\beta b)\, K_n(\beta c)\right]} \quad . \qquad \text{(AII.7)}$$

A second transformation from $b$ to $a$ gives the value of $Q(\beta a_+)$ just outside the plasma radius. Equating this to the value of $Q(\beta a_-)$ just inside the plasma radius gives

$$\left(1 - \frac{\omega_p^2}{\omega^2}\right) \frac{I_n'(\beta a)}{I_n\, \beta a} = \qquad \text{(AII.8)}$$

$$K_e \frac{K_e\left[I_n'(\beta a)\, K_n'(\beta b) - I_n'(\beta b)\, K_n'(\beta a)\right] + \frac{Q(\beta b)}{\epsilon_o}\left[I_n(\beta b)\, K_n'(\beta a) - I_n'(\beta a) K_n(\beta b)\right]}{K_e\left[I_n(\beta a)\, K_n'(\beta b) - I_n'(\beta b)\, K_n(\beta a)\right] + \frac{Q(\beta b)}{\epsilon_o}\left[I_n(\beta b)\, K_n(\beta a) - I_n(\beta a) K_n(\beta b)\right]}$$

where $Q(\beta b)$ is given by AII.7. Each of the quantities within the brackets in AII.7 and AII.8 are tabulated (28) for a limited number of cases permitting numerical solutions to be obtained with relative ease.

DISTRIBUTION OF TECHNICAL REPORTS

Chief of Naval Research 2
Navy Department - CODE 427
Washington 25, D. C.

Director, Naval Research Lab.
Washington 25, D. C.
Attn: Code 5240 1
Code 7130 1
Code 2000 6
Code 5430 1

Commanding Officer 1
Office of Naval Res.Branch Office
1000 Geary Street
San Francisco, California

Scientific Liaison Officer 25
Office of Naval Research, London
c/o Navy 100, Box 39, F.P.O.
New York, New York

Commanding Officer 2
Office of Naval Res.Branch Office
1030 E. Green Street
Pasadena, California

Commanding Officer 1
Office of Naval Research Branch Of.
The John Crerar Library Building
86 East Randolph Street
Chicago 1, Illinois

Commanding Officer 1
Office of Naval Res.Branch Office
346 Broadway
New York 13, New York

Officer-in-Charge 3
Office of Naval Research
Navy No. 100
Fleet Post Office
New York, New York

Chief, Bureau of Aeronautics EL 4 1
Navy Department EL 43 1
Washington 25, D. C. EL 45 1

Chief, Bureau of Ordnance
Navy Department Re 4 1
Washington 25, D.C. Re 9 1

Periodicals Librarian
General Library
California Inst. of Technology 1

Lincoln Laboratory
Massachusetts Inst. of Technology 1
Cambridge 39, Massachusetts

Signal Corps Resident Engineer
Electronic Defense Laboratory 1
Post Office Box 205
Mountain View, California

Cornell Aeronautical Laboratory 1
Cornell Research Foundation
Buffalo 21, New York

Director, Electronics Defense Gr. 1
Engineering Research Inst.
University of Michigan
Ann Arbor, Michigan

Georgia Inst. of Technology 1
Atlanta, Georgia
Attn: Librarian

Fred D. Wilimek 1
Varian Associates
611 Hansen Way
Palo Alto, California

John Dyer 1
Airborne Instrument Laboratory
Mineola, L.I., New York

Bell Telephone Laboratories
Murray Hill, New Jersey
Attn: Librarian 1
J. R. Pierce 1

Hughes Aircraft Company
Culver City, California 1
Attn: Mr. Milek, Tech.Librarian

RCA Laboratories
Princeton, New Jersey 1
Attn: Mr.Herold and H.Johnson

Federal Tele. Laboratories
500 Washington Avenue
Nutley, New Jersey
Attn: W. Derrick 1
K. Wing 1

Technical Library
G. E. Microwave Laboratory
601 California Avenue 1
Palo Alto, California

Chief of Naval Operations Op 20X 1
Navy Department Op 421 1
Washington 25, D. C. Op 55 1

Director, Naval Ordnance Laboratory 1
White Oak, Maryland

Director, Naval Electronics Lab. 1
San Diego 52, California

Dept. of Electronics and Physics 1
U.S. Naval Post Graduate School
Monterey, California

Commander Code 366 1
Naval Air Missile Test Center
Point Mugu, California

U. S. Naval Proving Ground 1
Attention: W. H. Benson
Dahlgren, Virginia

Commander 1
U.S. Naval Air Development Center
Johnsville, Pennsylvania

Committee on Electronics 1
Research and Development Board
Department of Defense
Washington 25, D. C.

Director, National Bureau of Stds. 1
Washington 25, D. C.
Attn: Div. 14.0 CRPL, Librarian

Commanding Officer 1
Engineering Res. and Dev. Lab.
Fort Belvoir, Virginia

Ballistics Research Laboratories 2
Aberdeen Proving Ground, Maryland
Attn: D. W. H. Delsasso

Chief, Ordnance Development Div. 2
National Bureau of Standards
Connecticut Ave and VanNess St, NW
Washington 25, D. C.

Commanding Officer 1
Frankford Arsenal
Bridesburg, Philadelphia, Pa.

Columbia Radiation Laboratory 1
538 W. 120th Street
New York 27, New York

Countermeasures Laboratory 1
Gilfillan Brothers, Inc.
1815 Venice Boulevard
Los Angeles, California

The Rand Corporation 1
1700 Main Street
Santa Monica, California
Attn: Librarian

Technical Library 1
Research and Development Board
Pentagon Building
Washington 25, D. C.

The Motorola Riverside Research Lab. 1
8330 Indiana Avenue
Riverside, California
Attn: Mr. John Byrne

Chief, Bureau of Ships CODE 816 1
Department of the Navy 820 1
Washington, D. C. 840 1

Panel on Electron Tubes 1
346 Broadway (8th Floor)
New York 13, New York

Supervisor of Research Laboratory 1
Electrical Engineering Building
Purdue University
Lafayette, Indiana

W. E. Lear 1
University of Florida
Department of Electrical Eng.
Gainesville, Florida

Director, Microwave Research Inst. 1
Polytechnic Institute of Brooklyn
55 Johnson Street
Brooklyn 1, New York

Material Laboratory Library, CODE 912B
New York Naval Shipyard 1
Brooklyn 1, New York

University of Washington
Department of Electrical Engineering
Seattle, Washington
Attn: E. A. Harrison 1
A. V. Eastman 1

Thermionics Branch 5
Signal Corps Eng. Laboratories
Evans Signal Lab, Bldg. 42
Belmar, New Jersey

Commanding General
Air Research and Dev.Command
Post Office Box 1395
Baltimore 3, Maryland
Attn: RDRR 1
RDDDE-3 1
RDDDE-5 1

Commanding General WCLC 1
Wright Air Devel.Center WCLRC 1
Wright-Patterson Air Force Base
Ohio

Commanding General CRRE 1
Air Force Cambridge Research Cen.
230 Albany Street
Cambridge 39, Massachusetts

Commanding General RCRW 1
Rome Air Development Center
Griffiss Air Force Base
Rome, New York

Armed Services Tech.Information 5
Document Service Center DSC-SA
Knott Building
Dayton 2, Ohio

Director CR4582 1
Air University Library
Maxwell Air Force Base, Alabama

Chief, Western Division 1
Air Research and Devel. Command
Office of Scientific Research
P.O. Box 2035, Pasadena, Calif.

Microwave Laboratory 1
Stanford University
Stanford, California
Attn: F.V.L. Pindar

University of Michigan 1
Electron Tube Laboratory
Ann Arbor, Michigan
Attn: E. Rowe

Mr. John S. McCullough 1
Eitel-McCullough, Inc.
San Bruno, California

University of Colorado 1
Department of Electrical Engineering
Boulder, Colorado

Ramo-Wooldridge Corporation 1
Control Systems Division
P.O. Box 900B
Hawthorne, California
Attn: Librarian

Electrical Engineering Dept. 1
Princeton University
Princeton, New Jersey

National Union Radio Company 1
350 Scotland Road
Orange, New Jersey
Attn: Dr. A. M. Skellet

Dr. J. E. Shepherd 1
Sperry Gyroscope Company
Great Neck, L.I., New York

W. L. Maxson Corporation 1
460 West 34th Street
New York 1, New York
Attn: M. Simpson

Mr. H. R. Argento
Raytheon Corporation 1
Waltham, Massachusetts

Dr. E. D. McArthur
Electron Tube Laboratory
General Electric Company 1
The Knolls
Schenectady, New York

General Electric Company 1
Electronic Components Division
Power Tube Department
Microwave Laboratory at Stanford
Palo Alto, California

Johns Hopkins University 1
Radiation Laboratory
1315 St. Paul Street
Baltimore 2, Maryland
Attn: Margaret Poole, Librarian

Raytheon Corporation 1
Waltham, Massachusetts
Attn: Librarian

Cascade Research
53 Victory Lane 1
Los Gatos, California

Engineering Library 1
Stanford University
Stanford, California

Research Laboratory of Electronics 1
Massachusetts Inst. of Technology
Cambridge 39, Massachusetts

Sloane Physics Laboratory 1
Yale University
New Haven, Connecticut
Attn: R. Beringer

Mr. H J Reich
Department of Electrical Eng. 1
Yale University
New Haven, Connecticut

Electron Tube Section 1
Electrical Engineering Dept.
University of Illinois
Champaign, Illinois

Chairman, Div. of Electrical Eng. 1
University of California
Berkeley 4, California

Technical Report Collection
303A, Pierce Hall 1
Harvard University
Cambridge 38, Massachusetts

Laboratory for Insulation Research
Massachusetts Inst. of Technology 1
Cambridge 39, Massachusetts
Attn: A. von Hippel

Chief, West Coast Office 1
Signal Corps Eng. Laboratories
75 So. Grand Avenue
Pasadena, 2, California

Office of Technical Services 1
Department of Commerce
Washington 25, D. C.

Professor W. P. Dyke 1
Linfield College
McMinnville, Oregon

Additional copies for Staff and
Future Requirements 25

Stanford Electronics Laboratories 1
Stanford University
Stanford, California

Attn: Applied Electronics Laboratory
Document Library

Mr. E. C. Okress, Technical Director
Westinghouse Microwave Center
310 N. Aurora Street 1
Ithaca, New York